การจำลองเชิงตัวเลขในการกักเก็บคาร์บอนไดออกไซด์ในพื้นที่สันทราย แอ่งฝาง

นางสาวนพวรรณ เรือนมั่น

วิทยานิพนธ์นี้เป็นส่วนหนึ่งของการศึกษาตามหลักสูตรปริญญาวิศวกรรมศาสตรมหาบัณฑิต
สาขาวิชาวิศวกรรมทรัพยากรธรณี ภาควิชาวิศวกรรมเหมืองแร่และปิโตรเลียม
คณะวิศวกรรมศาสตร์ จุฬาลงกรณ์มหาวิทยาลัย
ปีการศึกษา 2558

NUMERICAL SIMULATION ON CARBON DIOXIDE STORAGE IN SAN SAI AREA, FANG BASIN

Miss Noppawan Ruanman

A Thesis Submitted in Partial Fulfillment of the Requirements
for the Degree of Master of Engineering Program in Georesources Engineering
Department of Mining and Petroleum Engineering
Faculty of Engineering
Chulalongkorn University
Academic Year 2015

Thesis Title	NUMERICAL SIMULATION ON CARBON DIOXIDE STORAGE IN SAN SAI AREA, FANG BASIN
By	Miss Noppawan Ruanman
Field of Study	Georesources Engineering
Thesis Advisor	Assistant Professor Kreangkrai Maneeintr, Ph.D.

Accepted by the Faculty of Engineering, Chulalongkorn University in Partial Fulfillment of the Requirements for the Master's Degree

.....Dean of the Faculty of Engineering
(Professor Bundhit Eua-arporn, Ph.D.)

THESIS COMMITTEE

.....Chairman
(Associate Professor Dawan Wiwattanadate, Ph.D.)
.....Thesis Advisor
(Assistant Professor Kreangkrai Maneeintr, Ph.D.)
.....Examiner
(Assistant Professor Sunthorn Pumjan, Ph.D.)
.....External Examiner
(Siree Nasakul, Ph.D.)

นพวรรณ เรือนมั่น : การจำลองเชิงตัวเลขในการกักเก็บคาร์บอนไดออกไซด์ในพื้นที่สันทราย แอ่งฝาง (NUMERICAL SIMULATION ON CARBON DIOXIDE STORAGE IN SAN SAI AREA, FANG BASIN) อ.ที่ปรึกษาวิทยานิพนธ์หลัก: ผศ. ดร.เกรียงไกร มณีอินทร์, 131 หน้า.

จุดประสงค์ของงานวิจัยในครั้งนี้เป็นการศึกษาการกักเก็บคาร์บอนไดออกไซด์ในแหล่งน้ำมันที่หมดแล้ว โดยใช้แบบจำลองและคาดหวังการเคลื่อนที่ของคาร์บอนไดออกไซด์ในแหล่งน้ำมันที่โครงสร้างสันทราย แอ่งฝาง เพื่อเก็บเป็นข้อมูลเบื้องต้น ข้อมูลที่ใช้ในแบบจำลองมาจากศูนย์พัฒนาปิโตรเลียมภาคเหนือ กรมการพลังงานทหาร กระทรวงกลาโหม โปรแกรมซีเอ็มจีจะถูกใช้ในการสร้างแบบจำลองการกักเก็บคาร์บอน ตัวแปรที่ใช้ในแบบจำลองจะรวมความลึกระหว่าง 800-3000 เมตร อัตราการอัดฉีดที่ 1000 2000 และ 4000 ตันต่อวัน เวลาที่ใช้ในการศึกษาในครั้งนี้จาก 1 5 10 20 และ 50 ปี แบบจำลองได้ประยุกต์ใช้การแบ่งชั้นกริดโดยระเอียด (แอลจีอาร์) และแยกกรณีศึกษาออกเป็น 4 กรณีได้แก่ การเก็บคาร์บอนไดออกไซด์ในชั้นที่สอง ชั้นที่สี่ ชั้นที่หกและ ชั้นโดยรวม และยังได้ตรวจสอบความดันที่เพิ่มขึ้น และรัศมีการกระจายตัวอีกด้วย จากผลการศึกษาเป็ที่แน่ชัดว่า ความดันที่เพิ่มขึ้นจากการอัดฉีดคาร์บอนไดออกไซด์จนกระทั่งถึงเวลาปิดหลุม ซึ่งความดันที่เกิดขึ้นจะต้องน้อยกว่าความดันสูงสุด สำหรับอัตราการอัดฉีดที่ 2000 และ 4000 ตัน/วัน ความดันจะเพิ่มขึ้นและลดลงซึ่งต่างจากอัตราการอัดฉีดที่ 1000 ตัน/วัน นอกจากนี้รัศมีการกระจายตัวของคาร์บอนไดออกไซด์จะเพิ่มขึ้นจนถึงเวลาปิดหลุม และรัศมีจะลดลงเล็กน้อย แบบจำลองที่ศึกษาจะช่วยทำนายสิ่งที่จะเกิดขึ้นได้ตามช่วงเวลา ความลึกจะมีผลต่อปริมาณการกักเก็บ ความหนาของชั้นหินปิดกั้นผลกระทบต่อการรั่วของคาร์บอนไดออกไซด์ไปยังชั้นผิวดิน โดยอัตราการอัดฉีดและความดันที่เพิ่มขึ้นจะมีผลสัมพันธ์กัน

ภาควิชา วิศวกรรมเหมืองแร่และปิโตรเลียม ลายมือชื่อนิสิต .....

สาขาวิชา วิศวกรรมทรัพยากรธรณี ลายมือชื่อ อ.ที่ปรึกษาหลัก .....

ปีการศึกษา 2558

5570248721 : MAJOR GEORESOURCES ENGINEERING
KEYWORDS: CARBON DIOXIDE / CABON CAPTURE AND STORAGE / GEOLOGICAL STORAGE / LOCAL GRIDE REFINEMENT

NOPPAWAN RUANMAN: NUMERICAL SIMULATION ON CARBON DIOXIDE STORAGE IN SAN SAI AREA, FANG BASIN. ADVISOR: ASST. PROF. KREANGKRAI MANEEINTR, Ph.D., 131 pp.

The purpose of this work is to study the CO_2 storage in depleted oilfield with simulation and anticipate the movement of CO_2 in depleted oilfield at San Sai structure, Fang basin to collect a preliminary data. The data used in the simulation model come from Northern Petroleum Development Center, Defence Energy Department, Ministry of Defence. CMG program is used to create carbon storage model. The defined variable in modeling include depth between 800-3000 m., injection rate at 1000, 2000 and 4000 tons/day. The time this study from 1, 5, 10, 20 and 50 years. The simulation applies Local Grid Refinement (LGR) and separates case study into 4 cases as CO_2 storage at second, fourth, sixth and overall layers. Pressure buildup and radius of migration are investigated. From results, it is obvious the pressure buildup from CO_2 injection until shutin preiod. The pressure is still lower the maximum pressure. For 2000 and 4000 tons/day pressure buildup and decrease unlike that of 1000 tons/day injection rate. Furthermore, radius of migration of CO_2 will increase until shutin well preiod the radius will been slightly decreased. The simulation makes it possible to predict what will happen by the period. The depth will influence the amount of storage, thickness of caprock effect the CO_2 leakage into the surface, the injection rate and the pressure buildup are related.

Department:	Mining and Petroleum Engineering	Student's Signature	.....
		Advisor's Signature	.....
Field of Study:	Georesources Engineering		
Academic Year:	2015		

ACKNOWLEDGEMENTS

This report could not have been accomplished without the help of many persons. I am exceptionally grateful to my supervisor, Assistant Professor Krengkrai Maneeintr, Ph.D. His invaluable advice gave me guidance, direction toward the goals of research and he is always being very understanding.

I am gratefully acknowledge Associate Professor Dawan Wiwattanadate, Ph.D., Assistant Professor Sunthorn Pumjam, Ph.D. and Siree Nasakul, Ph.D. who are the thesis committee member for their kind comments and recommendations.

I am grateful to the Northern Petroleum Development Center, Defence Energy Department, Fang district and Chiang Mai province for supporting data used in this thesis.

This thesis is supported by Graduate School Thesis Grant, Chulalongkron University, Research Assistant Scholarship and Overseas Academic Presentation Scholarship for Graduate Students.

I would like to thanks all faculty members in the Department of Mining and Petroleum Engineering who have offered me knowledge, technical advices, and invaluable consultation.

I am very thankful to Miss Sujanya Gongpermpoon, my seniors, for her friendship, advices and help in entire course of study.

Finally, I extend gratitude to my family, especially my parents and my sister for support and encouragement. Thanks also to all who are not mentioned but involved in this thesis.

CONTENTS

Page

Page

LIST OF TABLES

LIST OF FIGURES

LIST OF ABBREVIATIONS

CCS	Carbon Capture and Storage
CMG	Computer Modeling Group Ltd
CO_2	Carbon dioxide
EOR	Enhanced Oil Recovery
FA	Fang
LGR	Local Grid Refinement
SS	San Sai

NOMENCLATURES

A	area
b	reservoir thickness
c_f	fluid compressibility
c_r	pore volume compressibility
c_t	total compressibility
E	efficiency
h	thickness
F_{min}	maximum pressure
g	gravitational acceleration
h	thickness
h_a	hydraulic head at point a
h_b	hydraulic head at point b
k	permeability
k_r	relative permeability
k_{rg}	gas relative permeability
k_{rw}	water relative permeability
k_{rog}	oil relative permeability for system with oil, gas and connate water
k_{rwo}	oil relative permeability for system with oil and water only
L	length
p	pressure
P/D	Pore pressure gradient
Q	volumetric flow rate
r_f	radius to the front
r_w	well radius
S_g	gas saturation
S_w	water saturation
t	time
T_s	mean annual ground surface temperature
x	Length
z	depth below ground surface

ρ	fluid density
ϕ	porosity
μ	viscosity
μ_w	viscosity of water

CHAPTER 1

INTRODUCTION

Currently, the problem of climate change and global warming has intensively increased. It is a worldwide issue to focus on the causes of the problem, which is mainly due to human activities such as combustion of fossil fuels leading to the amount of carbon dioxide increase in the atmosphere (Cantucci et al., 2009). In Thailand, the main sources of carbon dioxide that causes the most problems are fossil-fired power plant and industries (EGAT, 2015).

1.1 Carbon dioxide (CO_2) properties

Carbon dioxide is a chemical compound derived from the carbon element, which is an important element in variety of organism. The composition of carbon can be changed according to the conditions of the element itself. This is discussed in the carbon in gas phase. That is called “Carbon dioxide (CO_2)”. The advantages of CO_2 are their applications and uses in multi-industry. CO_2 in solid and/or liquid form is used for refrigeration and cooling, metals industry. CO_2 is used in the production of mold to enhance hardness, manufacturing and construction. CO_2 is used as a raw material in chemical processes and oil wells for oil extraction in petroleum industry, CO_2 gas is used as a soft drink, liquid CO_2 used to decaffeinate coffee and solid and liquid CO_2 is used to quick freezing, surface freezing and refrigeration in the transport of foods.

1.2 Source of CO_2

Source of CO_2 came from nature and human activities. The main sources of CO_2 emissions can be divided into many sections: electricity and heat, transportation, industry, residential, services and other sectors as shown in Figure 1.1(IEA, 2015). In this case, 49 percent (IPCC, 2005) of the CO_2 emission comes from fuel combustion for power generation. As a result, the trend of CO_2 release has been increasing.

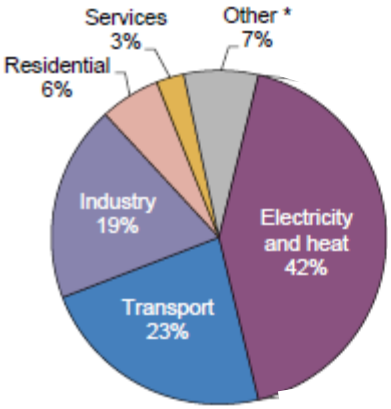

Figure 1.1World CO_2 emissions by sector in 2013 (IEA, 2015)

* Other includes agriculture/forestry, fishing, energy industries other than electricity and heat generation, and other emissions not specified elsewhere.

In Thailand, multiple parties focus on the problems with government agencies and the private sector together to find solutions of the problem by defining a national strategic level. Currently, Thailand is likely to increase CO_2 emissions by the growth of the population, thus establishing Thailand Greenhouse Gas Management Organization (TGO) as a guide to help reduce carbon dioxide and has a plan to reduce carbon dioxide emissions (EGAT, 2015). It is found that mainly CO_2 emission in Thailand is caused by combustion of fuels such as coal and oil to produce energy. Mae Moh power plant because of coal in large quantities. So it made CO_2 emissions into the atmosphere burns increased continuously in Figure 1.2.

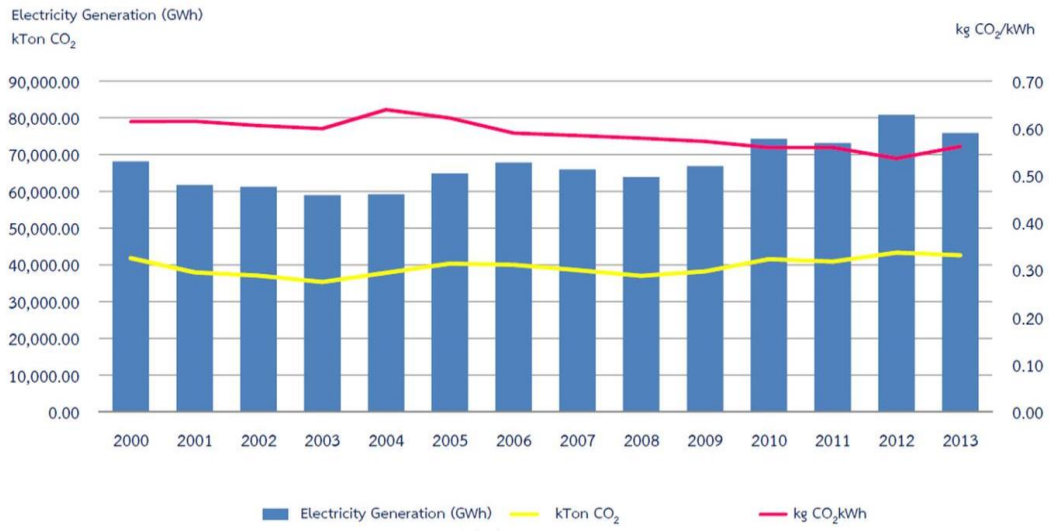

Figure 1.2 CO_2 Emissions from Electricity Generating Authority of Thailand (EGAT, 2015)

1.3 Carbon Capture and Storage Technology (CCS)

CCS is used to reduce the amount of CO_2 emissions from these sources. CCS can capture and store CO_2 approximately 85-95 percent of the CO_2 from total quantity emitted into the atmosphere (IPCC, 2005).

CCS technology is a process separated the CO_2 from the gas stream emitted from industrial processes or power generation. After separation CO_2 is compressed and transported to storage into the reservoir. CCS is an effective way of reducing emissions of CO_2 to the atmosphere. CCS process has 3 steps: capture, transportation and storage.

Capture

Current technology can be modified to capture CO_2 for about 85-95 percent of the total amount of CO_2 being released into the atmosphere (IPCC, 2005). The model in the capture of CO_2 has post combustion, pre combustion and oxyfuel combustion. Therefore, concentration, pressure and type of fuel used in the combustion are the parameters used to select the format for trapping carbon dioxide.

Transportation

Transportation of CO_2 mainly transports through pipeline because CO_2 can be transported in large quantity and the distance between the reservoir and capture plant is

very far. Transportation of CO_2 to the ocean may use ships. However, this is considering the method storage of transport that has a significant economic value.

Storage

This research is focusing on CO_2 storage especially in depleted oil field. Nowadays, there are 3 storage methods such as geological storage, ocean storage and mineral storage respectively (IPCC, 2005).

Geological storage is the storage of CO_2 in geological formation such as oil and gas wells, unmineable coal seams and deep saline formation as shown in Figure 1.3. CO_2 injection into geological layer involves various technologies such as survey, oil and gas production, drilling technology and injection technology. Furthermore, simulation and monitoring program to follow the migration have been developed for different types of geological storage as show below:

1. Depleted oil and gas reservoirs: this method injects CO_2 into the depleted oil and gas reservoirs. The originally accumulated traps don't leak. They are selected from geological structural and physical properties for oil and gas reservoirs. Simulation model is used to predict the movement, displacement behavior and trapping.
2. Enhanced oil recovery: this method injects CO_2 to enhance oil recovery (EOR). 5–40 percent of all is usually recovered by conventional primary production . Generally, reservoir depth is more than 600 m (IPCC, 2005).
3. Deep saline aquifer: the method selects deep sedimentary rock structure to inject CO_2 like the Sleipner project in the North Sea for saline formation storage. It is the first commercial project dedicated to geological storage by injects CO_2 in underground about 600-1000 m (IPCC, 2005).
4. Unmineable coal seams: this method injects CO_2 into unmineable coal seams for CO_2 storage.
5. Enhanced coal bed methane recovery: it method injects CO_2 into low affinity coal to produce methane to increase coal bed methane recovery.

CO_2 has been injected successfully at the Allison project in the Alberta Basin, Canada (Gunter et al., 2005).

6. Other suggested options (basalts, oil shale, cavities): this method is only injected CO_2.

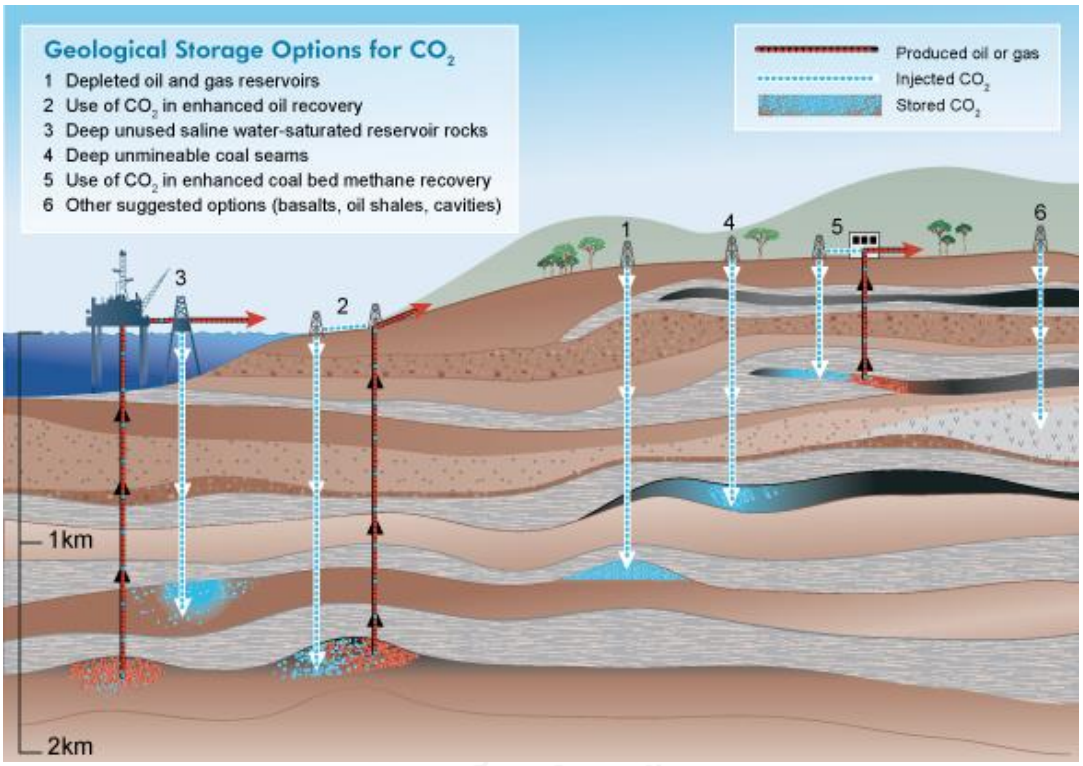

Figure 1.3 Geological storage of CO_2 (IPCC, 2005)

Ocean storage is to directly inject CO_2 into the sea by pipeline or ship at the level of 3 kilometer deep in water column and sea floor as presented in Figure 1.4. However, CO_2 can reduce pH affecting the environment, marine organisms, surface water are becoming more acidic, and there are chemical changes of the ocean. Moreover, the cost of ocean is higher compared to other methods. In 2002, there's a demonstration to inject 5 tons of CO_2 into deep ocean of Norway but it's opposed by the environment group (CRS, 2013). Therefore, ocean storage is no longer considered feasible (GreenFacts, 2015).

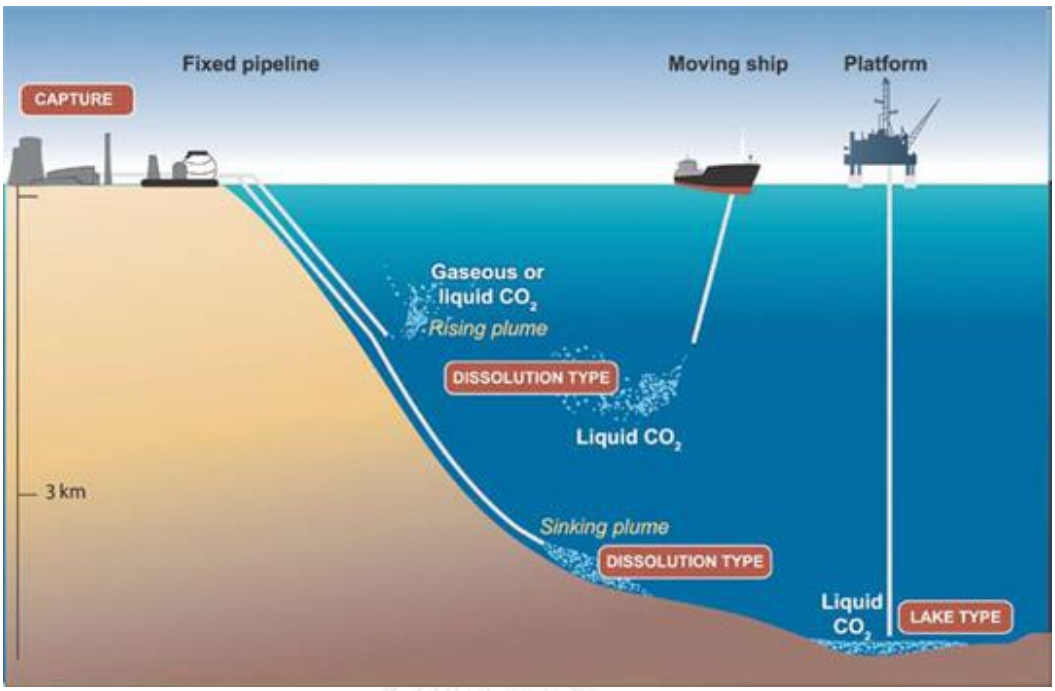

Figure 1.4 Ocean storage of CO_2 (IPCC, 2005)

Mineral storage is the process that CO_2 reacts with metal oxide such as magnesium oxide, calcium oxide and sodium oxide to form stable carbonate compounds as shown in Figure 1.5. The process occurs at very slow rate under ambient temperature and pressure and the process needs more energy. This process is demonstration. The Department Of Energy (DOE) did the survey for CO_2 storage at Columbia River Plateau flood basalt in the Pacific Northwest (CRS, 2013).

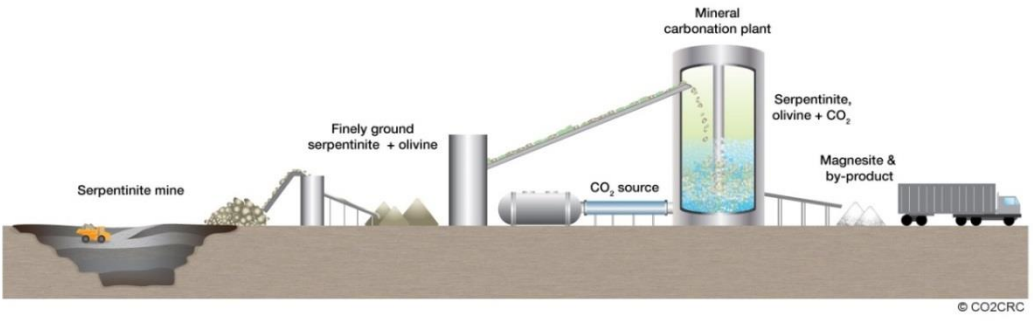

Figure 1.5 Mineral storage of CO_2 (CO2CRC, 2015)

Geological storage of CO_2, both onshore and offshore, has been developed starting from oil and gas industry. The recent development of storage in oil and gas field, saline formation and existing CO_2 storage project is presented in Table 1.1. Weyburn Project in Canada, Sleipner and Snohvit Projects in Norway and In Salah Project in Algeria.

Table 1.1 Site of CO_2 Storage

Project name	Country	Injection start (year)	Approximate average daily injection rate (tCO_2day^{-1})	Total (planned) storage (tCO_2)	Storage reservoir type
Weybum	Canada	2000	3000-5000	20000000	EOR
Sleipner	Norway	1996	3000	20000000	Saline formation
Snohvit	Norway	2006	2000	Unknown	Saline formation
In Salah	Algeria	2004	3000-4000	17000000	Gas field

Geological storage has advantages that are prompt data and economic benefit but it has disadvantage as well that it may is not worth efforts (IPCC, 2005). The good point of ocean storage is that it's a large amount of storage for CO_2 that can be directly injected into. But if it's injected less that 3 km, some of CO_2 will dissolve into sea water and some will float to water surface, in contrary, if injected area is more than 3 km, CO_2 will sink and be stored in form of fluid which is depend on area's pressure and temperature. For Mineral Storage, it's strong point is it's high stability but it's weakness is that it needs high investment but gain low value. From these 3 storage methods, the suitable method this CO_2 storage is Geological Storage.

1.4 Objectives of this research

The objective of the research is to study CO_2 storage in depleted oilfield at San Sai oilfield, anticipate the movements of CO_2 in depleted oil field evaluate the possibility. It is used as guidelines to develop methods and technology for CO_2 storage in the future of Thailand.

1.5 Scope of this research

Study CO_2 storage in depleted oilfield at San Sai oilfield, Fang basin base on only one well.

1.6 Contribution of this research

This research is aimed to the simulate CO_2 storage in oilfield in order to reduce CO_2 emission to the atmosphere. It can be used as a guideline to develop this technology in the future. Furthermore, it can be used to other application like oil and gas reservoir, and coal bed methane to increase project value.

The rest of the thesis will be presented in the next sections.

Chapter 2 explains theory about thermodynamic, rock properties, pressure, reservoir seals, storage capacity and literature review. General geology in the study area and reservoir simulation is illustrated in Chapter 3. The results and discussions are described about maximum pressure, storage capacity, and simulation results in Chapter 4. Chapter 5 presents the conclusions of this research.

CHAPTER 2

THEORY AND LITERATURE REVIEW

2.1 Theory

2.1.1 Thermodynamic properties of CO_2

Phase diagram shows the properties of temperature and pressure conditions at the various phases include: vapor, liquid and supercritical as show in Figure 2.1.

Supercritical Fluids are the area above critical point that has an unusual combination of liquid-like and gas-like properties: liquid like density, gas-like viscosity and diffusivity part way between the two.

CO_2 is found in state of supercritical with temperature of 31°C and the pressure of 73.8 bar on the critical point.

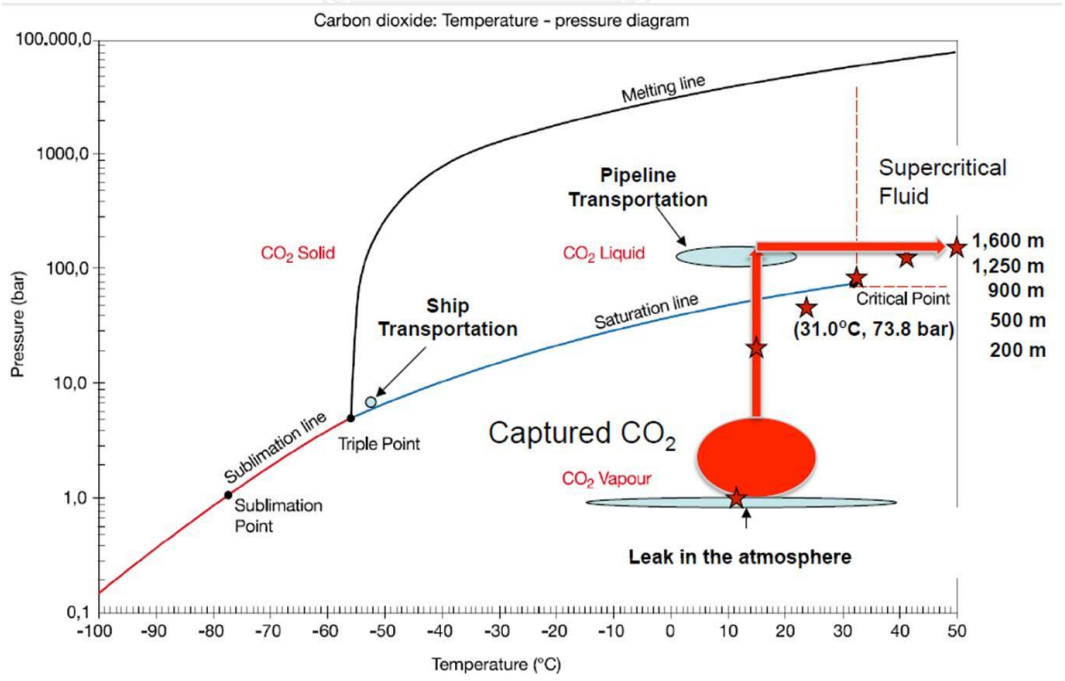

Figure 2.1CO_2: Temperature-pressure diagram (Wilcox, 2011)

2.1.2 Rock properties

2.1.2.1. Porosity

Porosity is the ratio of the volume of the space to total volume. The porosity is different in each rock. The porosity in the rock layer is controlled by the size of the shape and size distribution. High porosity, caused by deposition of ore with shape and size of grains about the same, but these sediments has cement between grains making porosity is decreased or sand layer is poor sorting, silt or clay included. It will replace the space between the grains. The porosity decreased as well. Normally, sandstones have porosity is 10-20 percent (Prakiat & Jeemsantia, 2011).

2.1.2.2. Permeability

Permeability is ability to allow water to percolate the rock. In addition, depend on porosity of rock, space and continuity between spaces.

$$k = \frac{-Q\mu}{A(\frac{p_b - p_a}{x})} \qquad (2.1)$$

When
μ Viscosity (Pas)
x Length (m)
Q Volumetric floe rate (m^3/s)
A Area (m^2)
p Pressure (Pa)

2.1.2.3. Density

Density is meaning the ratio between mass per volume of the substance itself. The symbol of density is ρ (kg/m^3).

2.1.2.4. Compressibility

Compressibility is meaning when fluid pressed or extruded cause cumulative elastic energy and smaller volume of compressed and back to the original volume. When the force or pressure exerted by compression used to be a symbol c with the unit of psi^{-1}.

2.1.2.5. Darcy's law

Darcy's law is describing the flow of fluid in reservoir. The discharge is proportional to area, head difference and inversely proportional to length. Darcy's law applies to steady state and laminar flow but not compatible with turbulent flow (size/font) and gas flow at very high or very low.

$$Q = -\frac{k\rho g A(h_b - h_a)}{\mu L} \qquad (2.2)$$

When Q = volumetric flow rate (m^3/s)

k = permeability (m^2)

ρ = fluid density (Kg/m^3)

g = gravitational acceleration (m/s^2)

A = cross section area (m^2)

μ = fluid viscosity (Pa-s)

h_a = hydraulic head at point a (m)

h_b = hydraulic head at point b (m)

L = length (m)

Immiscible fluid is that the fluid is unable to melt in the other flow and mix. CO_2 and brine are immiscible fluid.

2.1.2.6. Multi-phase flow

Injection pressure is an important part because the damage of storage can be avoided from the maximum pressure of injection. The maximum pressure of each formation depends on geological, depth and temperature etc. Limited pressure of injection is 90 percent of fracture pressure. The more injection pressure, the higher opportunities to break the caprock.

2.1.2.7. Geothermal gradient

When the depth increases, temperature increase respectively and $\frac{dt}{dz} \approx 25^{o}C$ to $30^{o}C/km$

$$T(z) = T_s + \int_0^z \frac{dT}{dz} dz = T_s + \frac{d\overline{T}}{dz} z \qquad (2.3)$$

When T_s mean annual ground surface temperature (◦C) ~14.7°C

z depth below ground surface (m)

2.1.3. Pressure

2.1.3.1. Fracture pressure

The fracture pressure formation must be calculated and set by using empirical relationships. Since the fracture pressure is affected by pore pressure served as a method or application the correlation of fracture pressure. Commonly used equations and the relationships include pressure fracture; the Hubbert and Willis equation, introducing basic principles are widely used at present. (Bourgoyne et al., 1986):

$$F = \frac{1}{3}\left(1 + \frac{2P}{D}\right) \qquad (2.4)$$

When F_{min} Maximum pressure

P/D Pore pressure gradient (psi/ft)

= 0.465 psi/ft (Normal Pore Pressure gradient)

2.1.3.2. Pressure buildup

When the pressure increases along with the function of time, usually it is observed after a shutin well or the rate of production declines. In general, the pressure buildup to measured at or near the bottom of the hole.

The parameters used to calculate are initial reservoir pressure (P), reservoir temperature (T), thickness (*b*), permeability (k), porosity (Ø), compressibility (c_t), flowrate of CO_2 (*Q*) and radius of injection well (r_w)

- Pressure buildup during CO_2 injection depends on flow in both the multiphase and single phase regions

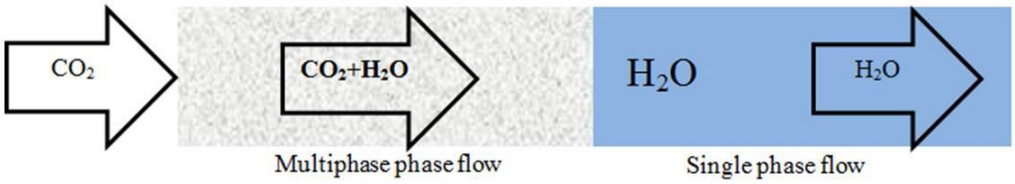

- Pressure buildup in the single phase region can be calculated with the this equation

$$\Delta P = \frac{Q \times \mu_W \times W}{4 \times \pi \times k \times b} + \frac{Q \times \mu_{CO_2}}{2 \times \pi \times k \times b} \times \left[\ln\left(\frac{r_f}{r_w}\right) + \left(\frac{f_{CO_2}}{K_{r_{CO_2}}} - 1\right)\left(1 - \frac{r_w}{r_f - r_w} \times \ln\left(\frac{r_f}{r_w}\right)\right)\right] \qquad (2.5)$$

When

b	Reservoir thickness (m)
c_t	Total compressibility (Pa^{-1})
k	Permeability (m^2)
Q	Injection rate (m^3/s)
r_f	Radius to the front (m)
r_w	Well radius (m)
t	Time (s)
ϕ	Porosity
μ_w	Viscosity of water (Pas)

The radius of influence can be used to estimate the extent of pressure buildup due to CO_2 injection

- Pressure buildup in the multiphase region can be calculated from the multiphase extension of Darcy's law combined with the Buckley-Leverett solution

-

2.1.3.3. Radial Geometry for Injection Pressure

Injection pressure

Injection pressure is an important factor to avoid the damage storage for CO_2 storage which depend on geological characteristic, depth and etc., in the injection ration determination and hole estimation. Over abundantly pressure will cause the caprock penetration.

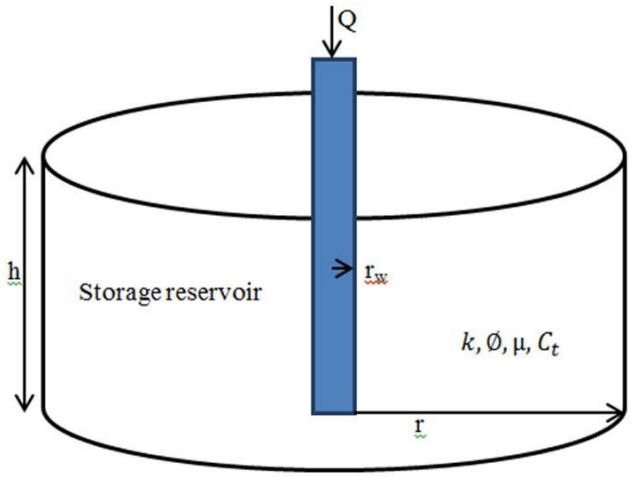

Figure 2.2 Radial geometry for injection pressure

$c_t = c_f + c_r$ (Pa^{-1})

$c_f = 1/\rho \, d\rho/dp = 4x10^{-10}$ Pa^{-1}

$c_r = 1/\emptyset \, d\emptyset/dp = 10^{-8}$ to 10^{-9} Pa^{-1}

When we inject CO_2

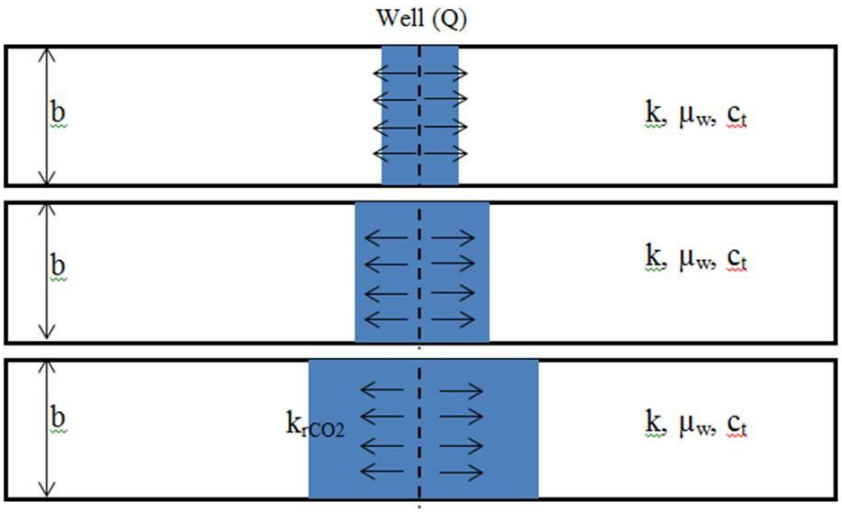

Figure 2.3 Growing plume multi-phase flow

Assume:

- The liquid can be compressed very little.
- Independent of pressure on k, μ_{CO2}, μ_w, k_r, density, c_t.
- Properties of the rocks as a uniform.
- The flow in radial direction in only a vertical direction.
- Infiltrate of CO_2 at constant thickness (h) throughout.
- Boundary conditions
    - The illumination is an infinite.
    - Boundary on top and bottom with impermeable layers.
    - Line source.
    - Rate of inject is fixed: t>0.
    - Initial pressure is same everywhere p_i.

2.1.4. Reservoir seals (caprocks)

1. Seals are needs to retain CO2 underground; CO2 requires a seal to remain underground:
    - Density water is greater than CO_2: $\rho_w > \rho_{CO2}$

- CO_2 is subject to buoyant forces that will drive it towards the ground surface:

  Buoyancy force = Volume x (ρ_w- ρ_{CO2}) x g

- A seal is needed to prevent upward migration

2. The properties of seals have two key
   - Permeability barrier
   - Capillary barrier (Membrane allows water flow but not CO_2)
3. Capillary pressure is the difference between the pressure in the wetting and non-wetting phases
4. Fine textured sedimentary rocks with small pores (r_{pore} << 1µm) have high capillary pressures
5. Capillary pressure can be accessed from the thickness of the CO_2 column in the storage reservoir
6. Capillary entry pressure >>capillary pressure to provide an effective seal

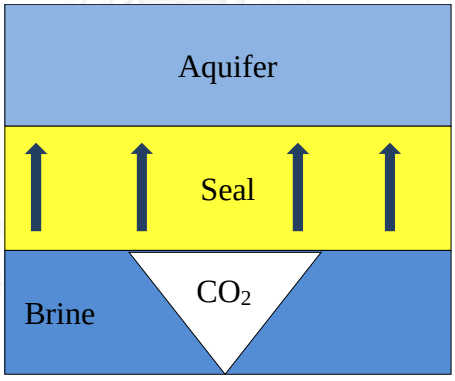

Figure 2.4 CO_2 trapping mechanisms of seals

2.1.5 Storage capacity

Storage capacity can be calculated for the area of CO_2 storage in each layer. When CO_2 injection into storage layer.

$$\text{Storage Capacity} = \emptyset A \rho_{CO2} h E \quad (2.6)$$

When ϕ Porosity
A Area

h	Thickness
ρ_{CO2}	Density of CO_2
E	Efficiency

Gorecki et al. (2009) explain three potential storage systems such as open system, close system and semiclosed system. The 3D model is applied to forecast the CO_2 injectivity in the geological formation and monitor CO_2 movement over the long period of time. Furthermore, the local grid refinement is applied to simulate to obtain the results with more accuracy. Also, many assumptions have been made to simplify and modify the unavailable data of the reservoir such as storage capacity and types of formation. This research is assumed to be open-system formation.

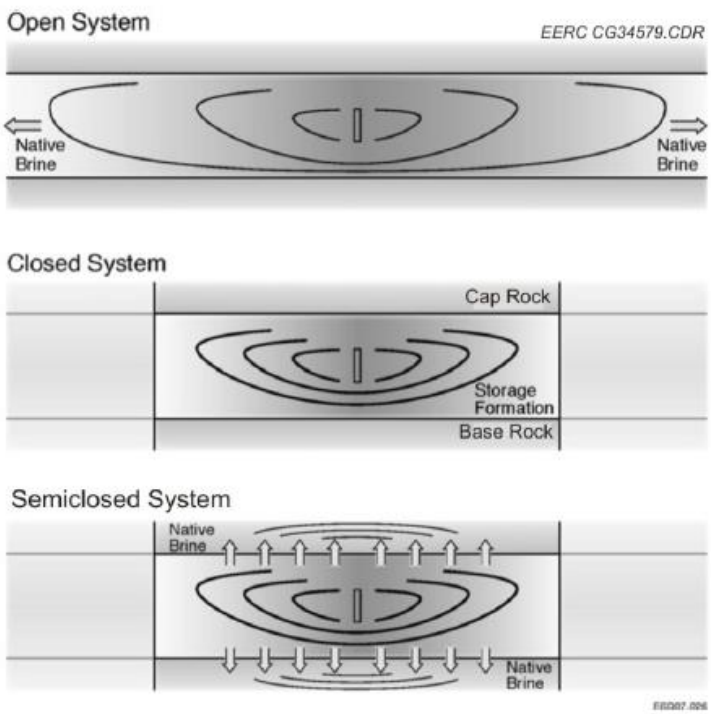

Figure 2.5 Diagram representing the three potential storage systems (Gorecki et al., 2009)

2.2 Literature Review

Benson (2010) explained in "Carbon Dioxide Capture and Storage in Underground Geologic Formations" hundreds of years ago, increasing trend of CO_2

concentration in atmospheric now increased to 370 ppm from the pre-industrial level of 280 ppm and the majority come from burning coal, oil and natural gas for electrical generation, transportation and industrial. Nowadays, worldwide have more than 20 billion tons of CO_2 emissions. Increased CO_2 will cause climate change. CCS in underground geologic formation is one of the options for decreasing CO_2 emissions. The idea CCS technology was developed in the last 1970. The last 1980 get the attention of scientists and engineers to reduce CO_2 emissions to the atmosphere. CCS technology has 4 step processes: capture, compression, pipeline transport and Underground injection respectively. CO_2 Capture has 3 type such as post-combustion, pre-combustion and oxygen-combustion that has different advantages and disadvantages. Compression and transport of CO_2 as the technology currently in use enhanced oil recovery, beverage carbonation, and fire suppression. CO_2 can be injected underground and stored in sedimentary basins. Sedimentary basins have tens of thousands feet thickness. The sandstone layers, that reservoir with high permeation, allow injection of CO_2. The shale or evaporites layers have very low permeability and seals protect CO_2 leak to surface quickly. The technology to inject underground is used in CO_2 enhanced oil recovery projects. CCS technology is significant benefits invaluable resources and developed over more than half a century by the oil and gas industry. The current and planned CCS projects such as Sleipner, North Sea (Statoil), Weyburn, Canada (Encana), In Salah, Algeria (BP), Gorgon, Australia (ChevronTexaco), Snohvit, Off-shore Norway (Statoil) and San Juan Basin, New Mexico (Burlington) respectively.

Torp and Gale (2004) studied Demonstrating storage of CO_2 in geological reservoirs: the sleipner and SACS projects. The studying is about the different scientific in the project: geology, geochemistry, geophysics and reservoir engineering/simulation. The project in the North Sea, was injected wuth CO_2 into a sand layer “Utsira formation”. In 1996, they started inject nearly 5 million ton of CO_2 and the project is the first commercial application of CO_2 storage in deep saline aquifers in the world. The project is called "The Saline Aquifer CO_2 Storage (SACS) project. The monitor used 3D seismic surveying in Utsira formation and repeat seismic surveys that can see the image the movement of CO_2 within the reservoir. Reservoir model is describing the storage of CO_2 movement in the reservoir and comparison seismic with itself.

Zakkour and Haines (2007) studied permitting issues for CO_2 capture, transport and geological storage: A review of Europe, USA, Canada and Australia. Discussing the environmental, health and safety issues by permitting regulatory action integrated. Review regulation at EU, North USA and Australia to evaluate the relevance to CCS and identified the ways to regulatory.

Bouc et al. (2009) studied determining safety criteria for CO_2 geological storage. The development of a methodology realised under the CRISCO$_2$ project, study of risk and objectives by using the model to evaluate the risk. This project's objective is to determine safety for geological storage. Using the basic methodology for determining impose various requirements and development of tools to identified risk, represent various rick events and assess the uncertainty of parameter and distribution of CO_2 in the format. Experiment at Paris basin for test the effect of safety criteria. The CRISCO$_2$ project is funds CO_2 capture and storage program of French National Research Agency (ANR).

Methods for Estimating CO_2 Storage in Saline Reservoirs were written by Frailey (2009). He explains; estimate CO_2 is an important for site selection of CO_2 geologic sequestration. The methods for estimating subsurface volumes in porous and permeable geologic formations are applied in oil and gas, ground water and underground natural gas storage. In general, these methods can be divided into two categories: static and dynamic. The static methods are volumetric and compressibility that require only rock and fluid properties. The dynamic methods are decline curve analyses, mass (or volumetric) balance, and reservoir simulation, and require information about active injection such as injection volumes and reservoir pressures. The different methods have advantages and disadvantages. Some methods are acceptable, depending on the data quality, data quantity, and geologic heterogeneity. The methods can be apply to basin-scale and specific site-scale storage estimates are discussed.

Dobossy et al. (2011) studied an efficient software framework for performing industrial risk assessment of leakage for geological storage of CO_2. This project is technology for geological storage of CO_2 emissions. Geological storage of CO2 has inherent risks. Two major concerns have been recognized: first leakage of CO_2 through the caprock and incomplete and second; Eliminate brine resulting in contamination of

drinking water sources. CO_2 and brine leakage have been identified to have three mechanisms: leakage through the faults and fractures in the caprock, leakage through man-made such as abandoned wells from oil and gas exploration and finally, diffuse leakage through the caprock. This paper describes a software for manage risk assessors and planners alike. The demonstrated through a case study of hypothetical injection site in the Alberta Basin show in Figure 18 is a 50 km by 50 km region. The area is a sediment sedimentary basin interest for the CO_2 store. The borehole exploration has resulted in over 1100 leave and active wells which a risk of unintended CO_2 leakage and brine displacement. The model used to describe using the extensive data describing the rock properties within the geological. This study data is regarding the location and depth of existing wells. The depth has related data related to stratigraphic data to assign an end formation for each well. There are two scenarios represent the two cases: know that the permeability of the hole and some research to reduce uncertainty. These results would be beneficial to risk assessors and planners. Case study useful in risk assessment and planning has three steps. First, the distribution of the leakage to formation can be used as a part of a cost assessment. Second, evaluate the reduction of CO_2 emissions by moving to deeper formation. Finally, conclusions information gives to the analysis.

Model is a tool that can make an effective risk assessment of geological storage of CO_2 a safe, reliable, and reduce emissions of CO_2. A case study assessment leakage of CO_2 and displacement of brine for a hypothetical injection in the Alberta Basin show useful information on software expectations and demonstrate knowledge and understanding of the scope of the risk assessment that can be performed.

Eiken et al. (2011) studied lessons learned from 14 years of CCS operations: Sleipner, In Salah and Snohvit. This paper share operational experience from three locations: Sleipner (14 years of injection), In Salah (6 years) and Snøhvit (2 years). These three locations have disposed 16 Mt of CO_2 by 2010. Three locations are contrasting in many respects. The surface conditions of Sleipner field be locate the Barents Sea in subsea development at ~330m water depth and storage depths ~700 m. below seafloor, In Salah field be locate the Sahara desert at ~470m water depth and storage depths ~1700 m. below surface and Snøhvit field be locate North Sea at ~80m water depth and storage depths ~2400 m. below seafloor. All these reservoirs are sandstones and used repeat 3D/4D seismic surveys to collect data to see the moving of

CO_2. Reservoir has development of CO_2 storage that occurs is controlled by geophysical monitoring, which some geological invisible. Snøhvit and Sleipner used 4D seismic monitoring is of sufficient quality to confirm the leakage into the overburden.

Goerke et al., (2011) studied "Numerical Simulation of Multiphase Hydromechanical Processes Induced by CO_2 Injection into Deep Saline Aquifers". They explain the concept modeling and numerical simulation of two-phase flow during CO_2 injection into deep saline aquifers. In 2005, the IPCC has published special report of the long term storage CO_2 in the underground. Three type of geological formation are important for storage of CO_2 such as depleted hydrocarbon reservoirs, deep saline aquifers and unminable coal seams. The depleted hydrocarbon reservoirs and deep saline aquifers are injected CO_2 in a denes form into porous rock formation. The deep saline aquifers have the largest storage capacity and are located near the power plant. The current, most CO_2 storage as a basis for simulation developed into oil, gas and geothermal energy produced by software. The case study utilizes the numerical methods to analyze the stress deformity. To this purpose, that set concept injection model. The two-phase flow process of CO_2 and brine, and deformity process near deep saline aquifer. Nowadays, deformity the flow and deformation of a simulation of the function of the base on the standard Galerkin finite element method. In this paper, it can be summarized as follows: The conceptual model and the numerical algorithm for the simulation of isothermal two phase flow in deformable porous media. The study is development of the theoretical and numerical framework for the solution of Thermo-Hydro-Mechanical-Chemical (THMC) coupled problems related to CO_2 storage in geological formations.

ADB (2013) has discussed CCS is a technology that reduces CO_2 emissions from fossil fuel in power plants and industrial. The energy consumption in Thailand has increased during 2000-2010. That has offered a road map for development of CCS in Thailand, which stage as follows: creation of CO_2 emission sources, study of possible storage sites and criteria for geological storage of capture CO_2. In Thailand source of CO_2 emissions in Thailand has four sectors as power, cement, natural gas processing and oil and gas production. The largest emission source from lignite power plant produces 18 Mt CO_2 per year. The study identified theoretical CO_2 storage capacity in

saline aquifer and rest in oil and gas fields. That study development of CO_2 storage is below 1,000 m. of saline aquifer and oil and gas field.

CHAPTER 3

SIMULATION

The area of this study is Fang district, Chiang Mai, Thailand. The data derived from Northern Petroleum Development Center, Energy Defense will study the Huai Ngu sub-basin, San Sai structure, Fang basin. The drill hole data from FA-SS-35-04 (DED, 1992) as used to create simulation by CMG-GEM to study CO_2 storage in depleted oilfield.

3.1 General Geology

Tertiary basin in Thailand

In Thailand, the age sedimentary basins in the Tertiary about 70 basins. That is diffusion in the northern, central and southern regions of Thailand as shown in Figure 3.1. Most of the positions of basins are N-S trending axes and independent basins. The structure of basins developed with EW direction has extensional stress in relation with NW-SE and NE-SW strike-slip faults. Two tectonic plates are moving and make developed of structure basins very complex. In the southern regions, offshore basins formed during the Middle Oligocene and onshore in the northern and central regions formed later in the Miocene. Normally, the Tertiary basins include alluvial fan deposit in the lower and upper parts, whereas the middle part is of lacustrine environment (Nuntajun, 2009).

3.2 General of Fang

The Fang basin is located in Fang intermountain basin northern Thailand, latitude 19° 43′ 00″ N to 20° 04′ 41″ N and longitude 89° 05′ 04″ E to 99° 43′ 00″ E as show in Figure 3.1. It is about 150 kilometer of Chiang Mai or about 850 kilometer

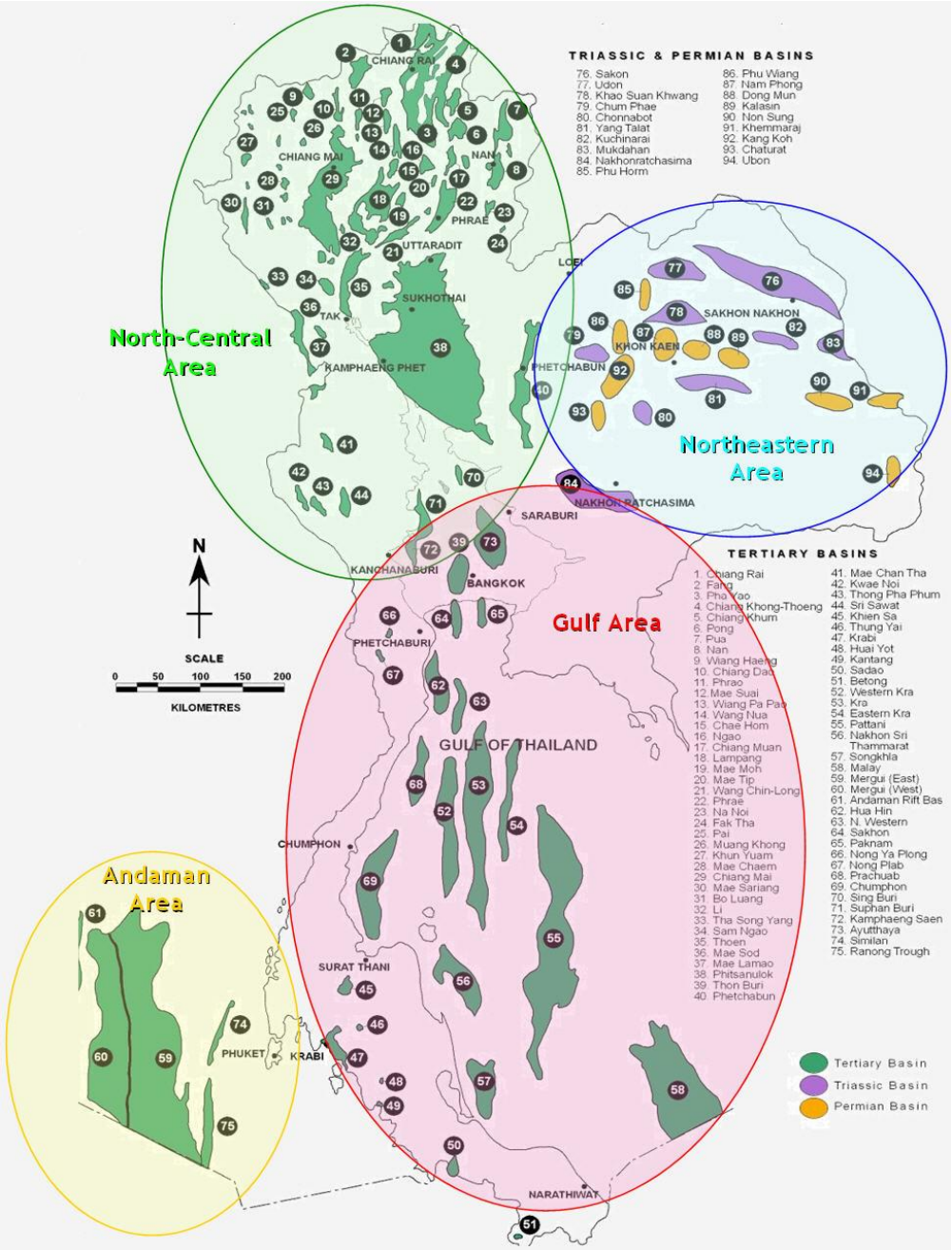

Figure 3.1Tertiary and Pre-Tertiary basins in Thailand (DMF, 2015).

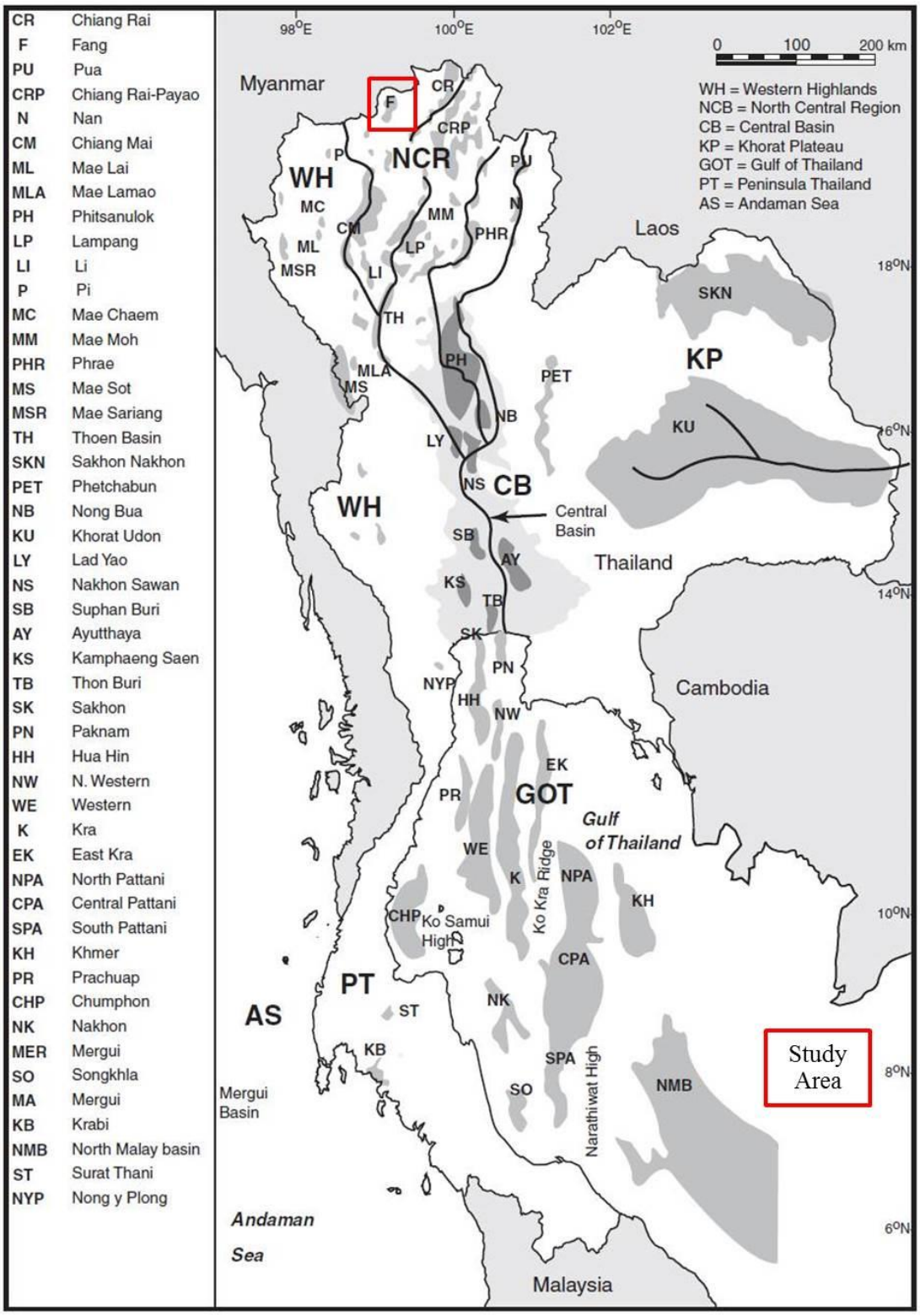

Figure 3.2 Tertiary basins in Thailand (Morley and Racey, 2011)

from Bangkok capital of Thailand. The surface area is around 670 km^2. The basin lies NE-SW with an elongated shape. The basin is about 500 m above mean sea level (Morley and Racey, 2011) .

Geology and Structure of Fang basin

The basin is a Tertiary basin in the northern onshore part of Thailand. The rock types include mudstone, sandstone, coal, oil shale and limestone depending on the location of the deposition in the basin as presented in Figure 3.2. From Khanthaprab and Kaewsaeng (1989) Fang basin is NNE-SSW trending and intracratonic basin. It is formed in early Tertiary and compression in middle Tertiary (Zollner and Moller, 1996). Braun and Hahn (1976) survey found that the stone in the Fang basin between Tertiary and Quaternary consist of silt, shale, sandstone, conglomerate, sedimentary rock and gravel. The basin is half graben structure and there will be increased depth to the SN of the basin will found major boundary fault cause deposit sediment basin in the Fang basin at the age of Oligocene to Resent composed of sedimentary type (Rodjanapo, 1998b). The Fang basin began to form deposition of coarse clastic sediments which later was followed by the deposition of fluvial and lacustrine sediments and changed to fluvial and alluvial in the Quaternary (Settakul, 1985).

Settakul (1984, 1985) and Belay (1992) explain around the Fang basin about most mountain range from 250 m up and the rock spread Precambrian Era to Quaternary Period.

From Water Resource Engineering CO. (1997) the survey, geological mapping in the northern side of the basin has found that the rocks are Ordovician to Triassic age. In the eastern side of the basin, it has found the rocks are Triassic to Jurassic age. In the western side of the basin it has found the rocks are Cambrian to Permian age and in the southern side of basin it has found the rocks are Carboniferous age.

The structure of the Fang basin has influenced the plate tectonic of the north for Triassic age. From Srihiran (1986), the Fang basin is an asymmetrical that has about 35^o and explained by drilling around Pong Nok oil field found basement inclined from east to west about 15^o and key bed almost parallel, dip about 15^o.

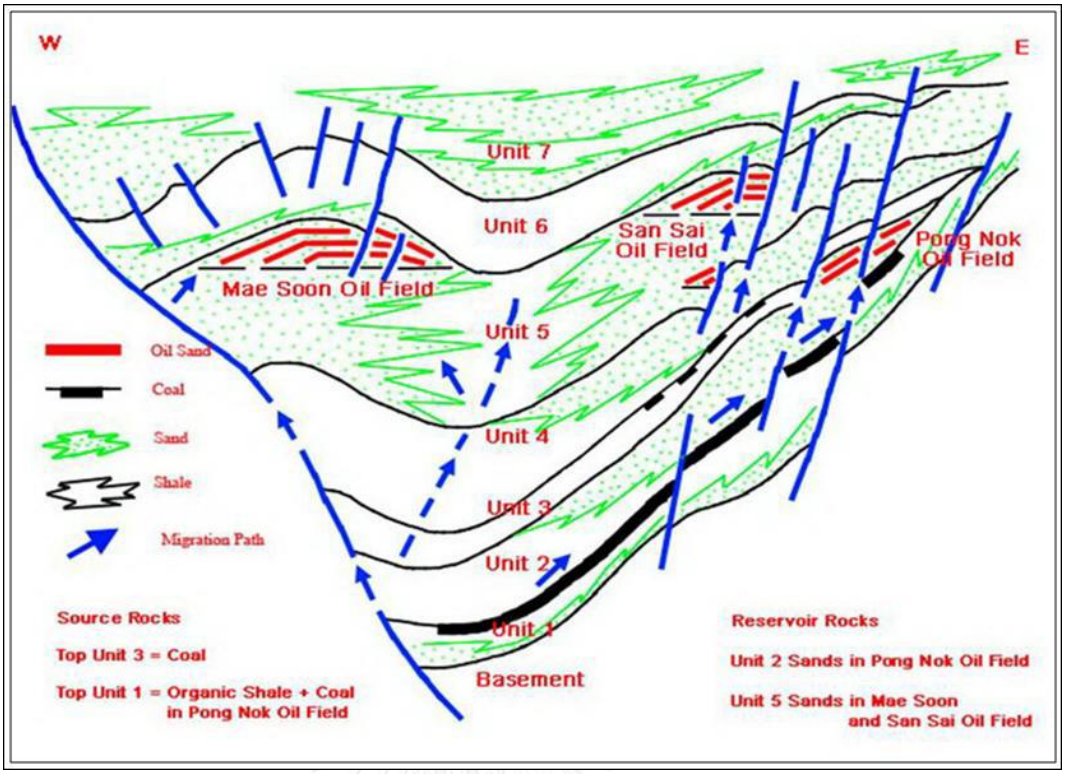

Figure 3.3 Cross section at Fang basin (ThaiDefenseEnergy & Schlumberger, 2013)

Seismic results of survey support depth of Fang basin have a depth to the west and the east shallow.

Settakul (1985) structure of Fang basin is a half-graben and dip to eastern. The basin can separate in three sub-basins such as Huai Pasang, Huai Ngu and Pa Ngew sub-basins. It separate by saddle formed by older rocks as shown in Figure 3.2. The deepest part of the Fang basin in the central Huai Ngu sub-basin is a sedimentary about 3000 meters.

PCR (1988) has studied geological area to find evidence in the petroleum and created a relationship between the sedimentary and the evolution of tectonics of the Fang basin. The Fang basin can be divided into 3 extensional sub-basins which are as follows Huai Pa Sang sub-basin, Huai Ngu sub-basin and Pa Ngew sab-basin from north to south, respectively.

Rodjanapo (1998a) studied and found the Fang basin caused by subsidence of the crust. Chiang Saen fault cuts through the basin margin in the western side. It was making the western has collapsed over the eastern. The area of interest is in parts of

Huai Ngu sub-basin. The Huai Ngu sub-basin have 6 structure as Ban Thi, Mae Soon, Nong Yao, Pong Nok, Sam Jang and San Sai structure.

Lithostratigraphy

Settakul (1984),(1985) has classified the sedimentary in Fang basin into 2 formations from top to bottom such as Mae Fang formation and Mae Sod formation. In 1984, the report can separate Mae Sot formation into 3 sub-formations such as Lower Mae Sot, Middle Mae Sot and Upper Mas Sot by electric log data.

Chumkratoke (2004) has classified sedimentary in Fang basin into 4 formations such as Lower syn-rift sequence (Lower Mae Sot), Middle syn-rift sequence (Upper Mae Sot), Upper syn-rift sequence (Lower Mae Fang) and Post-rift sequence (Upper Mae Fang) which consistent with the classified formation by Settakul (1984).

Geology and Structure of San Sai Oil field

The San Sai structure is located in the east of the Fang basin and half graben as shown in Figure 3.3. Nuntajun (2009) did geophysics survey began in 1961 by gravity and magnetic survey, 1985 and 1992 2D seismic survey. The environment of sedimentation occurs in the Tertiary-Quaternary. The San Sai structure is a monocline and dips about 10^{o}-20^{o} in the central of Fang basin. It has two major faults in eastern of the structure that trap oil (Settakul, 1985).

Lithostratigraphy

Stratigraphy of San Sai structure is based on seismic data, well logs and drill cutting. CORELABORATORIES (1992) does survey and analysis of the data by wireline log and seismic section of FA-SS-35-04 well and it can be divided into 2 formations follows;

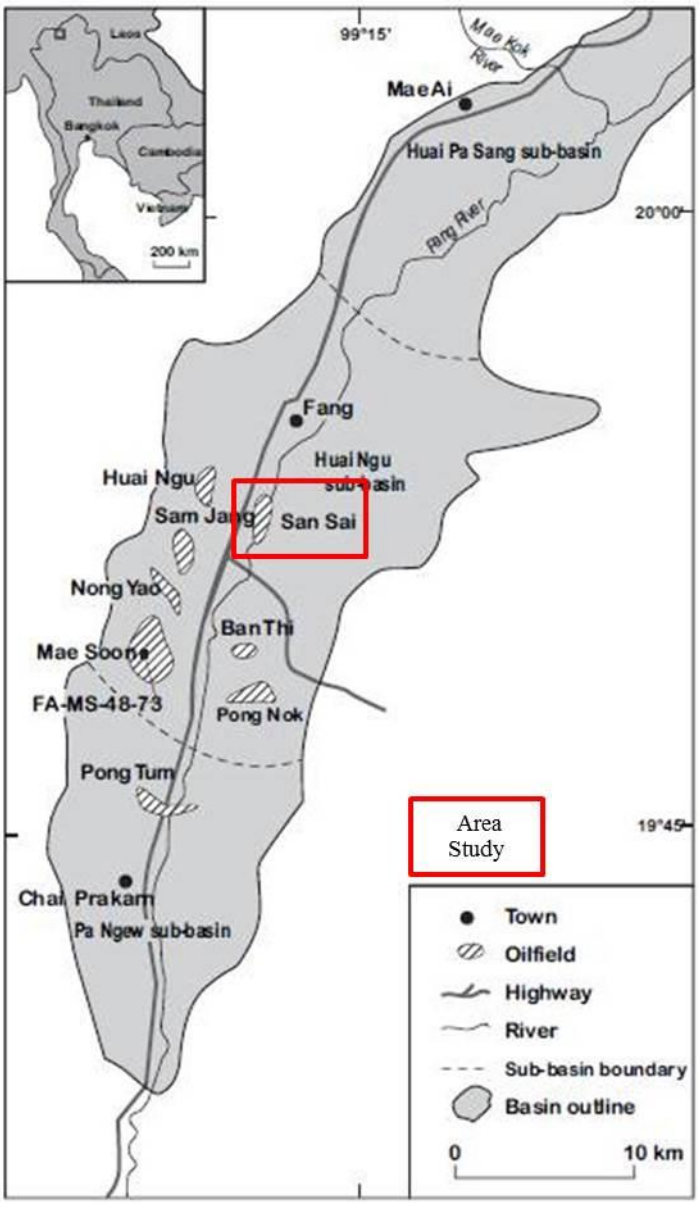

Figure 3.4 Three sub-basins in Fang basin (Nuntajun, 2009)

Mae Fang formation occurs in the Pleistocene-Resent. This formation depth to 4500 ft. (approximate 1370 m.) comes from seismic data and finds a lot of coarse sand-very coarse sand, clay and sedimentary coming from fluvial deposition environment.

Mae Sod formation occurs in the late Eocene-Pliocene. This formation separates into 3 ranges. First, upper Mae Sod formation occurring in the late Miocene-Pliocene depth to 2500-4500 ft. (approximate 762-1370 m.) to include sandstone

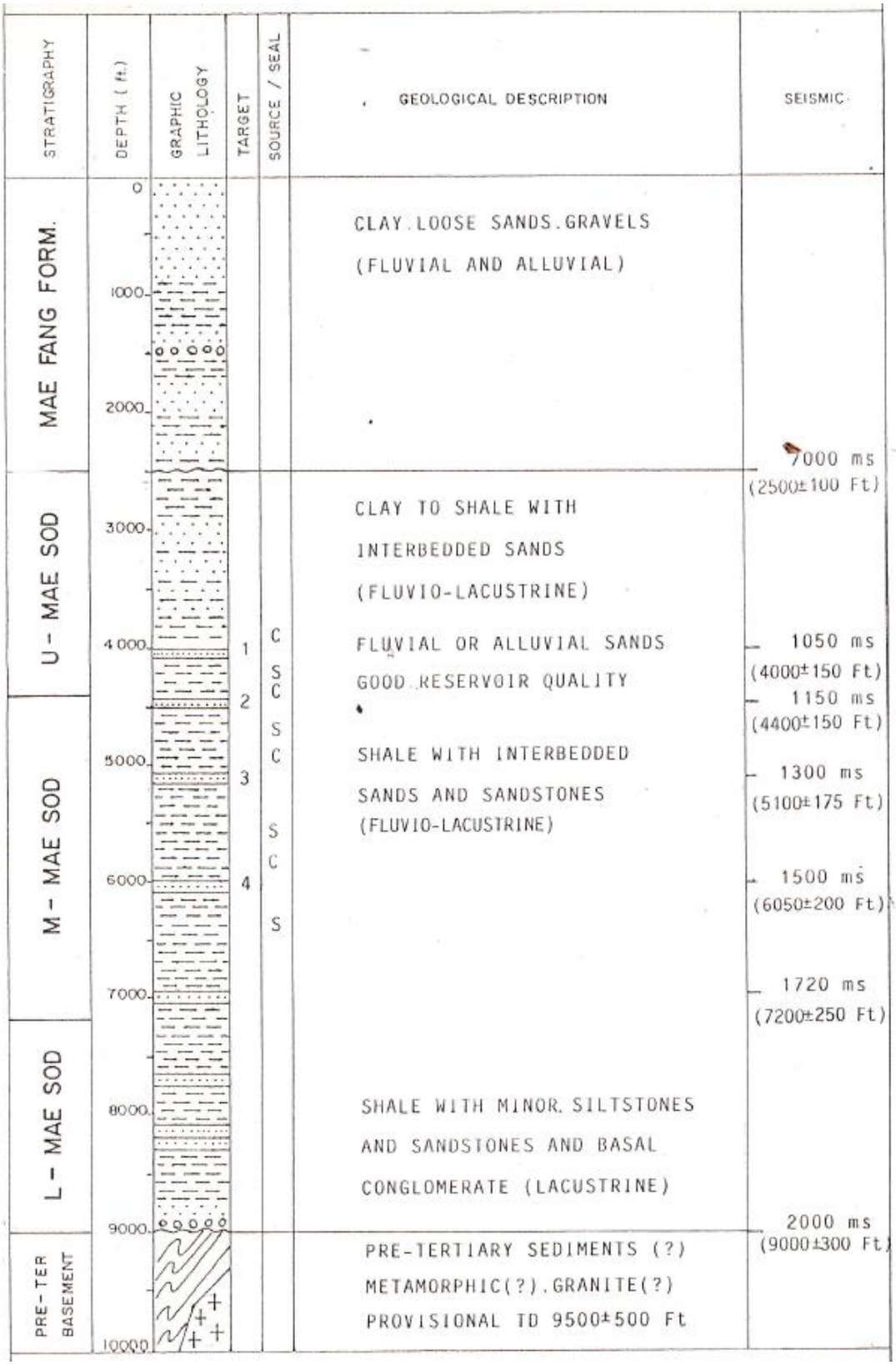

Figure 3.5 Geological prognosis at FA-SS-35-04 in San Sai area (DED, 1992)

thickness 5-30 ft. (estimate 1.5-9 m.) insert shale and lacustrine depositional environment. Second, middle Mae Sod formation occurs in the Oligocene-Miocene depth to 4500-6700 ft. (approximate 1370-2040 m.) This layer has lot of shale and inserts sandstone, silt, part of thin coal, fluvial and continental deposition environment and some part lacustrine depositional environment. This layer is harder than upper Mae Sod formation. Third, lower Mae Sod formation occurs in the late Eocene depth ranging from 6700 ft. (approximate 2040m.) until basement. The upper of this layer is coal bed thickness approximate 100 ft. (about 30 m.) rang 6800-6900 ft. (about 2070-2100 m.)

3.3 Reservoir simulation

The CMG software from Computer Modeling Group Ltd. is used to create the reservoir simulation. The software simulates hydrocarbon reservoir by inserting the reservoir data. CMG includes 3 reservoir simulation applications. IMEX is a three-phase black oil reservoir simulator forecasts the primary, secondary, enhanced oil recovery and models production from conventional sandstone and carbonate reservoirs. GEM is the reservoir simulation software for compositional and unconventional model that simulates the flow of three-phase and multi-component fluids. STAR is a thermal, k-value compositional, chemical reaction, and geomechanism reservoir simulator used for model recovery processes (CMG, 2011). In this thesis, CMG (2011) is selected for creating reservoir simulation model for CO_2 injection into geological formation and monitor CO_2 movement over the long period of time because the GEM model is specifically for storage of CO_2. A 3D model is set up using the formation characteristics as shown in Table 3.1 creating of reservoir simulation. Cartesian grid reservoir simulation is constructed by using GEM. The components of GEM simulation consist of reservoir, components, rock property, initial conditions and well. The methodology on produce of this study is presented in Figure 3.4. The detail of reservoir simulation is shown in Appendix A. Furthermore, the local grid refinement is applied to obtain the results with more accuracy. Also, many assumptions have been made to simplify and modify to calculate the unavailable research data such as storage capacity (Gorecki et al., 2009).

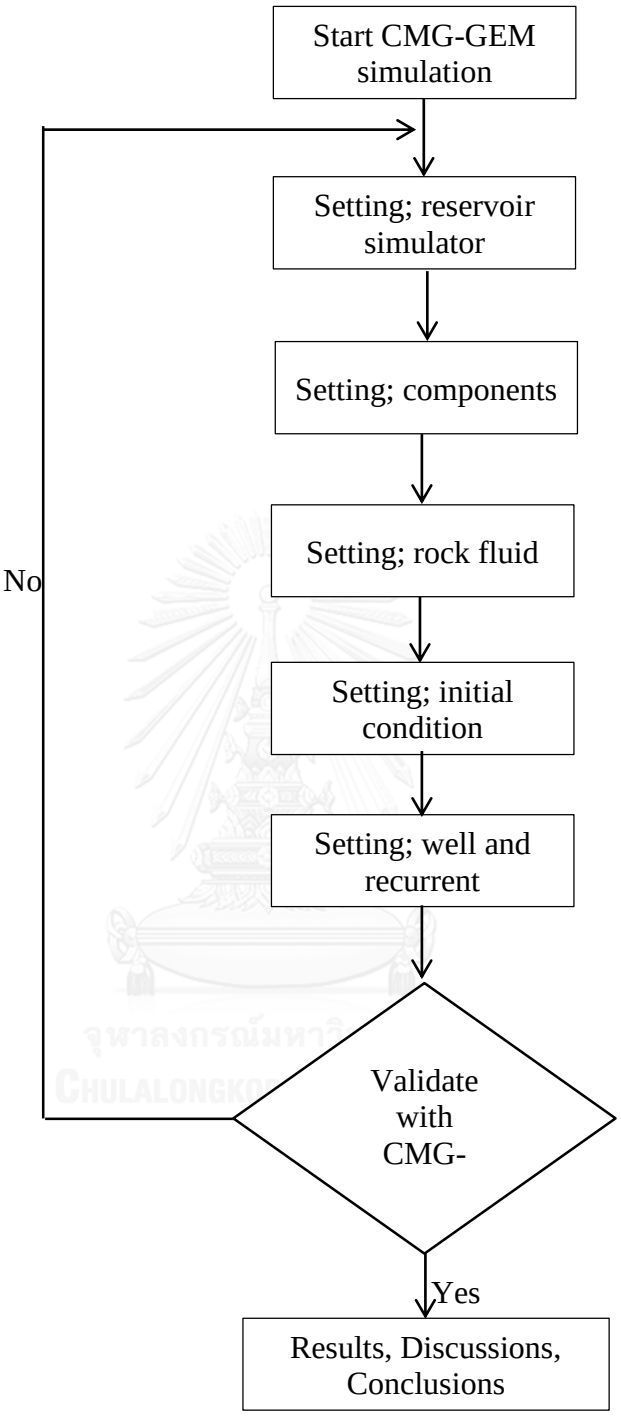

Figure 3.6 Diagram of methodology of this study

Initially, the information in the model must be set in the order to calculate grid block. It will still be under the limitations of the academic license which has less than 10000 grids. The model requires parameters such as; cartesian grid, reservoir properties, component, rock fluid, initial conditions and well and recurrent. In this study, the model will be divided into 3 cases to determine the behavior for different formations as shown in Table 3.1 and Figure 3.5-3.6. Also rich property such as relation permeability in presented in Table 3.2 and Figure 3.7-3.8. The data of San Sai structure comes from the Northern Petroleum Development Center. The simulation is homogeneous model. The fracture pressure is important to run simulation in CO_2 storage. If the pressure is over fracture, pressure will break the caprock and let CO_2 leak into the surface. The fracture pressure is calculated base on equation (2.4) for Hubbert and Willis equation. The maximum values will be shown in each case study.

Rock properties are set depending on the different types of rocks and related information. In this case it will be set to rock fluid type is show in Table 3.2 and Figure 3.7-3.8. The keyword include; *ROCKFLUID, *SWT, and *SGT.

Table 3.1 Case study detail to set up in GEM

Parameters		Value	Unit
Grid block		35x35x8	grid (m)
Depth;	2rd layer	2119.88-2161.03	m
	4th layer	2340.86-2369.82	
	6th layer	2465.83-2535.94	
Thickness;	2rd layer	41.15	m
	4th layer	28.96	
	6th layer	70.10	
Density of CO_2;	2rd layer	434	kg/m^3
	4th layer	444	
	6th layer	450	
Formation		Sand	-
Porosity		23.6	%
Permeability		110-190	mD
Temperature;	2rd layer	119.53	^oC
	4th layer	128.67	
	6th layer	135.93	
Bottom Hold Pressure;			kPa
	2rd layer	20681.45	
	4th layer	22669.79	
	6th layer	24251.76	
Maximum pressure;	2rd layer	27763.38	kPa
	4th layer	30657.47	
	6th layer	32294.14	
Flow rate		1,000, 2,000, 4,000	tons/day
Gas injection		99.99% CO_2, 0.01% CH_4	-

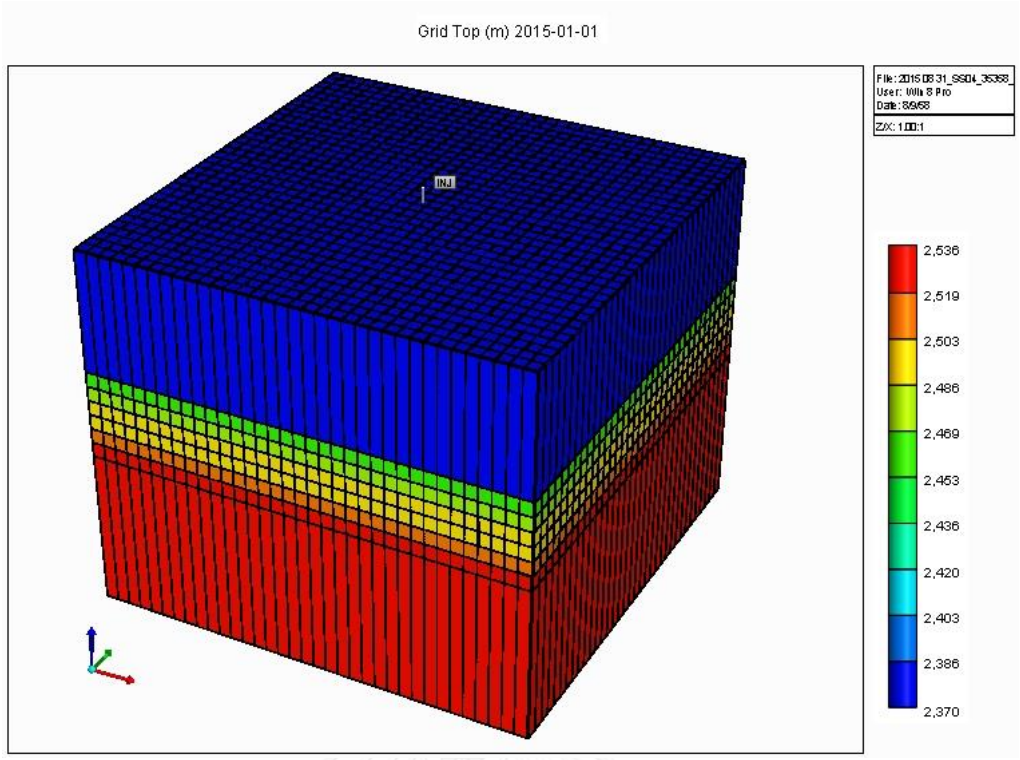

Figure 3.7 Three dimension view of reservoir simulation show formation depth

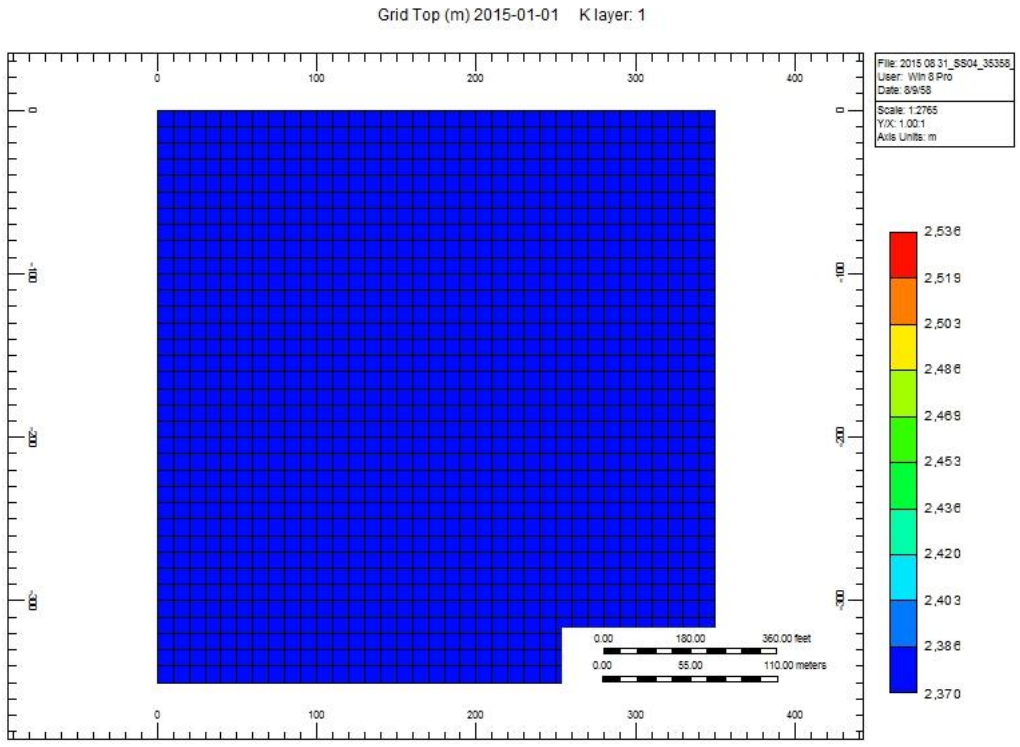

Figure 3.8 Top view of reservoir simulation

Table 3.2 Relative permeability of Gas-Liquid (Gas saturation)

S_g	k_{rg}	k_{rog}	S_w	k_{rw}	k_{row}
0.005	0	0	0.16	0	0
0.04	0.005	0	0.2	0.002	0
0.08	0.013	0	0.24	0.01	0
0.12	0.026	0	0.28	0.02	0
0.16	0.04	0	0.32	0.033	0
0.2	0.058	0	0.36	0.049	0
0.24	0.078	0	0.4	0.066	0
0.28	0.1	0	0.44	0.09	0
0.32	0.126	0	0.48	0.119	0
0.36	0.156	0	0.52	0.15	0
0.4	0.187	0	0.56	0.186	0
0.44	0.222	0	0.6	0.227	0
0.48	0.26	0	0.64	0.277	0
0.52	0.3	0	0.68	0.33	0
0.56	0.348	0	0.72	0.39	0
0.6	0.4	0	0.76	0.462	0
0.64	0.45	0	0.80	0.54	0
0.68	0.505	0	0.84	0.62	0
0.72	0.562	0	0.88	0.71	0
0.76	0.62	0	0.92	0.8	0
0.8	0.68	0	0.96	0.9	0
0.84	0.74	0	0.995	1	0

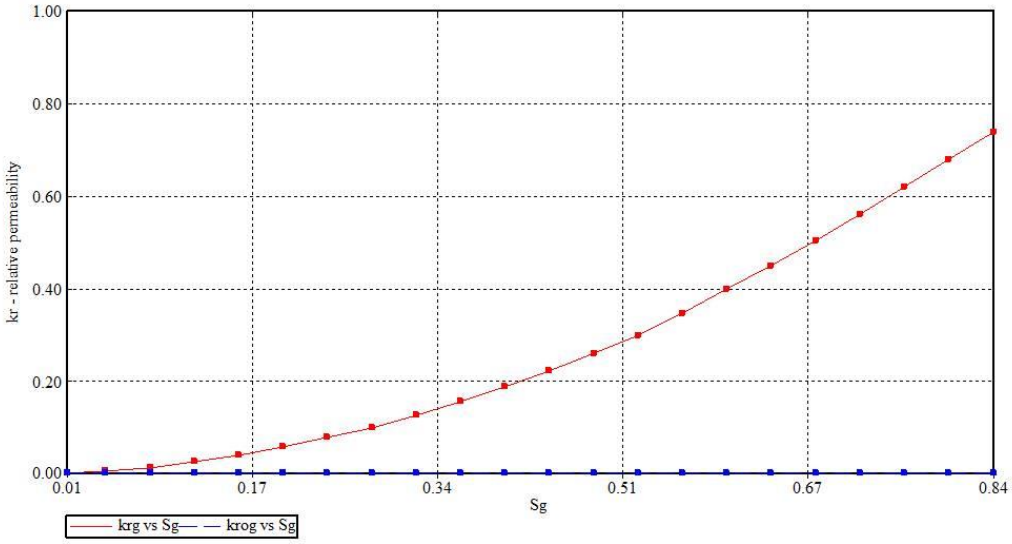

Figure 3.9 Relative permeability to liquid and gas as function of gas saturation

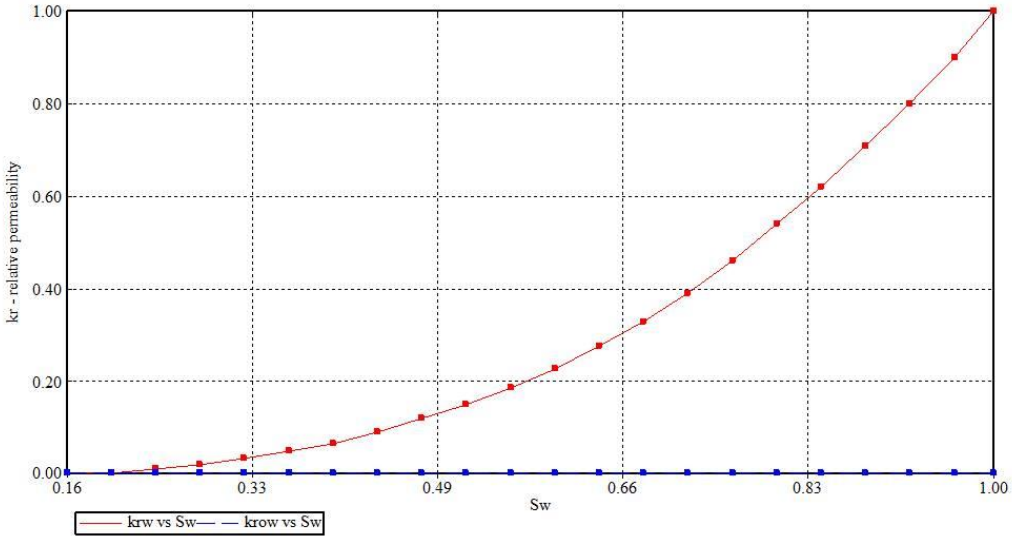

Figure 3.10 Relative permeability to water fraction at the given water saturation

The conditions and parameters that will be studied in the CMG-GEM simulation as presented in Table 3.3. This research will be studied in the depth at 1800 to 2700 m. in sand layer. By the rate of injection of 1000, 2000 and 4000 tons/day and set the maximum pressure on each layer from the calculated of the 90 percent of equation (2.4). When CO_2 injected into the each layer the pressure buildup will increase but less than

maximum pressure. The simulation program will be shutin well to avoid broken of caprock because of the pressure buildup over the maximum pressure.

Table 3.3 Detail condition and parameter to be study

Parameter	Unit
Depth	m
Flow rate	ton/day
Pressure buildup	kPa
Radius of migration	m

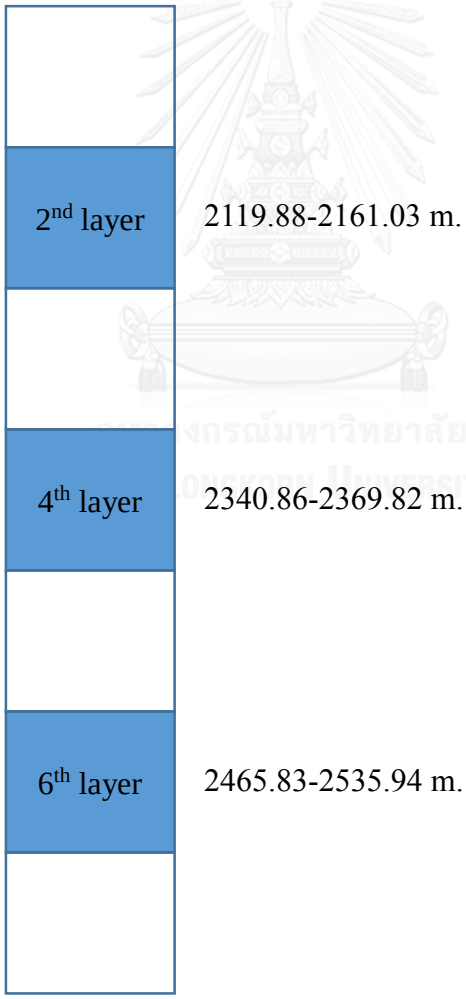

Figure 3.11 CO_2 injection into second, fourth and sixth layer from top to bottom

CHAPTER 4

RESULTS AND DISCUSSION

This chapter describes the effects of the parameters on CO_2 storage from simulation of the injection rate at 1000, 2000 and 4000 ton/day and time storaging from 1, 5 10, 20 to 50 years. The San Sai structure for this study is; FA-SS-35-04.

4.1 Maximum pressure

The data shown in Table 4.1 for information on each formation for the depth 800 to 3000 m., thickness from DED (1992), formation temperature is 77 ^{o}C (Chumkratoke, 2004),

The bottom hole pressure is calculated from equation (4.1). The pressure gradient is 9.5233 kPa/m (0.421 psi/ft) from DED (1992) and surface pressure is 101.3529 kPa (14.7 psi).

$$BHP = (pressure\ gradient\ x depth) + sueface\ pressure \qquad (4.1)$$

4.2 Storage capacity

The density is calculated from website (Peacesoftware, 2015). Storage capacity is calculated in depleted oil, from equation (2.6) used in the calculation based on porosity at 0.236 and 185000 m^2 for Fang area. Thickness is based on DED (1992) and efficiency is based on 2.51 percent (Gorecki et al., 2009).

The temperature is calculate from equation (2.4) include; geothermal gradient at FA-SS-35-04 is 0.024 ^{o}F/ft (DED, 1992) and surface temperature is 25 ^{o}C.

The facture pressure is calculated from equation (2.5). The facture pressure used 14.5518 kPa/m (0.6433 psi/ft). Fracture pressure and maximum pressure assume at 90 percent (Mathias and Roberts, 2013) to prevent the caprock cracking due to excessive fracture pressure.

4.3 Simulation result

4.3.1 Effect of injection rate and depth on pressure buildup

From Figure 4.1-4.4 the orange line represents the maximum pressure which is 90 percent of fracture pressure. When CO_2 injected underground, pressure in the formation is buildup

Figure 4.1 illustrates the change in pressure buildup when CO_2 injected into the depleted oilfield at the second layer with the injection rate from 1000-4000 tons/day. The maximum pressure of this layer is 27.76 MPa which is used as criteria to stop the injection. The initial pressure for this formation is 20.08 MPa. At 1000 tons/day injection rate, the injection period is 46 years and that formation will be shutin with shutin pressure of 26.69 MPa. Four more years will be observed for CO_2 monitoring as well as radius of migration until 50 years of this study. The final pressure at year 50^{th} is 26.76 MPa. For injection rate at 2000 tons/day, injection period is 20 years with 26.02 MPa shutin pressure and 30 more years for monitoring. The final pressure after 50 years is 26.12 MPa. For injection rate at 4000 tons/day, the injection period takes 8 years and 42 years for monitoring. The shutin pressure and final pressure are 24.42 and 24.68 MPa, respectively as shown in Table 4.2.

Table 4.1 Data to setting in model for FA-SS-35-04 area

Layer	Top	Bottom	Thickness	BHP	Temperature	Density	Flow rate (Q)			Frecture pressure	Max. pressure
	m	m	m	MPa	^{o}C	kg/m^3	ton/day			MPa	
1	1856.23	2119.88	263.65	20.2896	117.7333	432	1000	2000	4000	30.85	27.76
2	2119.88	2161.03	41.15	20.6814	119.5333	434					
3	2161.03	2340.86	179.83	22.3940	127.4000	443				34.06	30.66
4	2340.86	2369.82	28.96	22.6698	128.6667	444					
5	2369.82	2465.83	96.01	23.5841	132.8667	448				35.88	32.29
6	2465.83	2535.94	70.10	24.2518	135.9333	450					
7	2535.94	2659.99	124.05	25.4332	141.3600	452				38.71	34.84

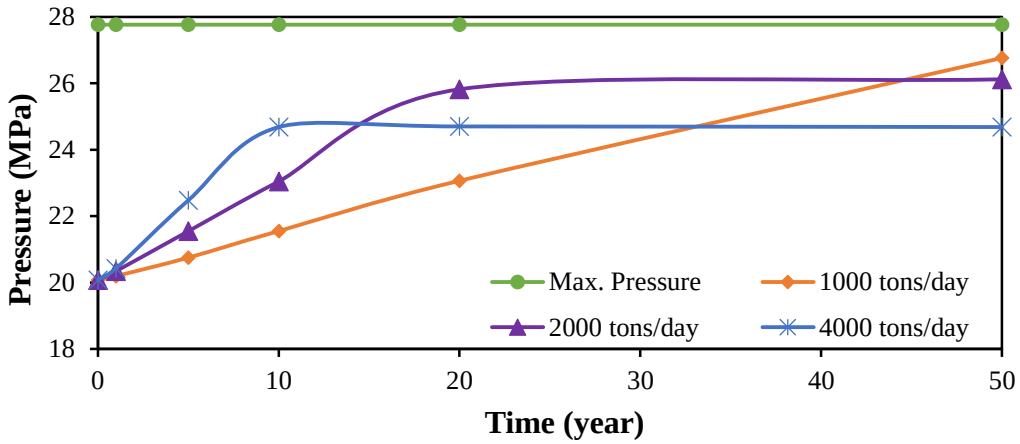

Figure 4.1 second layer of FA-SS-35-04

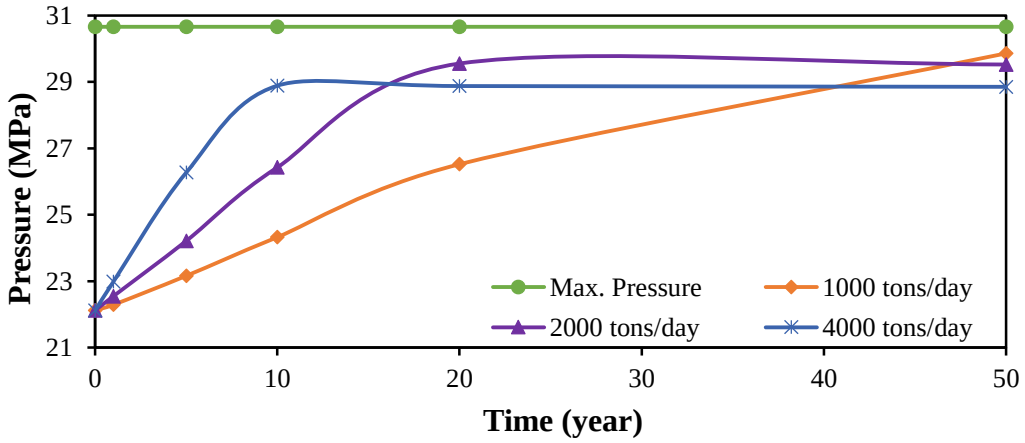

Figure 4.2 fourth layer of FA-SS-35-04

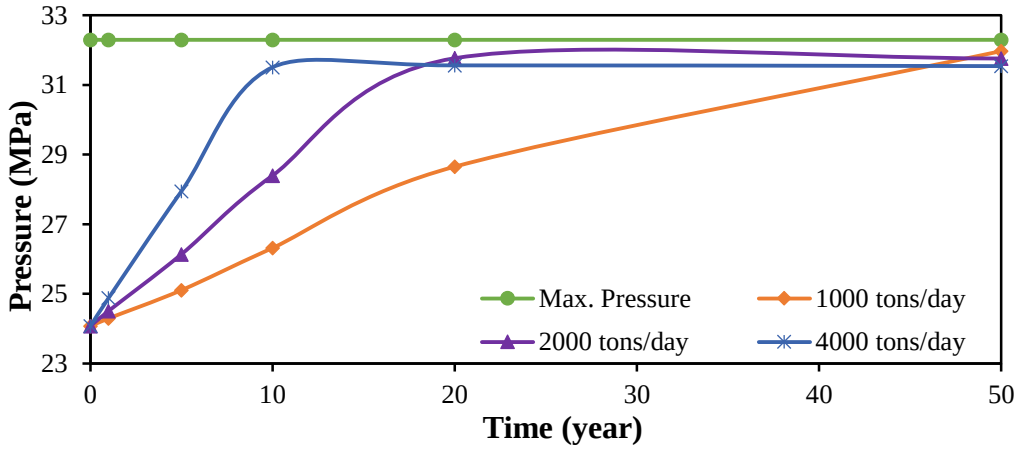

Figure 4.3 sixth layer of FA-SS-35-04

Table 4.2 The pressure buildup by period

Layer	Initial Pressure (MPa)	Maximum Pressure (MPa)	Injection Time/Pressure buildup		
			1000 tons/day	2000 tons/day	4000 tons/day
2	20.08	27.76	46 years 26.69 MPa	20 years 26.02 MPa	8 years 24.42 MPa
			50 years 26.76 MPa	50 years 26.12 MPa	50 years 24.68 MPa
4	22.13	30.66	36 years 29.84 MPa	17 years 29.46 MPa	8 years 28.62 MPa
			50 years 29.86 MPa	50 years 29.52 MPa	50 years 28.85 MPa
6	24.07	32.29	35 years 31.94 MPa	17 years 31.66 MPa	9 years 31.19 MPa
			50 years 31.97 MPa	50 years 31.76 MPa	50 years 31.54 MPa

Table 4.3 The storage capacity when shutin well

Layer	Storage Capacity (Million ton)		
	1000 tons/day	2000 tons/day	4000 tons/day
2	16.98	15.16	12.41
4	13.33	12.78	11.69
6	12.78	12.97	13.15

The pressure buildup change at overall layers. This case can divides 7 layers from top to bottom layer is shale switch sand respectively (Figure 3.9) and the maximum pressures are 27.76, 30.66 and 32.39 MPa, respectively. When CO_2 is injected into depleted oilfield will injection rate from 1000-4000 tons/day. The initial pressure is 20.08, 22.13 and 24.07 MPa, respectively. Injection rate at 1000 tons/day,

the injection pressure is 35 years and that formation will be shutin with shutin pressure of 24.31 MPa in sixth layer. And then open the fourth layer, the final pressure at 50 years is 25.14 MPa.

The pressure build up for injection rate at 2000 and 4000 tons/day are present in Table 4.4-4.5.

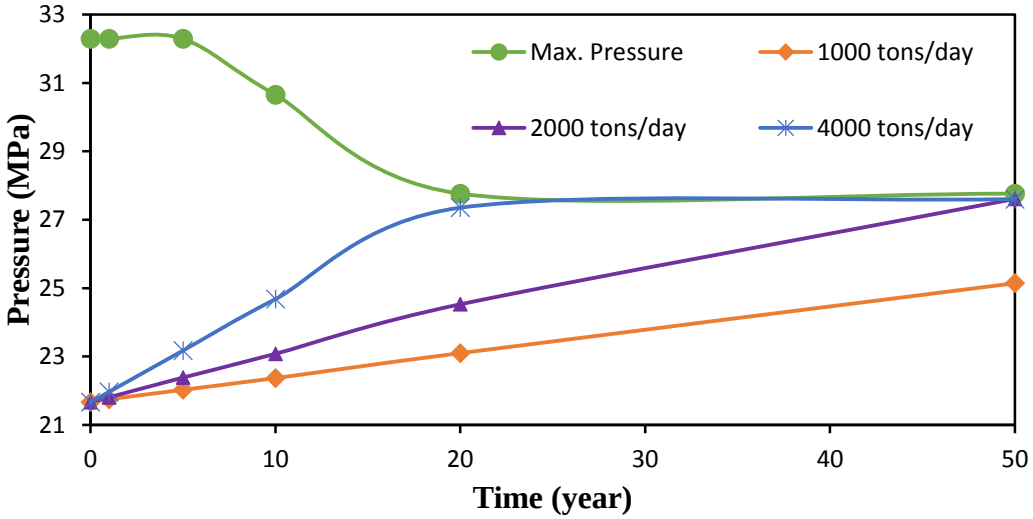

Figure 4.4 FA-SS-35-04 overall layers

Table 4.4 The pressure buildup by period at overall layers

Layer	Initial Pressure (MPa)	Maximum Pressure (MPa)	Injection Time/Pressure buildup		
			1000 tons/day	2000 tons/day	4000 tons/day
2	20.08	27.76	-	50 years 27.61 MPa	50 years 27.60
4	22.13	30.66	50 years 25.14 MPa	36 years 26.71 MPa	16 years 26.62
6	24.07	32.29	35 years 24.31 MPa	18 years 24.37 MPa	9 years 24.56 MPa

Table 4.5 The storage capacity when shutin well at overall layers

Layer	Storage Capacity (Million ton)		
	1000 tons/day	2000 tons/day	4000 tons/day
2	-	30.32	28.18
4	17.92	26.04	24.76
6	12.76	13.39	13.75

4.3.2 Radius of migration of CO_2 storage

The time period of CO_2 injection into 3 storage layers ranges from 1, 5, 10, 20 and 50 years at the injection rate from 1000 to 4000 tons/day. The results of radius of migration as presents in Table 4.2-4.3 and Figure 4.1-4.4 for 2nd layer, 4th layer and 6th layer and overall layers, respectively. At 4000 tons/day injection rate, the radius of migration of the well FA-SS-35-04 will increase as pressure from injection increases. Later, after shutting in well, it continues increasing until it reaches the maximum pressure depending on depth and injection rate. Then, after year 10th, the pressure becomes lower, thus making radius of migration relatively smaller as well. In contrast, at 1000 tons/day injection rate after shutting well, pressure keep increasing, as the radius of migration. Therefore, the radius of migration after 50 years becomes layers. The reason of the decrease of pressure and radius of migration is that the injection is high and the formation has less time to reach equilibrium. When maximum pressure has reached, the system adjusts itself to equilibrium for the whole formation. Therefore the pressure is lower and the radius of migration becomes smaller. But for the ease for lower injection rate, the system can adjust itself gradually. Consequently, the pressure and the radius of migration keep increasing.

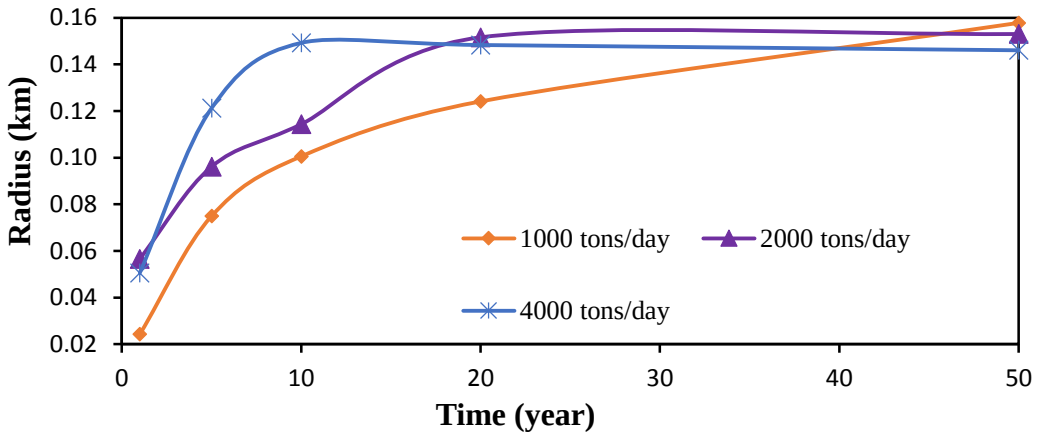

Figure 4.5 FA-SS-35-04 in the second layer

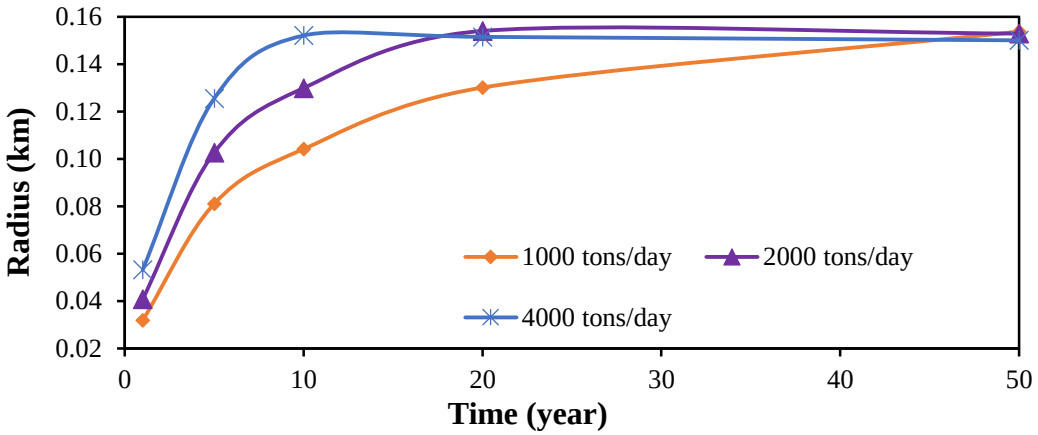

Figure 4.6 FA-SS-35-04 in the fourth layer

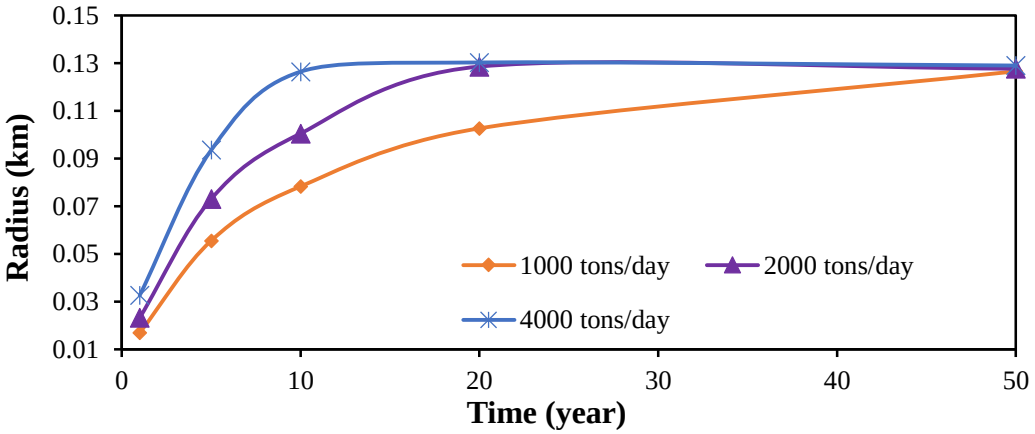

Figure 4.7 FA-SS-35-04 in the sixth layer

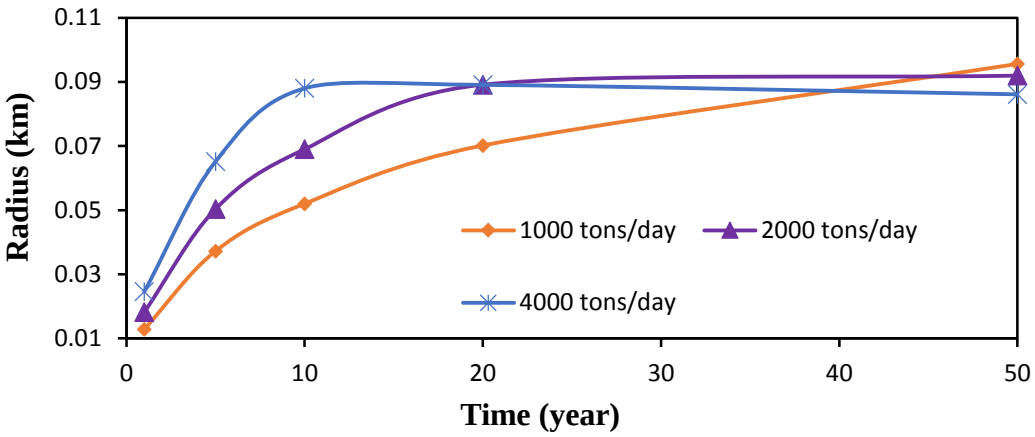

Figure 4.8 FA-SS-35-04 in the overall layers

Furthermore This section parameters the simulation results of the effects of parameters such as pressure buildup, injection rate, depth and radiuses of migration with time changing with time 1, 2, 3, 4, 5, 10, 20 and 50 years as shown in Figure 4.9-4.16 which are presented in 3D model and cross section view of FA-SS-35-04 area in sixth layer at the rate of injection at 4000 tons/day. This model applies local grid refinement (LGR) to shown more detail in layer of interest to the simulation model. Migration of CO_2 has changed clearly and in greater detail. Another results injection rate will be shown in Appendix B.

Table 4.6 presents the radius of migration, area at the top layer and storage capacity for each year for 2nd layer as shown in Figure 4.9-4.16 for 1, 2, 3, 4, 5, 10, 20 and 50 years, respectively. In second layer, the expansion of the CO_2 to the most increases in the 10 years and after that, the expansion will decrease until 50 years.

Table 4.6 The effects of parameters for second layer by period at injection rate 4000 tons/day

n^{th} Year	Radius (m)	Area (m^2)	Storage Capacity (Million ton)	CO_2 storage at layer
1	50.51	8034	1.46	Top sublayer
2	84.07	22204.04	2.92	
3	99	30790.75	4.38	
4	111.44	39015.75	5.84	
5	121.18	46133.01	7.30	
10	149.21	69943.24	12.41	
20	148.3	69092.70	12.41	
50	146.03	66993.71	12.41	

Table 4.7 presents the radius of migration, of area at top layer and storage capacity for each year. In fourth layer, when the CO_2 injection starts, the expansion of the CO_2 increases until year 10^{th} after that the expansion will decrease until the end of simulation at 50 years.

Table 4.7 The effects of parameters for fourth layer by period

n^{th} Year	Radius (m)	Area (m^2)	Storage Capacity (Million ton)	CO_2 storage at layer
1	53.3	8924.92	1.46	Top sublayer
2	84	22167.08	2.92	
3	103.47	33634.02	4.38	
4	115.4	41837.09	5.84	
5	125.55	49520.3	7.30	
10	152.09	79669.34	11.69	
20	151.51	72116.14	11.69	
50	150.05	70731.97	11.69	

Table 4.8 explains the radius of migration, of area at the 2nd layer in 1st year and at top layer in each year, storage capacity for sixth layer. Figure 4.25-4.32 as shown CO_2 migrations from injection for 1, 2, 3, 4, 5, 10, 20 and 50 years, respectively. The sixth layer, when the CO_2 injection starts, the expansion of the CO_2 increases until year 20th after that the expansion will decrease until the end of simulation at 50 years.

Table 4.8 The effects of parameters for sixth layer by period

n^{th} Year	Radius (m)	Area (m^2)	Storage Capacity (Million ton)	CO_2 storage at layer
1	32.60	3338.76	1.46	Top sublayer
2	43.84	6037.97	2.92	
3	68.80	14870.54	4.38	
4	83.00	21642.43	5.84	
5	93.55	27.493.97	7.30	
10	126.44	50.224.87	13.15	
20	130.29	53330.06	13.15	
50	129.01	52287.35	13.15	

Table 4.9 presents the radius of migration, storage capacity for each year for overall layer and of area at the top layer of 6th layer in 1, 2, 3, 4 and 5 years, at 4th layer in 10 years and in 20 and 50 years at 2nd layer. In overall layer, when the CO_2 injection starts, the expansion of the CO_2 increases until year 20th after that the expansion will decrease until the end of simulation at 50 years.

Table 4.9 The effects of parameters for overall layer by period

n^{th} Year	Radius (m)	Area (m^2)	Storage Capacity (Million ton)	CO_2 storage at layer
1	24.58	1898.09	1.45	Top of 6th layer
2	40.42	5132.66	2.90	Top of 6th layer
3	50.97	8161.67	4.35	Top of 6th layer
4	59.24	11025.03	5.79	Top of 6th layer
5	65.24	13371.43	7.24	Top of 6th layer
10	87.99	24322.96	14.29	Top of 4th layer
20	89.06	24918.12	28.18	Top of 2nd layer
50	86.11	23294.70	28.18	Top of 2nd layer

a.

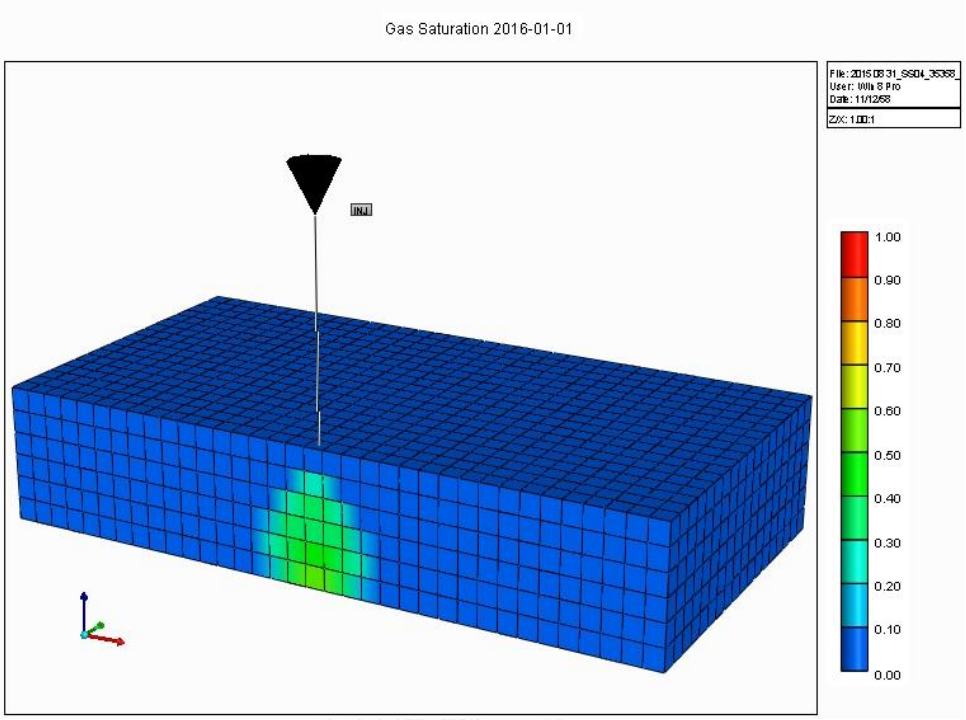

b.

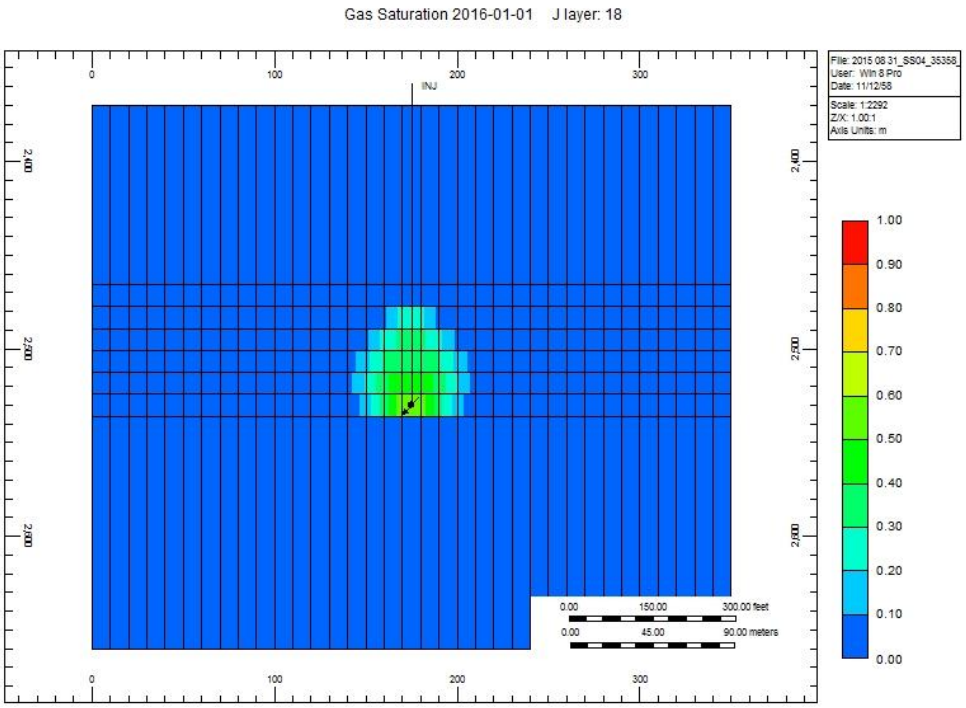

Figure 4.9 (a) 3D view, 1 year injection and (b) side view, 1 year injection at 2465.83-2535.94 m.

a.

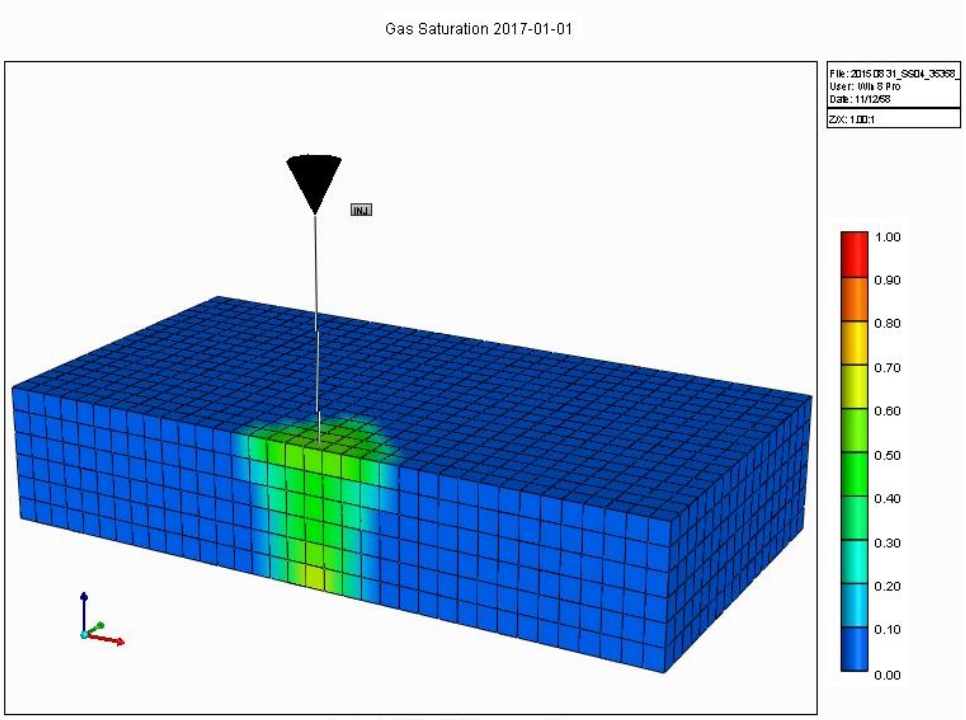

b.

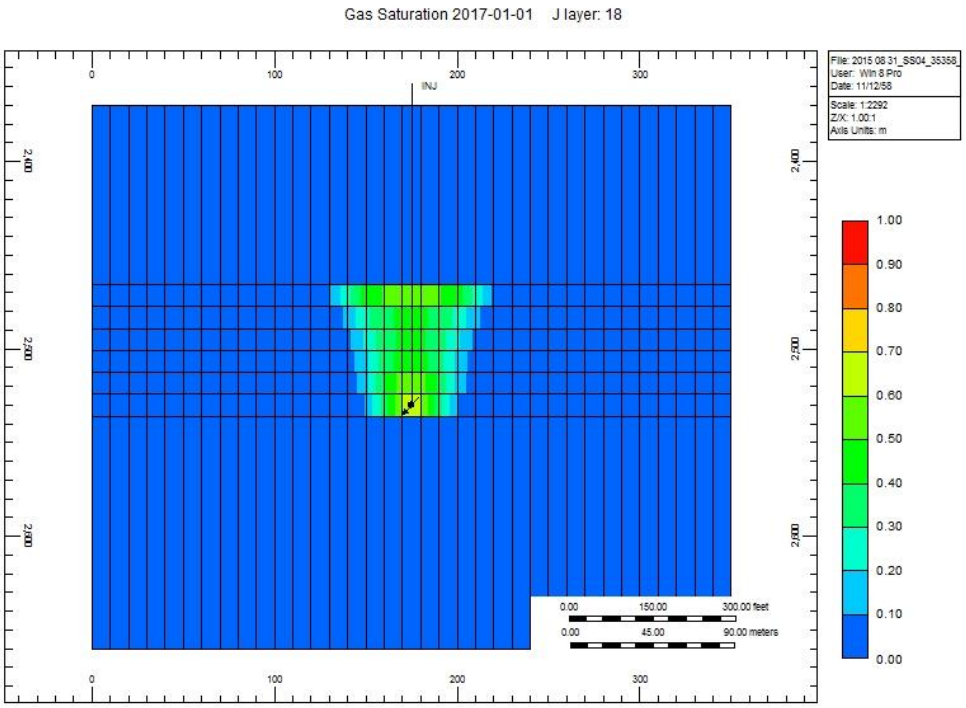

Figure 4.10(a) 3D view, 2 year injection and (b) side view, 2 year injection at 2465.83-2535.94 m.

a.

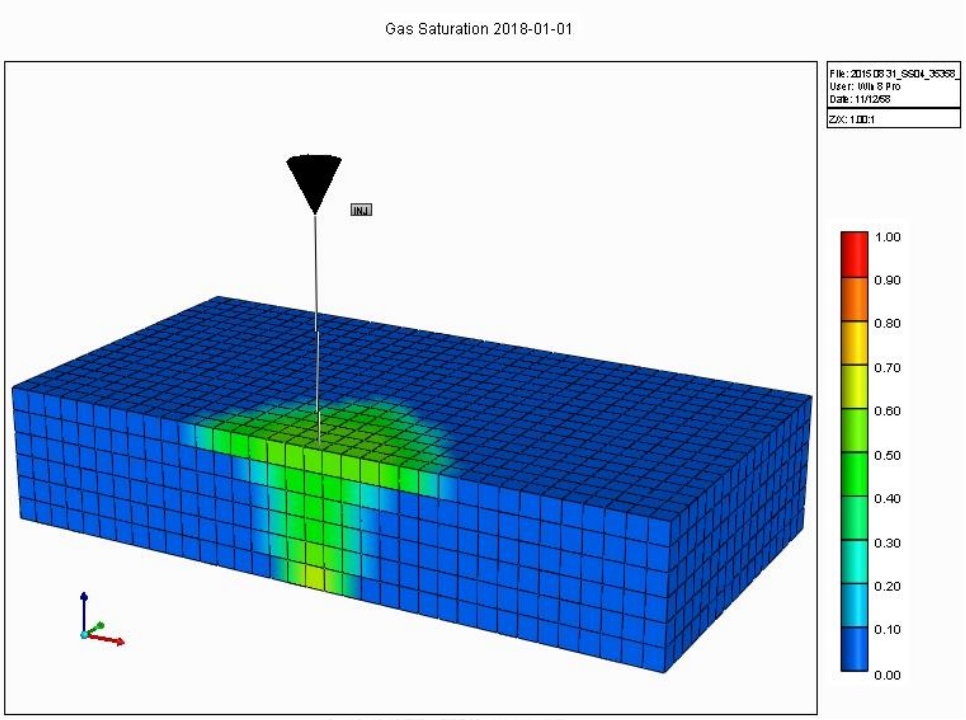

b.

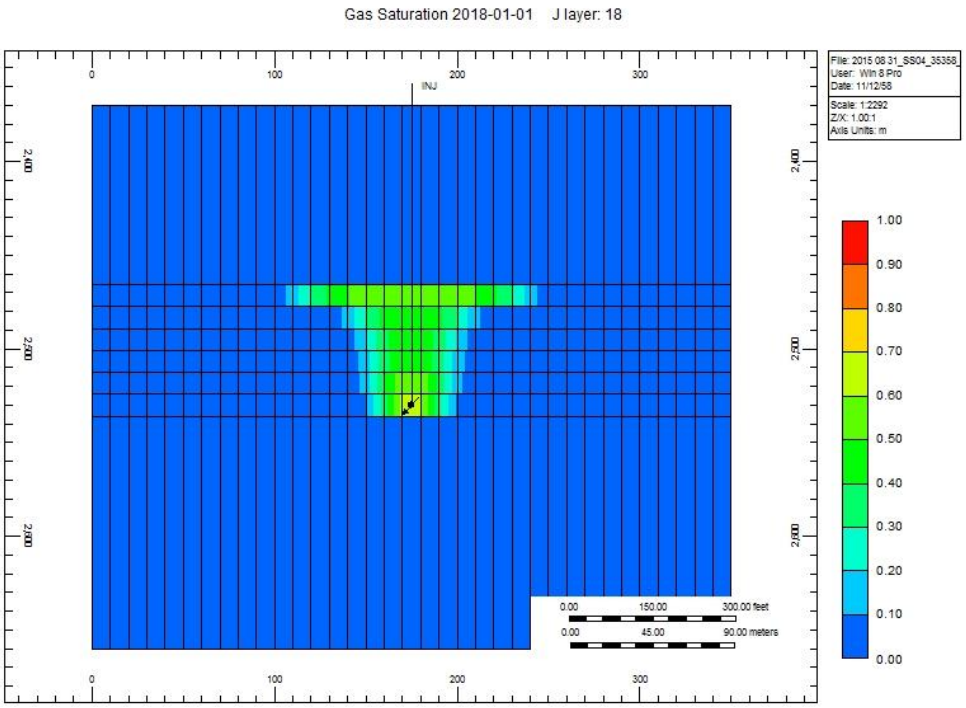

Figure 4.11 (a) 3D view, 3 year injection and (b) side view, 3 year injection at 2465.83-2535.94 m.

a.

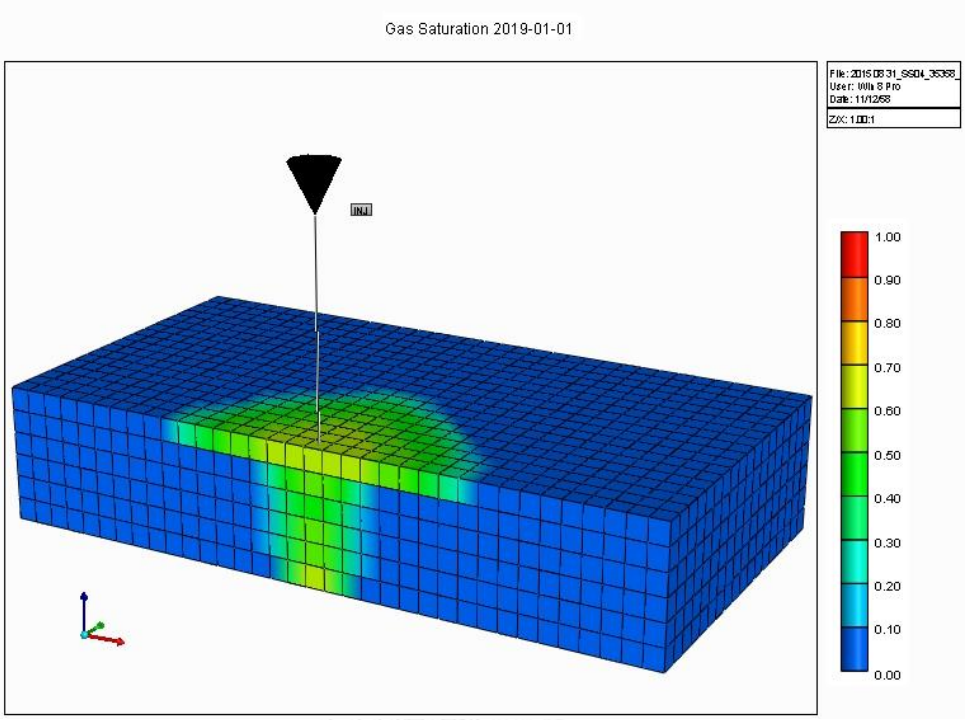

b.

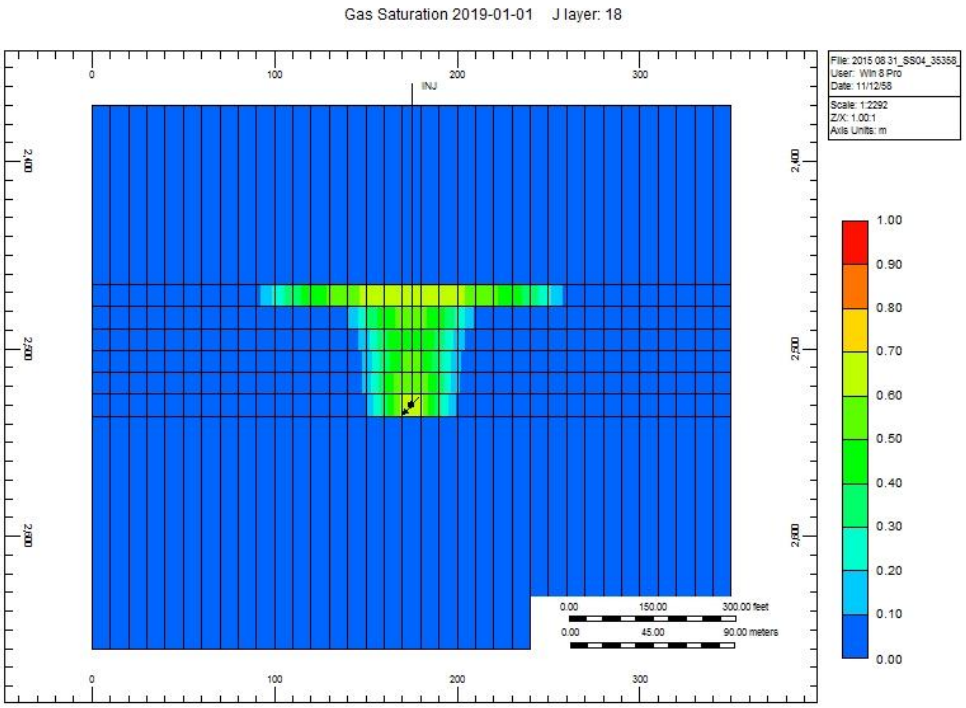

Figure 4.12 (a) 3D view, 4 year injection and (b) side view, 4 year injection at 2465.83-2535.94 m.

a.

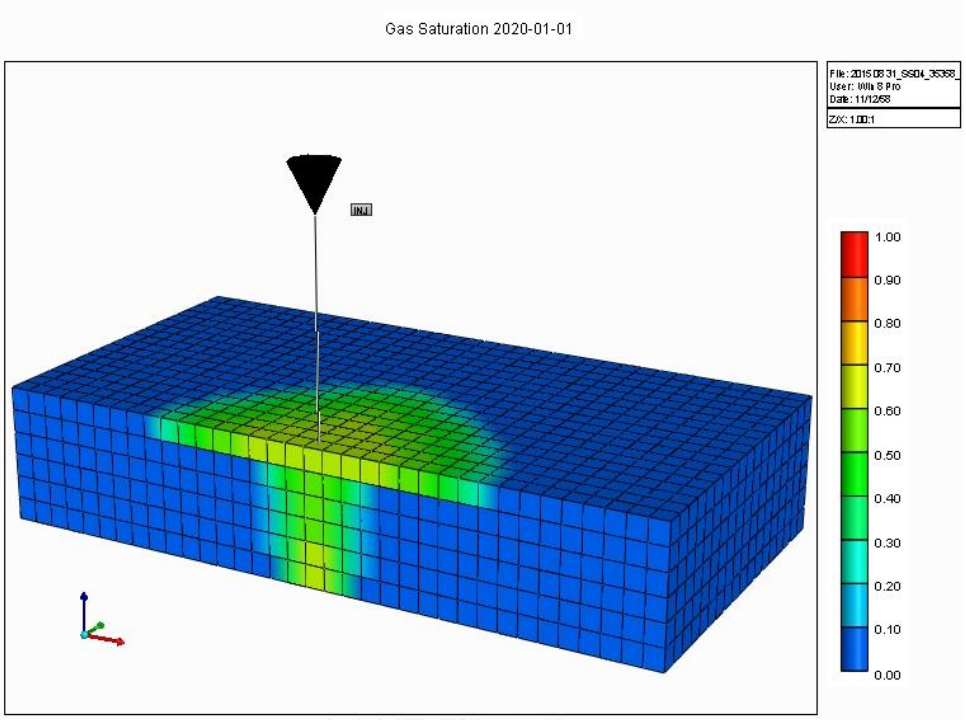

b.

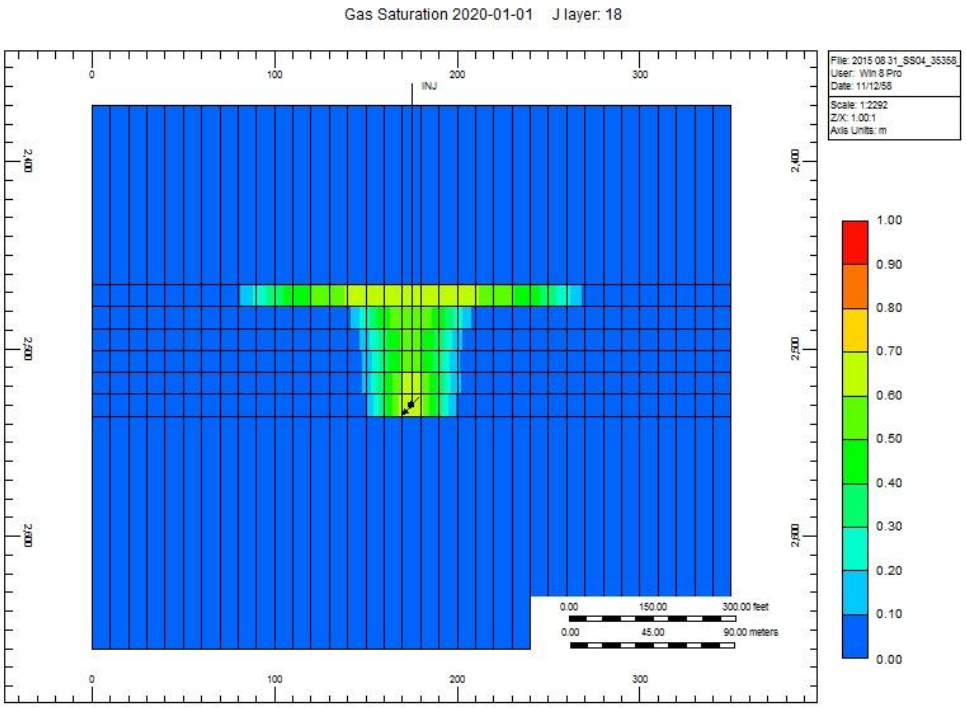

Figure 4.13 (a) 3D view, 5 year injection and (b) side view, 5 year injection at 2465.83-2535.94 m.

a.

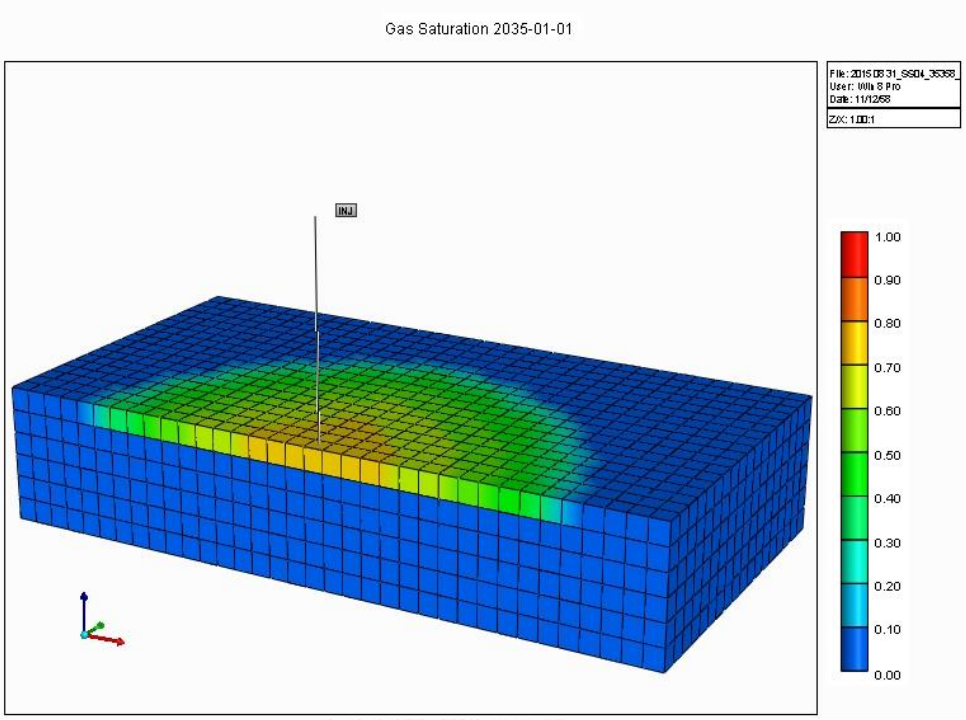

b.

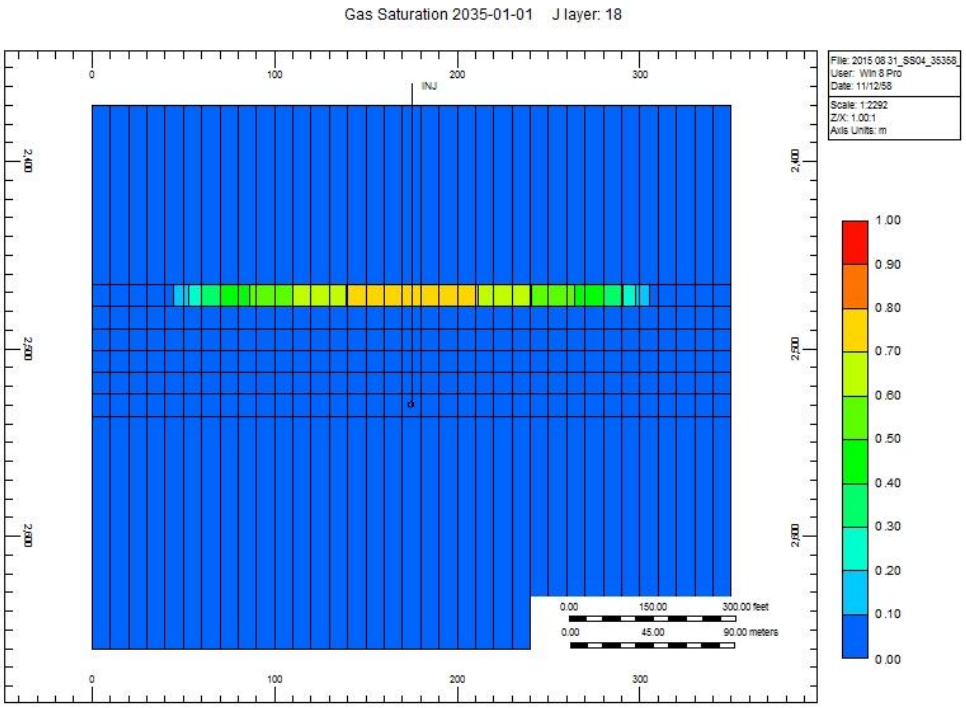

Figure 4.14 (a) 3D view, 10 year injection and (b) side view, 10 year injection at 2465.83-2535.94 m.

a.

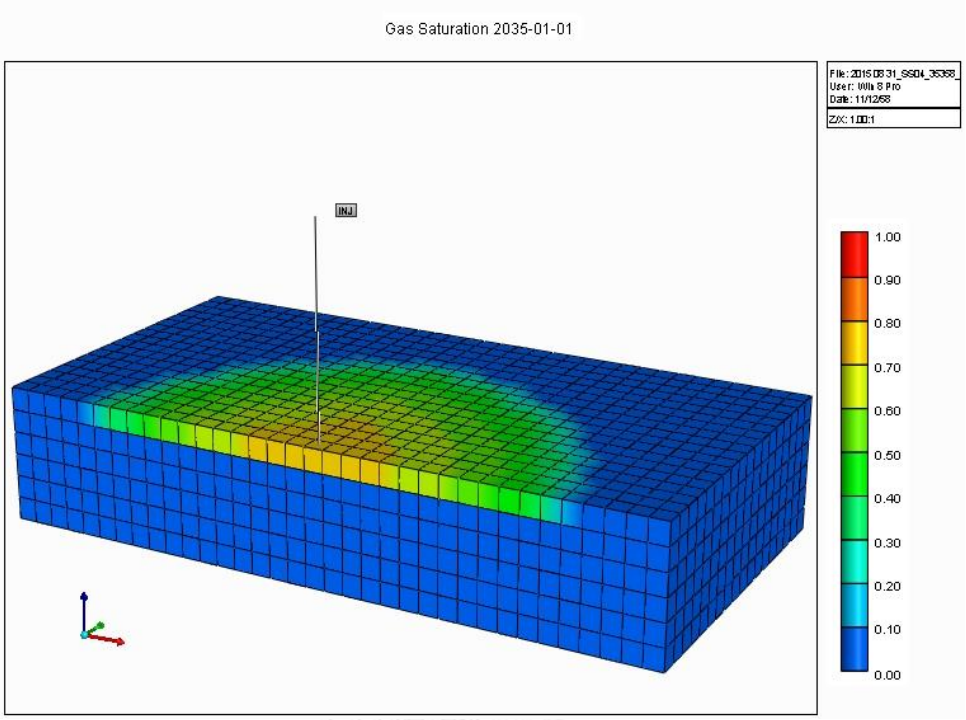

b.

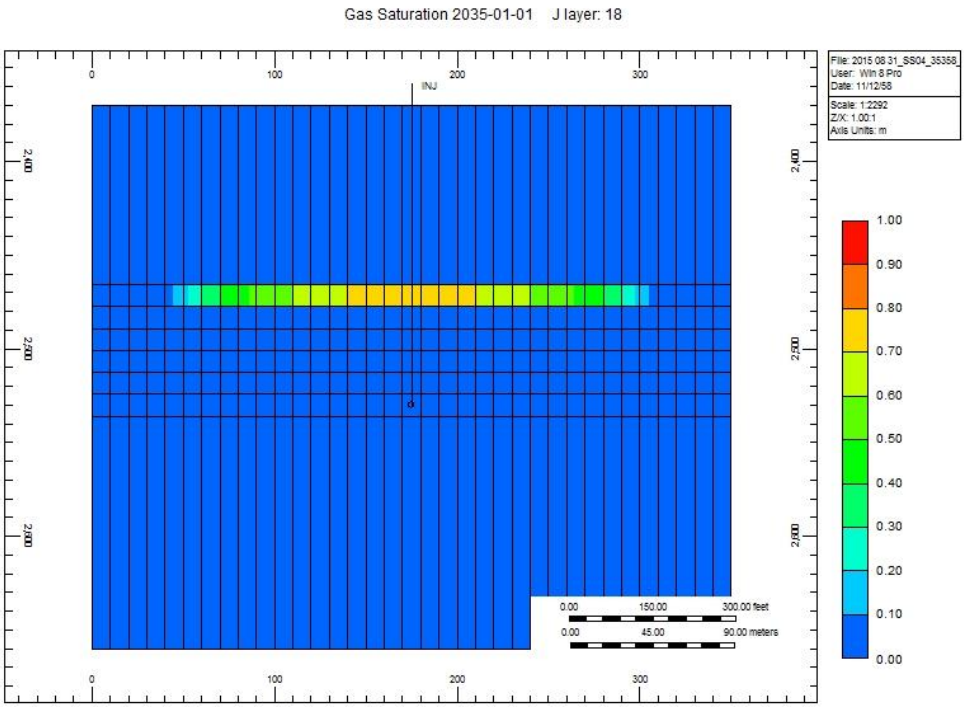

Figure 4.15 (a) 3D view, 20 year injection and (b) side view, 20 year injection at 2465.83-2535.94 m.

a.

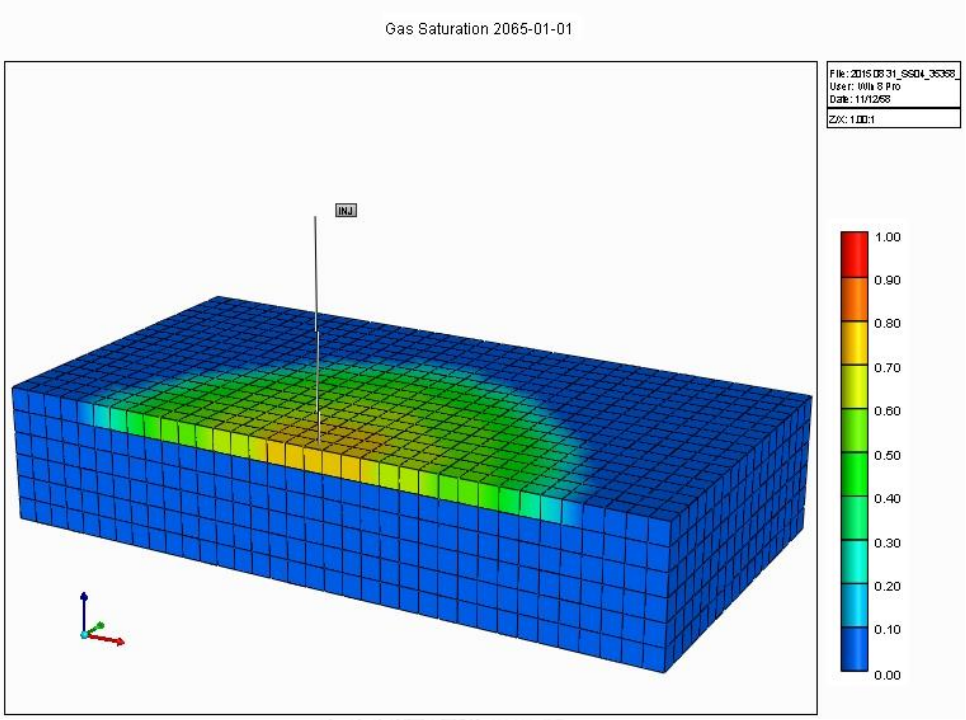

b.

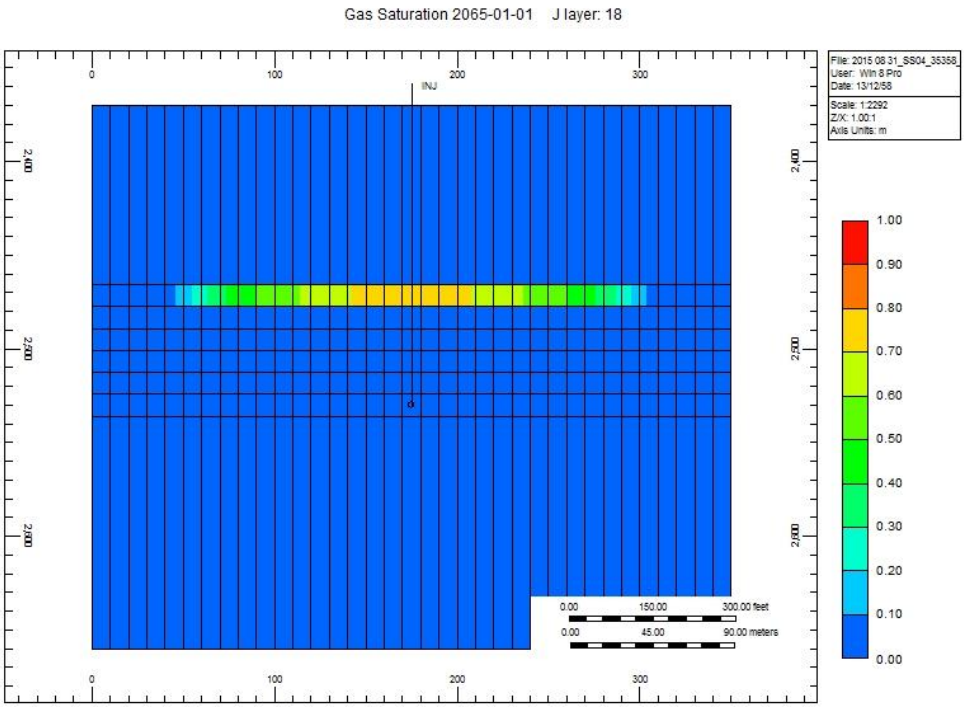

Figure 4.16 (a) 3D view, 50 year injection and (b) side view, 50 year injection at 2465.83-2535.94 m.

CHAPTER 5

CONCLUSIONS AND RECOMMENDATIONS

In this chapter, the effects of parameters for simulation of CO_2 storage in depleted oil reservoir are concluded. The conclusions provide the possibilities of CO_2 storage by following conditions such as depth, injection rate, pressure buildup and radius of migration to demonstrate the change in each layer. It divides the layer of injection such as layer 2, 4, 6 and overall layers respectively. The conclusion and recommendation can shown below;

5.1 Conclusions

- When the depth increases the pressure, temperature and density are affected in that these properties increase as depth increase because density increases and volumes decreases.
- Depth is related to the amount of CO_2 storage.
- Fracture pressure indicates the highest value that doesn't make caprock crack.
- Maximum pressure indicates the maximum value that safety pressure at 90 percent of fracture pressure
- Mostly, the trend of pressure buildup is going in the same direction during the first injection for 2000 and 4000 tons/day injection rate. The pressure buildup increased until the pressure buildup is near the maximum pressure and shutin well. Then the pressure buildup is slightly increased. However, for 1000 tons/day injection rate pressure buildup will increase until 50 years.
- The radius migration, the trend is same as the pressure buildup but the volume in the each layer when CO_2 injection depends on the injection rate and pressure buildup of storage layers.

- In term of capacity and pressure buildup, the suitable inject rate is 1000 tons/day. However in term of number of working days on economic, 4000 tons/day is much better because it takes time less.

5.2 Recommendations

- This research studies the homogenous simulation model but heterogeneous simulation model might be more realistic.
- The depth that the author's choosing in the range of 800-3000 m. When it's applied to the simulation models, it should be deeper than 1000 m. because the depth affects the amount of CO_2 storage, it the more depth will make the reservoir storage increased.
- Site selection is important. Therefore geology study should study further.

REFERENCES

ADB. (2013). *Prospects for CARBON CAPTURE and STORAGE in SOUTHEAST ASIA*.

Belay, G. (1992). *DISIRIBUTION AND CHARACTERISTICS OF PETROLEUM SOURCE ROCKS IN OIL WELL IF 30 03s BAN TAO FANG BASIN NORTHERN THAILAND*. (Master of Science in Geology), Chiang Mai, Chiang Mai University.

Benson, S. M. (2010). *Carbon Dioxide Capture and Storage in Underground Geologic Formation*. Paper presented at the The 10-50 Solution: Technologies and Policies for a Low-Carbon Future.

Bouc, O., et al. (2009). Determining safety criteria for CO2 geological storage. *Energy Procedia*, *1*(1), 2439-2446. doi:10.1016/j.egypro.2009.02.005

Bourgoyne Jr, A. T., et al. (1986). *Applied Drilling Engineering*: Society of Petroleum Engineers Richardson, TX.

Braun, E. V., andHahn, L. (Cartographer). (1976). Geological Map of Northern Thailand, Scale 1:250,000, Sheet Chiang Rai II

Cantucci, B., et al. (2009). Geochemical modeling of CO2 storage in deep reservoirs: The Weyburn Project (Canada) case study. *Chemical Geology*, *265*(1-2), 181-197. doi:10.1016/j.chemgeo.2008.12.029

Chumkratoke, C. (2004). *SIMULATION STUDY OF OIL RECOVERY IMPROVEMENT BY WATER FLOODING IN FANG OIL FIELD*. (Master of Engineering in Geotechnology), Suranaree University of Technology, Suranaree University of Technology.

CMG. (2011). *User's Guide GEM Advanced Compositional and GHG Reservoir Simulator Version 2011*.

CO2CRC. (2015). Storage images.

CORELABORATORIES. (1992). *INTEGRATED REPORT PREPARED FOR DEFENSE ENERGY DEPARTMENT WELL: FA-WR-35-04*.

CRS. (2013). *Carbon Capture and Sequestration (CCS): A Primer*. Retrieved from

DED. (1992). *GEOLOGICAL REPORT FA-SS-35-04 (FA-WR-35-04)*.

DMF. (2015). Petroleum Province.

Dobossy, M. E., et al. (2011). An efficient software framework for performing industrial risk assessment of leakage for geological storage of CO2. *Energy Procedia, 4*, 4207-4214. doi:10.1016/j.egypro.2011.02.368

EGAT. (2015). CO_2 emission.

Eiken, O., et al. (2011). Lessons learned from 14 years of CCS operations: Sleipner, In Salah and Snøhvit. *Energy Procedia, 4*, 5541-5548. doi:10.1016/j.egypro.2011.02.541

Frailey, S. M. (2009). Methods for estimating CO2 storage in saline reservoirs. *Energy Procedia, 1*(1), 2769-2776. doi:10.1016/j.egypro.2009.02.048

Goerke, U. J., et al. (2011). Numerical Simulation of Multiphase Hydromechanical Processes Induced by CO2Injection into Deep Saline Aquifers. *Oil & Gas Science and Technology – Revue d'IFP Energies nouvelles, 66*(1), 105-118. doi:10.2516/ogst/2010032

Gorecki, C. D., et al. (2009). Development of Storage Coefficients for Determining the Effective CO_2 Storage Resource in Deep Saline Formations *Society of Petroleum Engineers*, 35.

GreenFacts. (2015). Ocean storage

Gunter, W. D., et al. (2005). CO2 storage and enhanced methane production: Field testing at Fenn-Big Valley, Alberta, Canada, with application. *Greenhouse Gas Control Technologies 7*, 413-421.

Holt, T., et al. (1995). Undergeound Storage of CO, In Aquifers and Oil Reservoirs. *Energy Conversion and Management*, 535-538.

IEA. (2015). *CO_2 EMISSIONS FROM FUEL COMBUSTION*. Retrieved from

IPCC. (2005). *CARBON DIOXIDE CAPTURE AND STORAGE*: the United States of America by Cambridge University Press, New York.

Khanthaprab, C., andKaewsaeng, K. (1989). *Sedimentary Facies and Petroleum Poteneial of Fang Basin* Paper presented at the International Symposium on Intermontane Basins.

Mathias, S. A., andRoberts, A. W. (2013). A Lambert W function solution for estimating sustainable injection rates for storage of CO2 in brine aquifers. *International Journal of Greenhouse Gas Control, 17*, 546-548. doi:10.1016/j.ijggc.2013.04.007

Morley, C. K., andRacey, A. (2011). *Tertiary stratigraphy*.

Nuntajun, R. (2009). *SEISMIC STRATIGRAPHY OF THE FANG BASIN, CHIANG MAI PROVINCE.* (Master of science), Chiang Mai, Chiang Mai University.

PCR. (1988). *Technical appaisal of the Defense Energy Department Blocks Northern Thailand*.

Peacesoftware. (2015). Thermodynamics Online calculation of thermodynamic properties

Prakiat, D., andJeemsantia, A. (2011). *Opportunity for Carbon Dioxide Storage in Thailand: Mae Moh Power Station Case Study.* (Bachelor), Chulalongkorn.

Rodjanapo, S. (1998a). *Facies Analysis of Tertiary Rocks in Mae Soon and Nong Yao Oilfields Fang Basin Northern Thailand.* (Master of Science), Chiang Mai, Chiang Mai University.

Rodjanapo, S. (1998b). *Facies Analysis of Tertiary Rocks in Mae Soon and Nong Yao Oilfileds, Fang Basin Northern Thailand*.

Settakul, N. (1984). *Pong Nok oil field, Proceeding of the Symposium on Cenozoic Basins of Thailand: Geology and Resources*.

Settakul, N. (1985). *Petroluem Geology of Fang Basin Part I*.

Srihiran, S. (1986). *SURFACE RESISTIVTY MEASUREMENT FOR OIL EXPLORATION AT MAE SOON OIL POOl, FANG BASIN CHANGWAT CHIANG MAI.* (Master of Sciecne), Chiang Mai, Chiang Mai University.

ThaiDefenseEnergy, andSchlumberger. (2013). *Reservoir Modeling Study and Field Development Planning in Fang Basin, Chapter 1 Data Gathering and Assumptions*.

Torp, T. A., andGale, J. (2004). Demonstrating storage of CO2 in geological reservoirs: The Sleipner and SACS projects. *Energy Procedia, 29*, 1361-1369.

Water Resource Engineering CO., L. (1997). *Survery and assessment of coal Fang Basin Chiang Mai*.

Wilcox, J. (2011). *Workshop on Carbon Capture and Storage. This workshop is part of Stanford-Chulalongkorn University Collaboration Program financially supported by Chevron Corporation and Chevron Offshore*.

Zakkour, P., andHaines, M. (2007). Permitting issues for CO2 capture, transport and geological storage: A review of Europe, USA, Canada and Australia.

International Journal of Greenhouse Gas Control, 1(1), 94-100. doi:10.1016/s1750-5836(06)00008-9

Zollner, E., andMoller, U. (1996). *3D Seismic Interpretation, Central Fang Basin, Thailand*.

APPENDIX

APPENDIX A

This section explains for reservoir model construction by the use of CMG-GEM reservoir simulator. The parameter used to reservoir model in base case condition is follows:

Table A.1 Setting of builder reservoir simulator

Simulator	GEM
Working Units	SI
Porosity	Single Porosity

Table A.2 Setting data for 2^{nd}, 4^{th}, 6^{th} layers

Detail	FA-SS-35-04 (2^{nd}, 4^{th}, 6^{th} layers)
Grid Type	Cartesian
K Direction	Down
Number of blocks (i x j x k)	35 x 35 x 8
Block widths in I direction	35 x 10
Block widths in J direction	35 x 10

Table A.3 Setting data for overall layers

Detail	FA-SS-35-04 (overall layers)
Grid Type	Cartesian
K Direction	Down
Number of blocks (i x j x k)	35 x 35 x 8
Block widths in I direction	35 x 10
Block widths in J direction	35 x 10

Reservoir-Array properties

Table A.4 The FA-SS-35-04 at 2nd layer.

	Grid Top (m)	Grid Thickness (m)	Porosity	Perm-I (md)
whole			0.236	
Layer 1	1856.23	263.65		0.1
Layer 2	2119.88	6.86		150
Layer 3	2126.74	6.86		190
Layer 4	2133.60	6.86		130
Layer 5	2140.46	6.86		160
Layer 6	2147.32	6.86		180
Layer 7	2154.18	6.85		190
Layer 8	2161.03	179.83		0.1

Table A.5 The FA-SS-35-04 at 4th layer.

	Grid Top (m)	Grid Thickness (m)	Porosity	Perm-I (md)
whole			0.236	
Layer 1	2161.03	179.83		0.1
Layer 2	2340.86	4.83		120
Layer 3	2345.69	4.83		140
Layer 4	2350.52	4.83		130
Layer 5	2355.35	4.83		150
Layer 6	2360.18	4.83		160
Layer 7	2365.01	4.81		190
Layer 8	2369.82	96.01		0.1

Table A.6 The FA-SS-35-04 at 6th layer.

	Grid Top (m)	Grid Thickness (m)	Porosity	Perm-I (md)
whole			0.236	
Layer 1	2369.82	96.01		0.1
Layer 2	2465.83	11.68		130
Layer 3	2477.52	11.68		150
Layer 4	2489.20	11.68		190
Layer 5	2500.88	11.68		170
Layer 6	2512.56	11.68		120
Layer 7	2524.24	11.70		190
Layer 8	2535.94	124.05		0.1

Table A.7 The FA-SS-35-04 at overall layers.

	Grid Top (m)	Grid Thickness (m)	Porosity	Perm-I (md)
whole			0.236	
Layer 1	1856.23	263.65		0.1
Layer 2	2119.88	41.15		170
Layer 3	2161.03	179.83		0.1
Layer 4	2340.86	28.96		190
Layer 5	2369.82	96.01		0.1
Layer 6	2465.83	35.05		180
Layer 7	2500.88	35.05		190
Layer 8	2535.94	124.05		0.1

APPENDIX B

This section explains the simulation results changing with time 1, 5, 10, 20 and 50 years. It presented in 3D model and cross section view of FA-SS-35-04 area in second layer, fourth layer, sixth layer and overall layers at the rate of injection at 1000 and 2000 tons/day are follows.

Table B 1. The effects of parameters for second layer by period at injection rate 1000 tons/day

n^{th} Year	Radius (m)	Area (m^2)	CO_2 storage at layer
1	24.23	1844.41	Top sublayer
5	74.9	17624.37	
10	100.55	31762.45	
20	124.1	48383.07	
50	157.8	78228.30	

Table B 2. The effects of parameters for second layer by period at injection rate 2000 tons/day

n^{th} Year	Radius (m)	Area (m^2)	CO_2 storage at layer
1	56.61	10067.84	Top sublayer
5	96.1	29013.27	
10	114.31	41050.49	
20	151.59	72191.32	
50	153.01	73551.16	

Table B 3. The effects of parameters for fourth layer by period at injection rate 1000 tons/day

n^{th} Year	Radius (m)	Area (m^2)	CO_2 storage at layer
1	31.92	3200.93	Top sublayer
5	81.09	20657.82	
10	104.17	34090.64	
20	130.11	53182.80	
50	153.7	74216.01	

Table B 4. The effects of parameters for fourth layer by period at injection rate 2000 tons/day

n^{th} Year	Radius (m)	Area (m^2)	CO_2 storage at layer
1	40.81	5232.19	Top sublayer
5	102.7	33135.29	
10	129.9	53011.27	
20	154	74506.01	
50	152.88	73426.23	

Table B 5. The effects of parameters for fourth layer by period at injection rate 4000 tons/day

n^{th} Year	Radius (m)	Area (m^2)	CO_2 storage at layer
1	53.3	8924.92	Top sublayer
5	84	22167.08	
10	103.47	33634.02	
20	115.4	41837.09	
50	125.55	49520.3	

Table B 6. The effects of parameters for sixth layer by period at injection rate 1000 tons/day

n^{th} Year	Radius (m)	Area (m^2)	CO_2 storage at layer
1	16.9	897.27	5^{th} sublayer
5	55.53	9687.36	Top sublayer
10	78.3	19260.76	
20	102.65	33103.03	
50	126.58	50336.16	

Table B 7. The effects of parameters for sixth layer by period at injection rate 2000 tons/day

n^{th} Year	Radius (m)	Area (m^2)	CO_2 storage at layer
1	23.2	1690.93	5^{th} sublayer
5	73.06	16769.08	Top sublayer
10	100.5	31730.87	
20	128.57	51931.30	
50	127.68	512114.82	

Table B 8. The effects of parameters for sixth layer by period at injection rate 4000 tons/day

n^{th} Year	Radius (m)	Area (m^2)	CO_2 storage at layer
1	32.6	3338.76	5^{th} sublayer
5	43.84	6037.97	Top sublayer
10	68.8	14870.54	
20	83	21642.43	
50	93.55	27493.97	

Table B 9. The effects of parameters for overall layer by period at injection rate 1000 tons/day

n^{th} Year	Radius (m)	Area (m^2)	CO_2 storage at layer
1	12.86	519.56	Top of 7^{th} layer
5	37.23	4354.48	Top of 6^{th} layer
10	52	8494.87	Top of 6^{th} layer
20	70.17	15468.66	Top of 6^{th} layer
50	95.59	28706.14	Top of 4^{th} layer

Table B 10. The effects of parameters for overall layer by period at injection rate 2000 tons/day

n^{th} Year	Radius (m)	Area (m^2)	CO_2 storage at layer
1	18.21	1041.77	Top of 7^{th} layer
5	50.36	7967.49	Top of 6^{th} layer
10	69	14957.12	Top of 6^{th} layer
20	89.12	24951.71	Top of 6^{th} layer
50	91.95	26561.55	Top of 4^{th} layer

Table B 11. The effects of parameters for overall layer by period at injection rate 4000 tons/day

n^{th} Year	Radius (m)	Area (m^2)	CO_2 storage at layer
1	24.58	1898.08	Top of 7^{th} layer
5	65.15	13334.56	Top of 6^{th} layer
10	87.99	24322.96	Top of 6^{th} layer
20	89.06	24918.12	Top of 6^{th} layer
50	86.11	23294.70	Top of 6^{th} layer

FA-SS-35-04 at the rate of injection at 1000 tons/day

a.

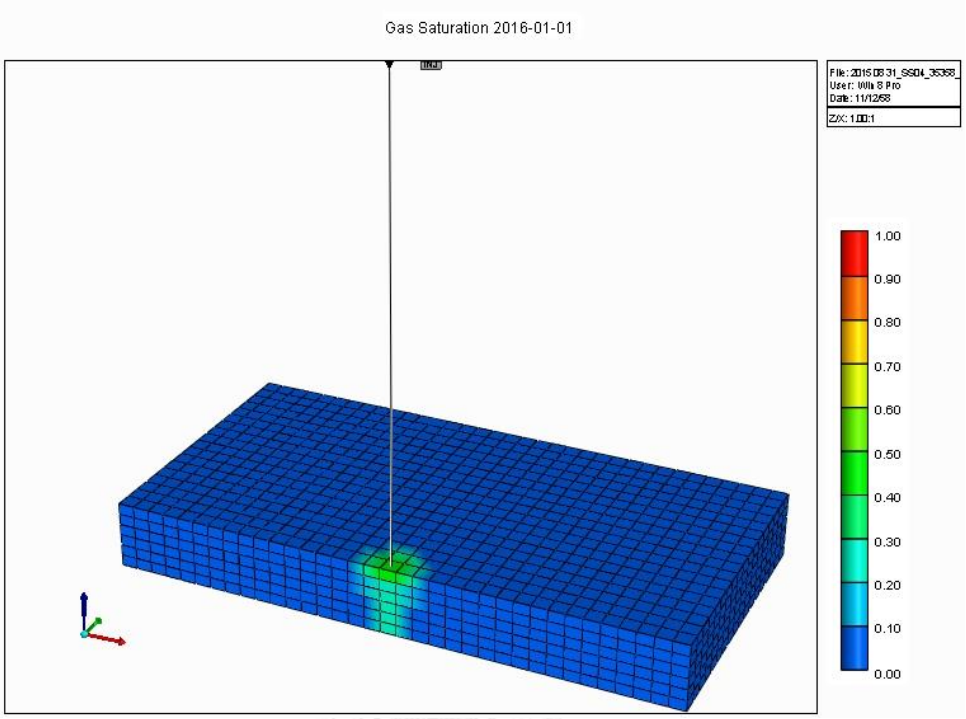

b.

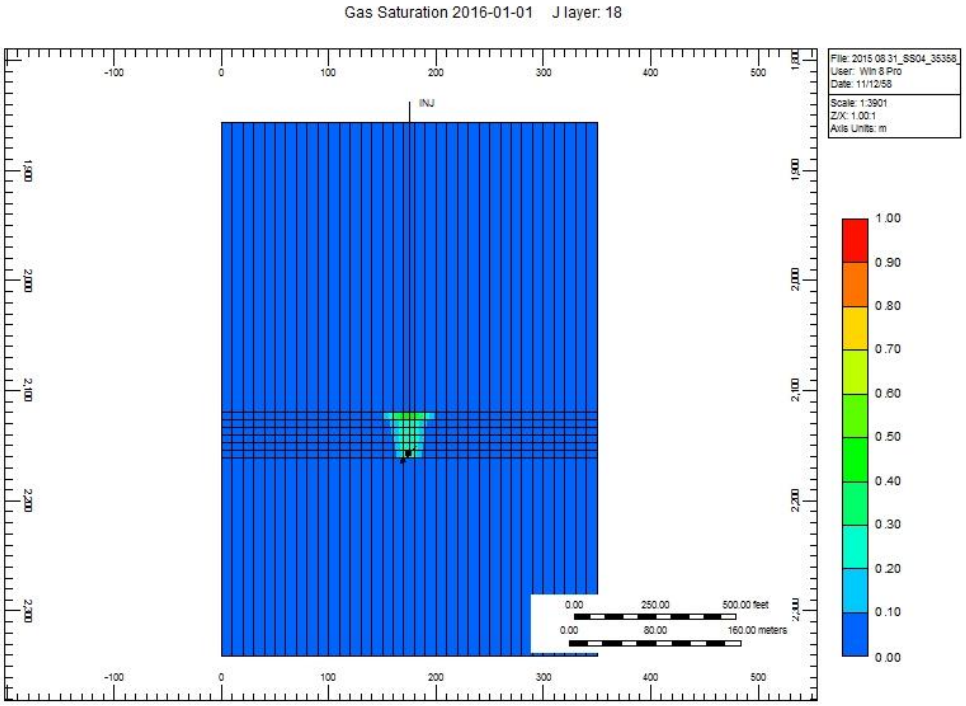

Figure B 1 (a) 3D view, 1 year injection and (b) side view, 1 year injection at. 2119.88-2161.03 m.

a.

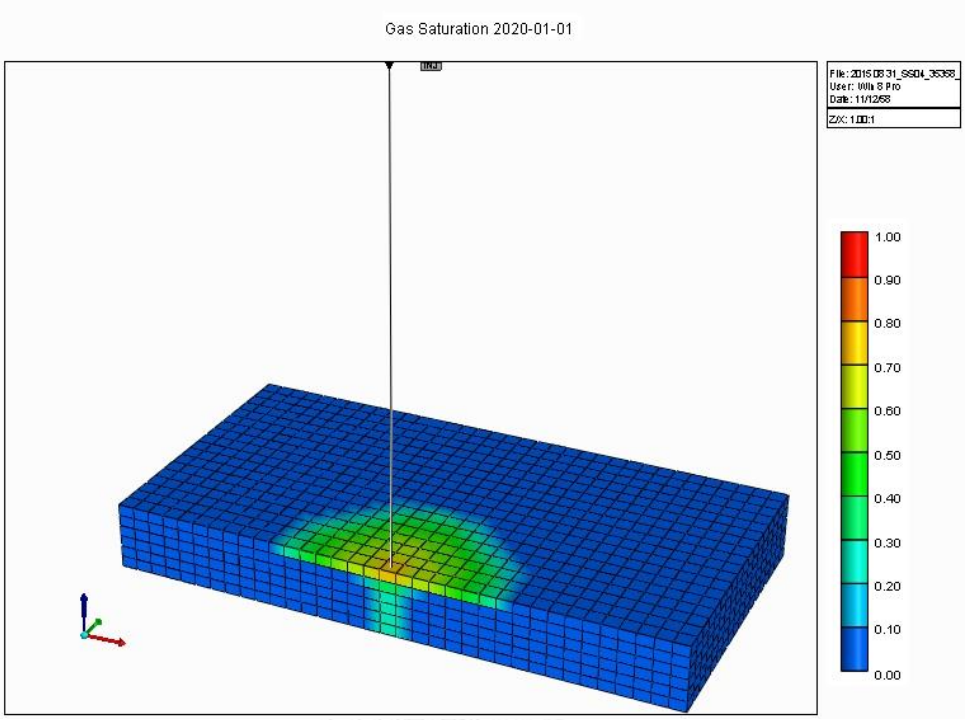

b.

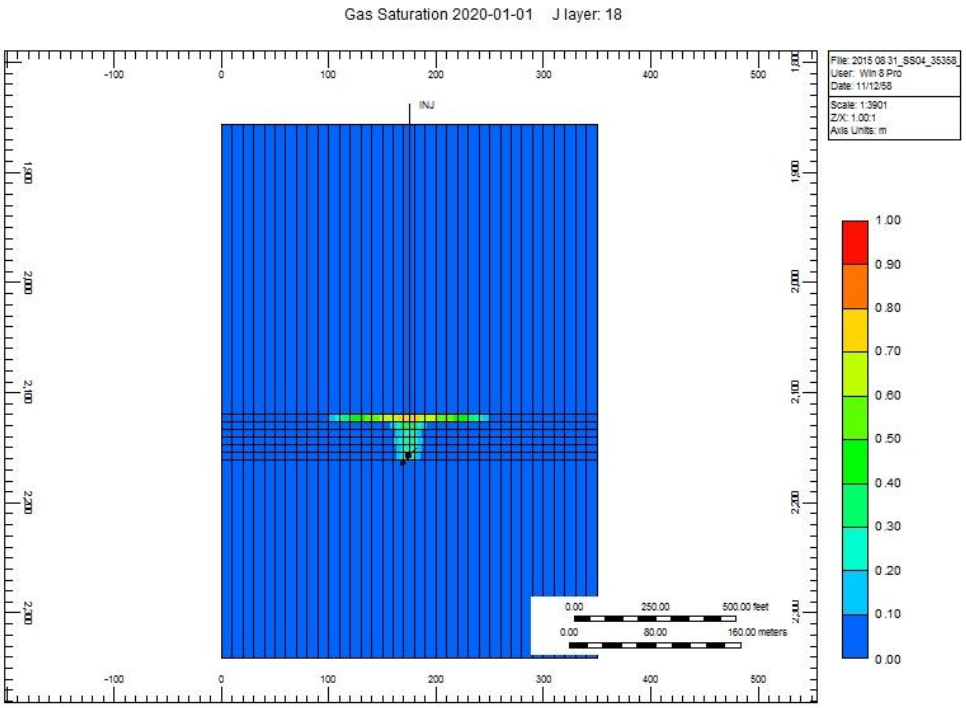

Figure B 2 (a) 3D view, 5 year injection and (b) side view, 5 year injection at. 2119.88-2161.03 m.

a.

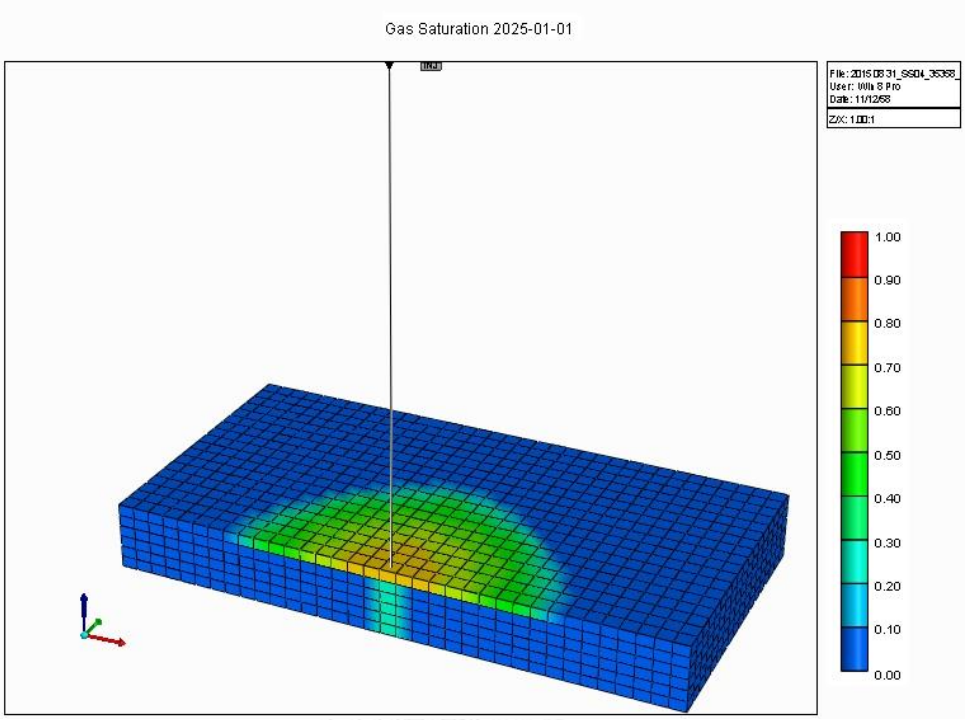

b.

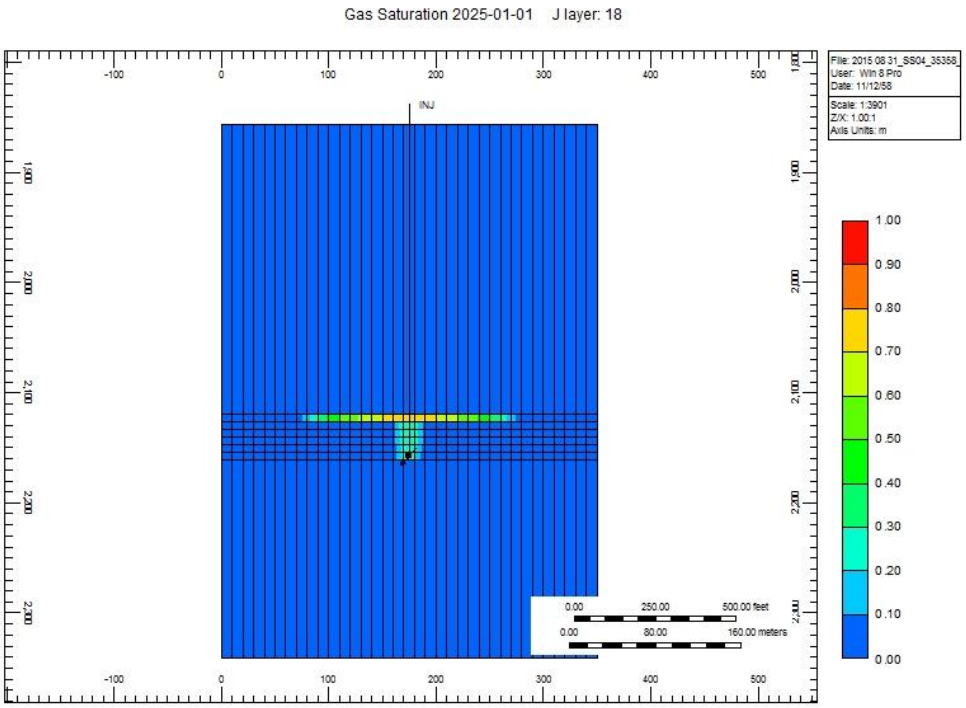

Figure B 3 (a) 3D view, 10 year injection and (b) side view, 10 year injection at. 2119.88-2161.03 m.

a.

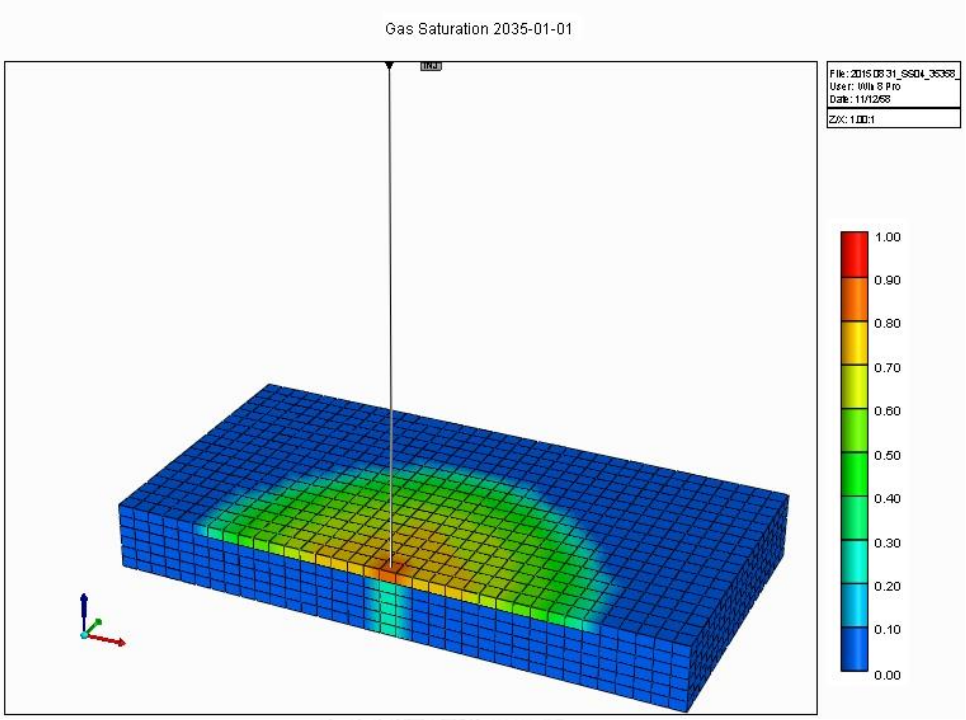

b.

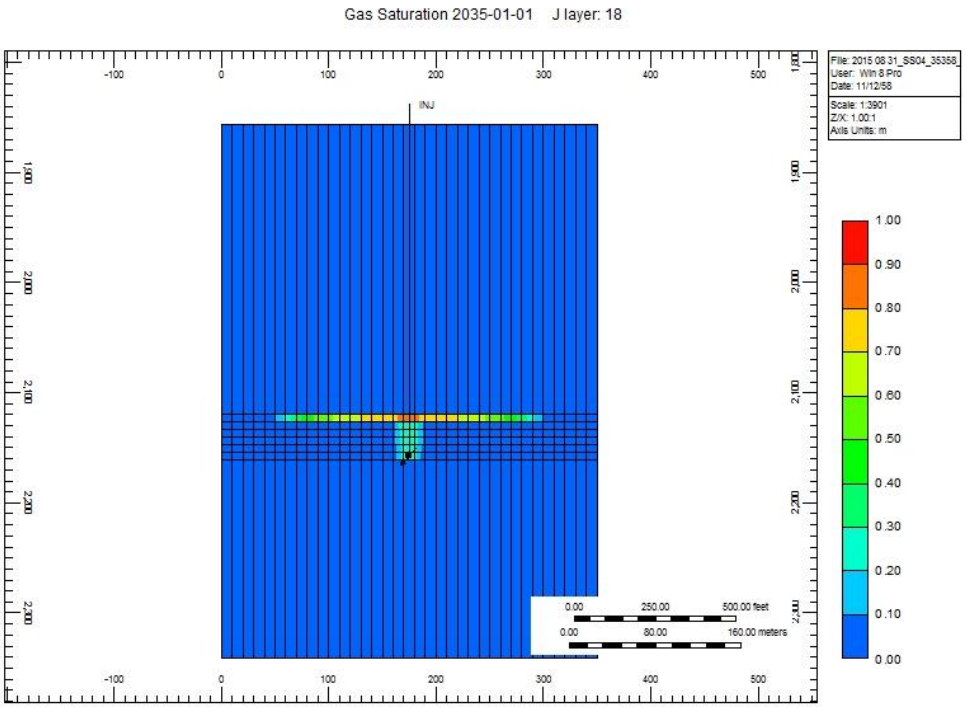

Figure B 4 (a) 3D view, 20 year injection and (b) side view, 20 year injection at. 2119.88-2161.03 m.

a.

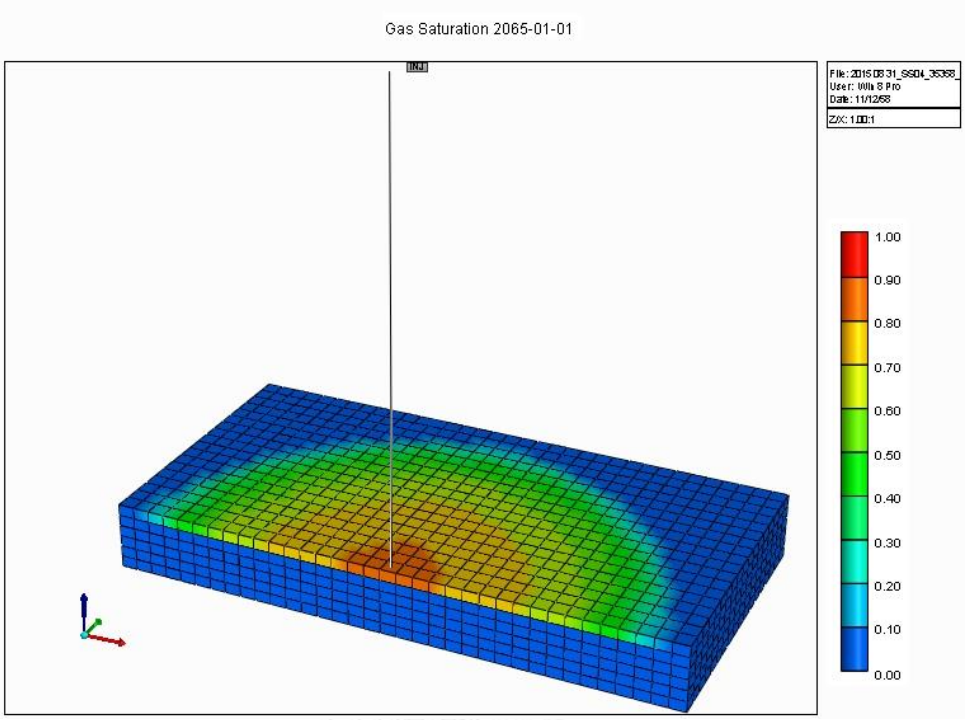

b.

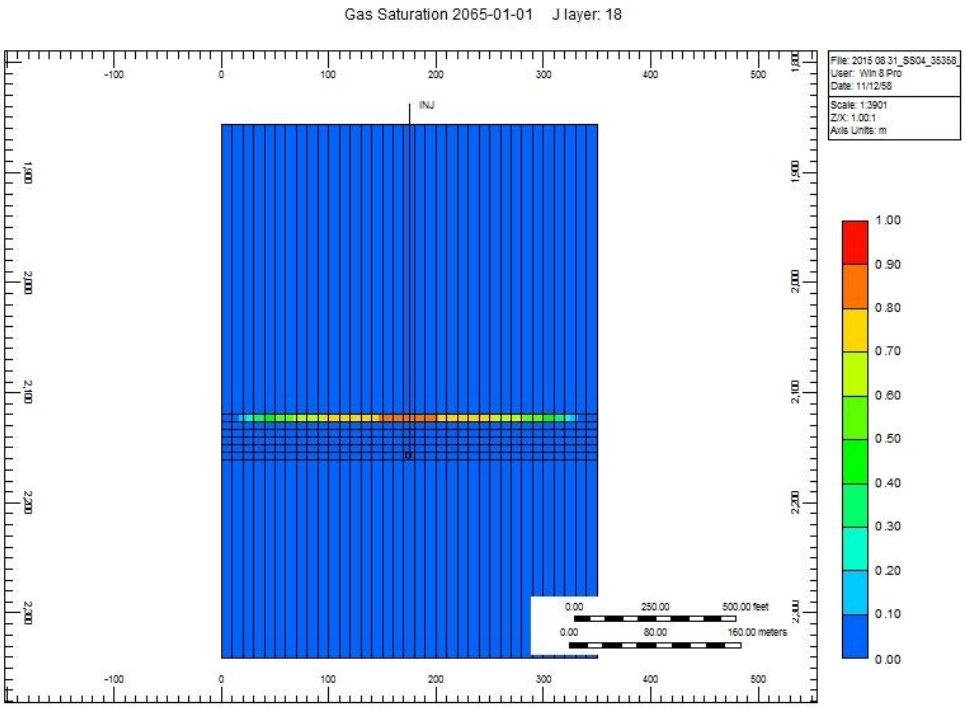

Figure B 5 (a) 3D view, 50 year injection and (b) side view, 50 year injection at. 2119.88-2161.03 m.

a.

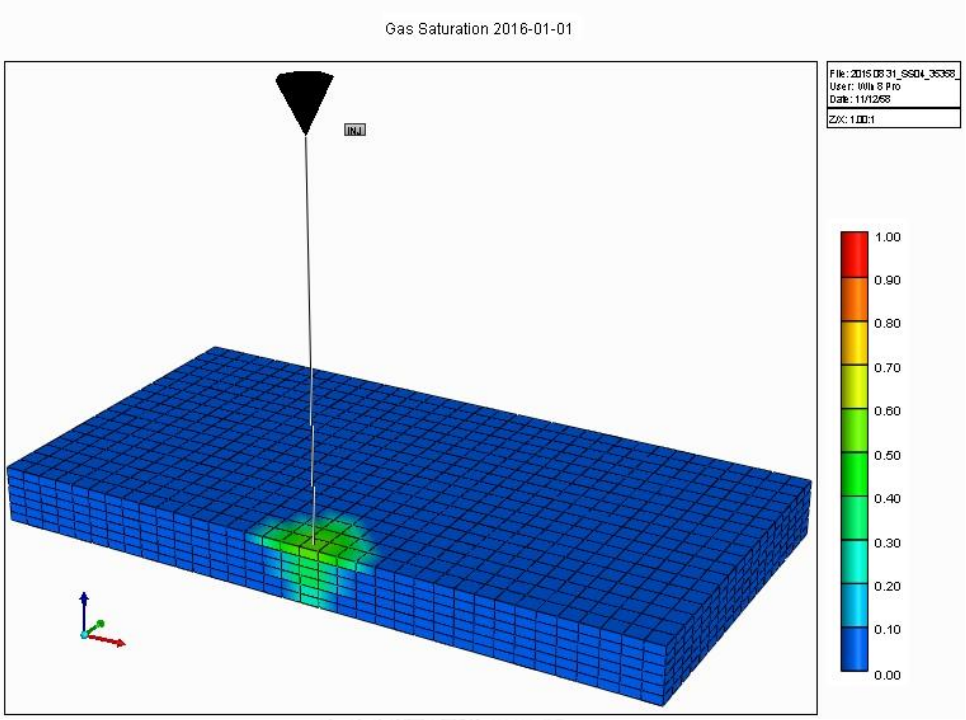

b.

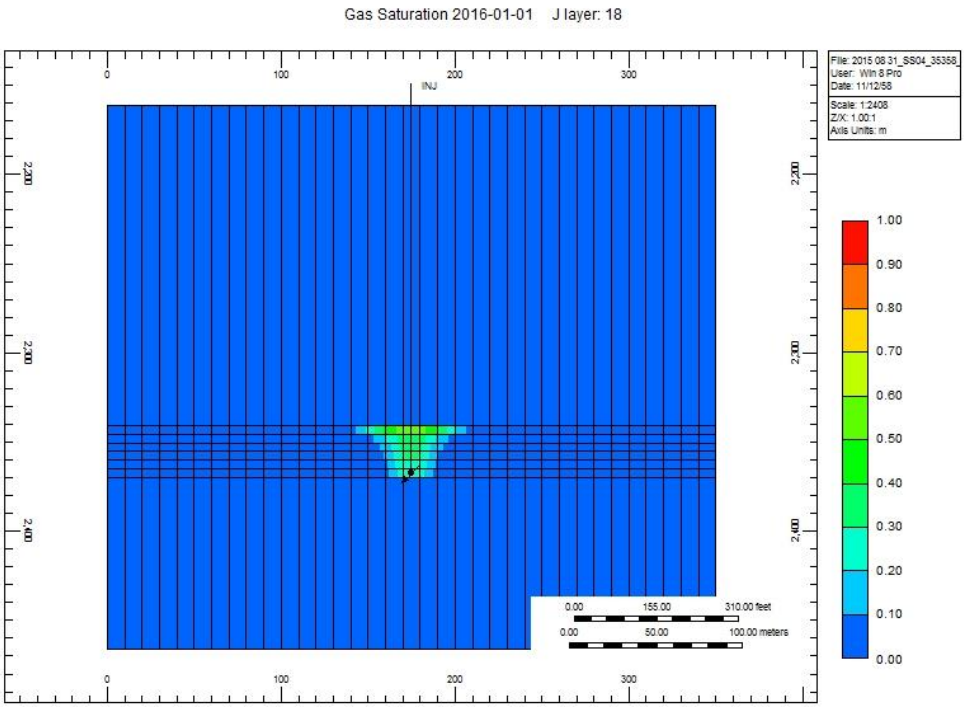

Figure B 6 (a) 3D view, 1 year injection and (b) side view, 1 year injection at. 2340.86-2369.82 m.

a.

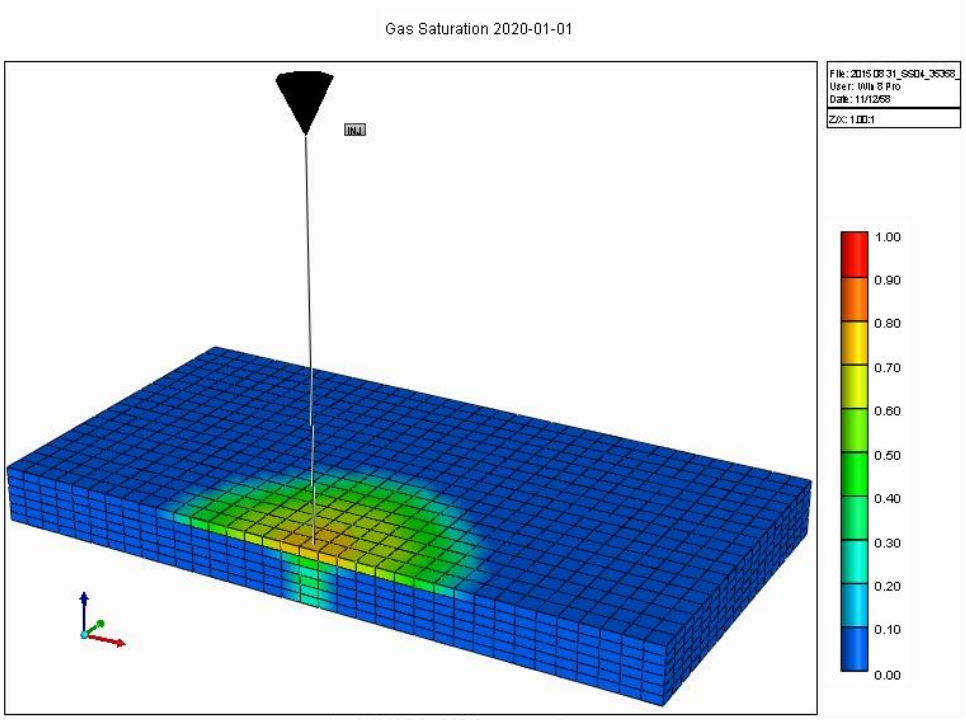

b.

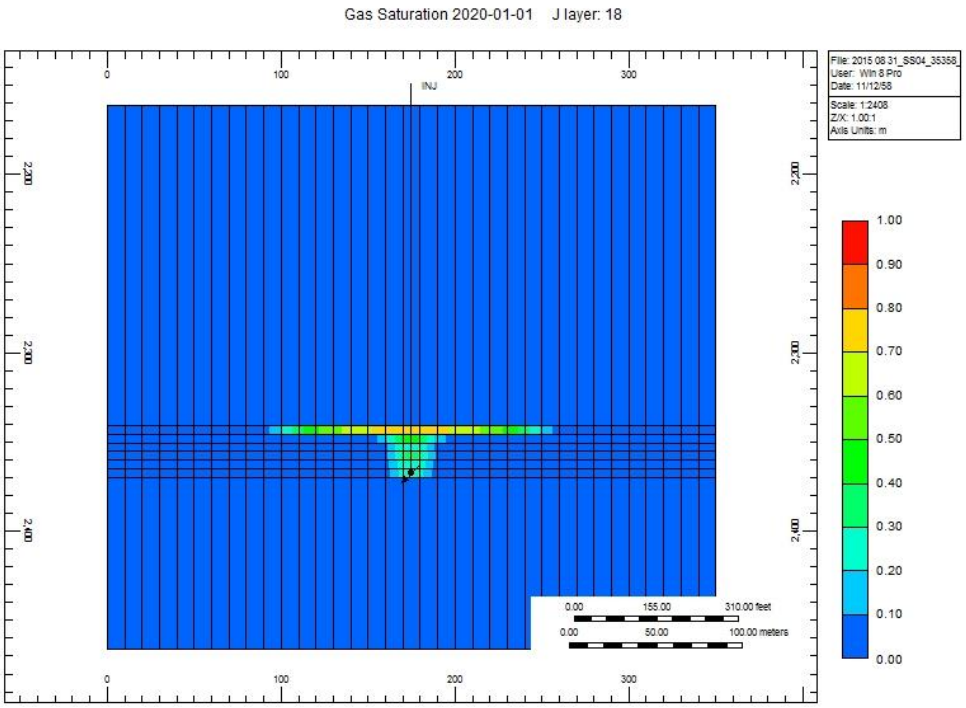

Figure B 7 (a) 3D view, 5 year injection and (b) side view, 5 year injection at. 2340.86-2369.82 m.

a.

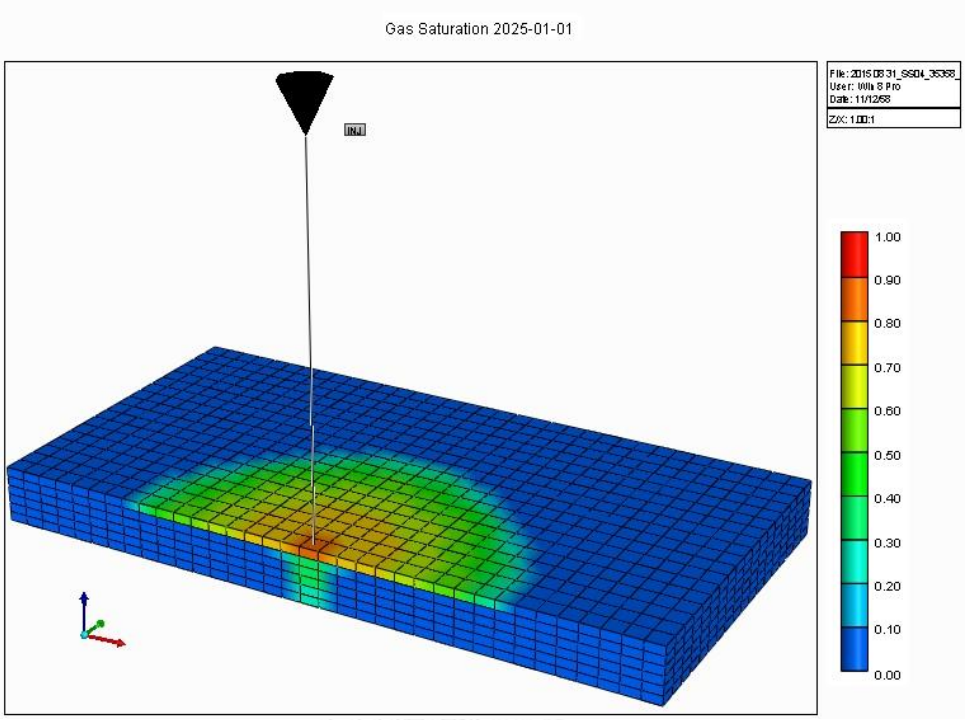

b.

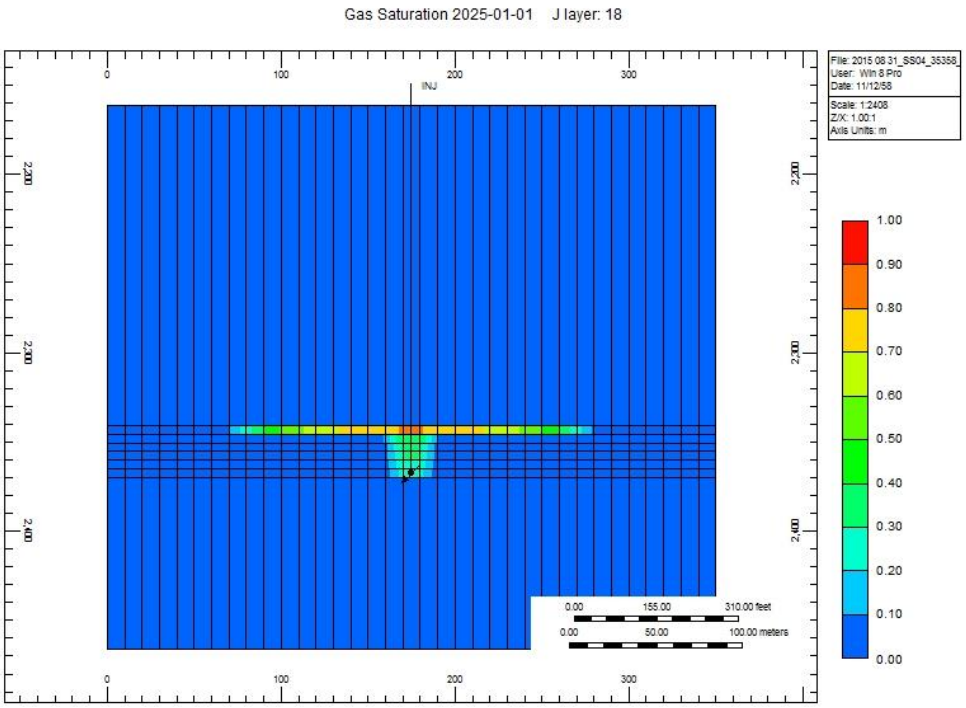

Figure B 8 (a) 3D view, 10 year injection and (b) side view, 10 year injection at. 2340.86-2369.82 m.

a.

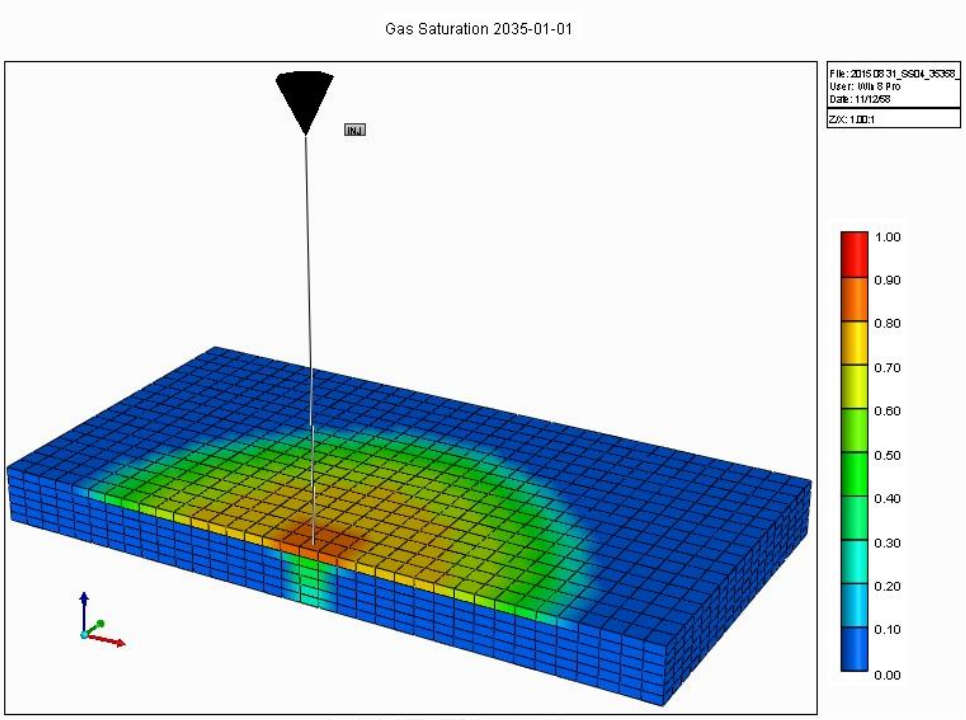

b.

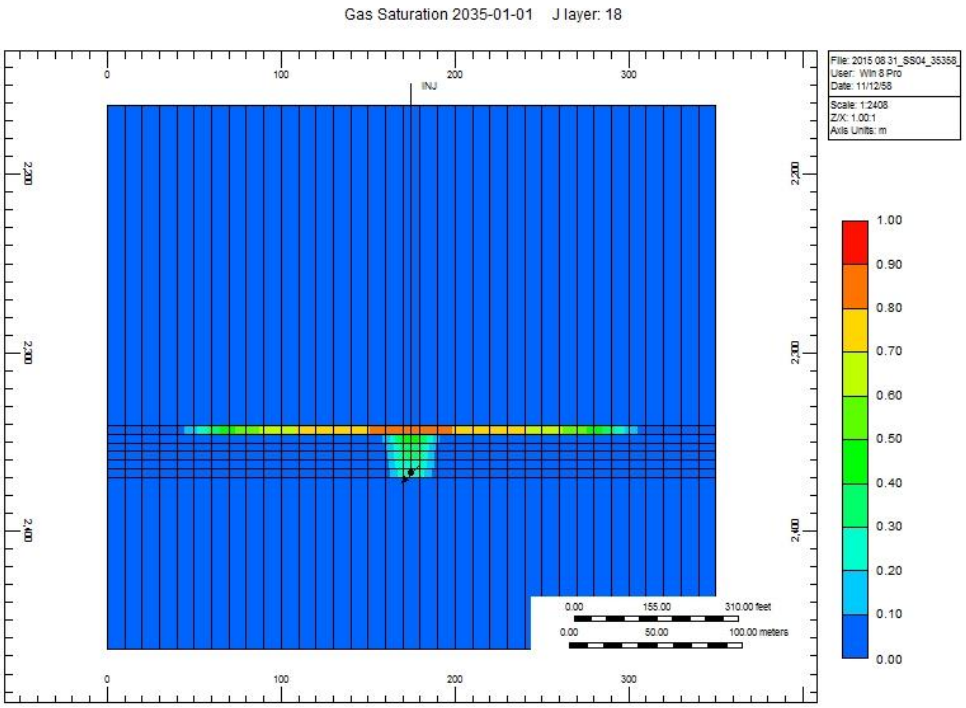

Figure B 9 (a) 3D view, 20 year injection and (b) side view, 20 year injection at. 2340.86-2369.82 m.

a.

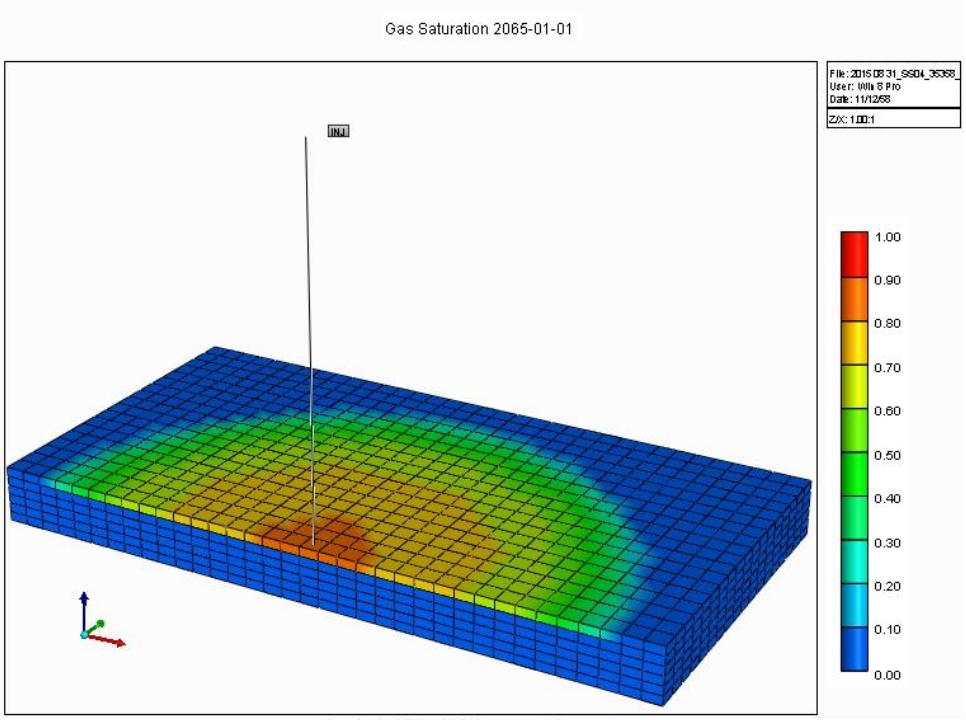

b.

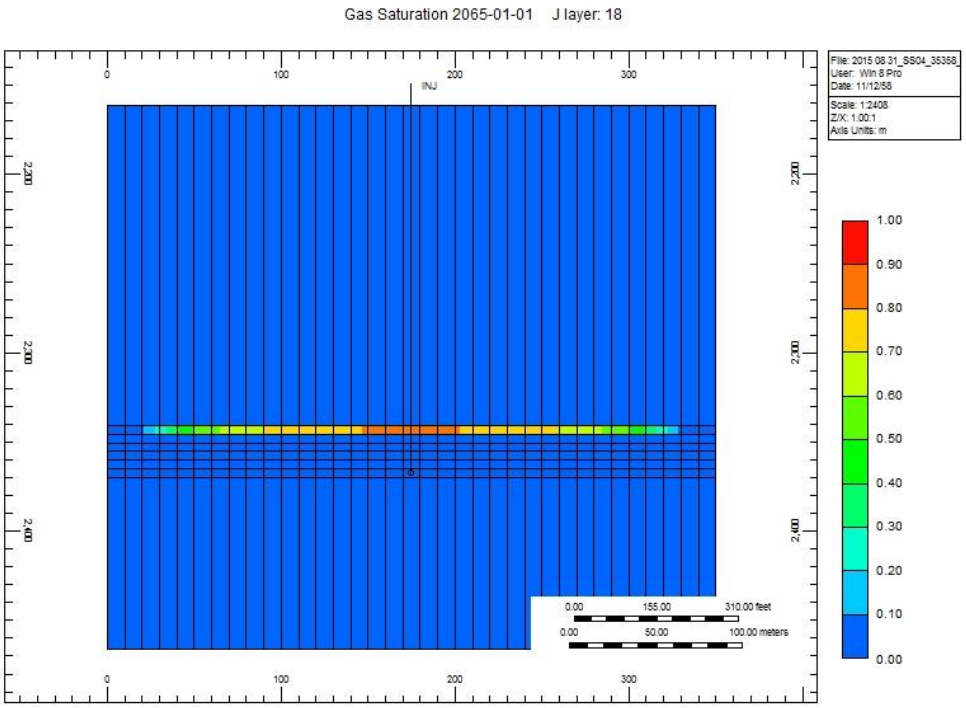

Figure B 10 (a) 3D view, 50 year injection and (b) side view, 50 year injection at. 2340.86-2369.82 m.

a.

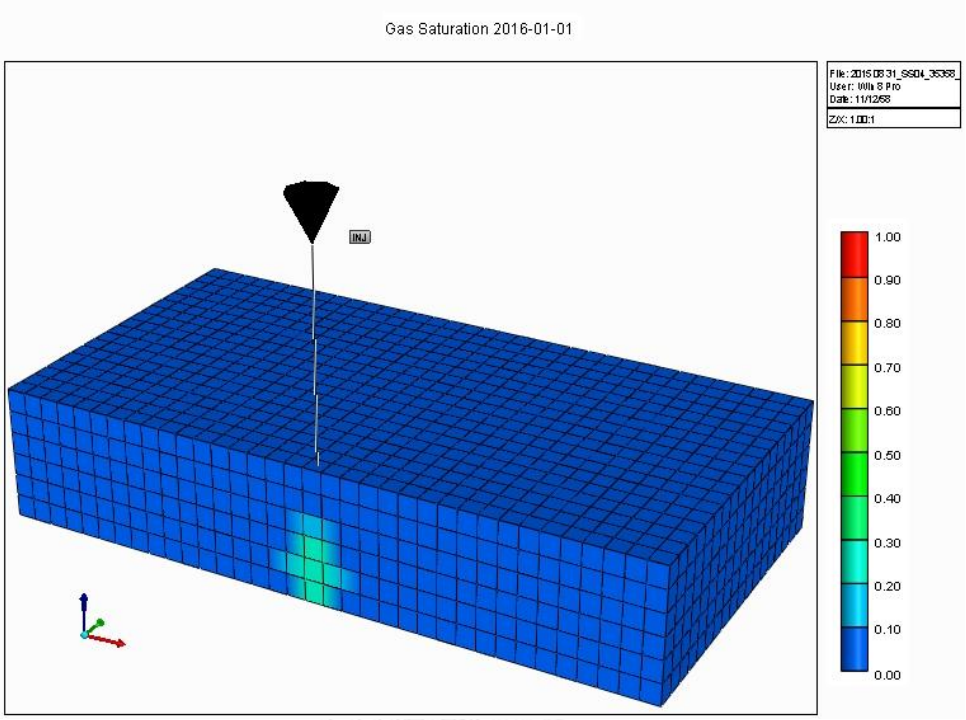

b.

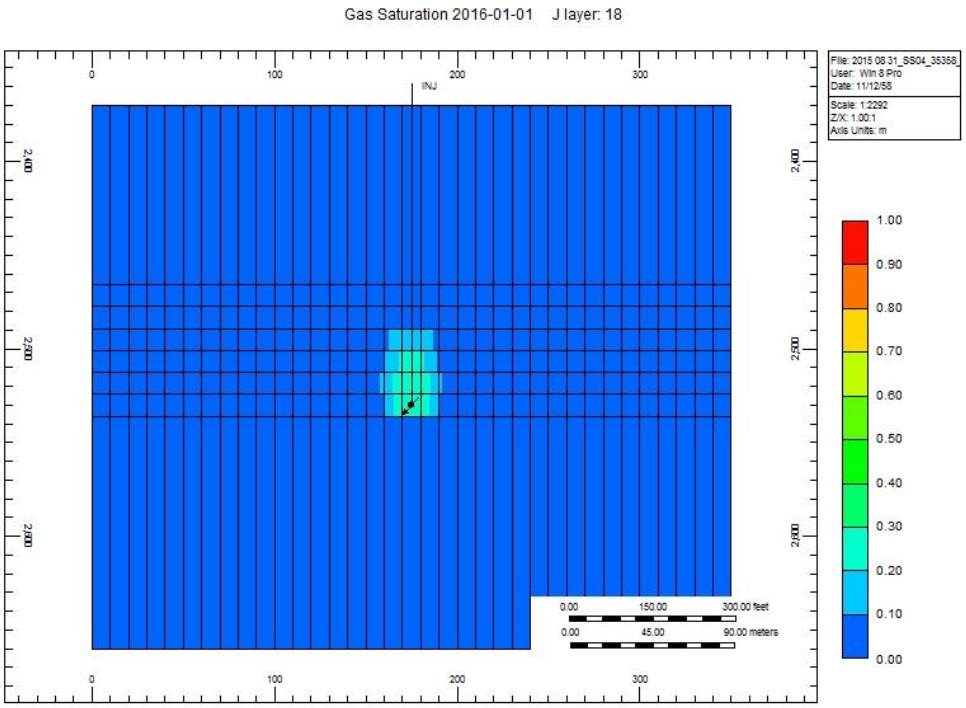

Figure B 11 (a) 3D view, 1 year injection and (b) side view, 1 year injection at. 2465.83-2535.94 m.

a.

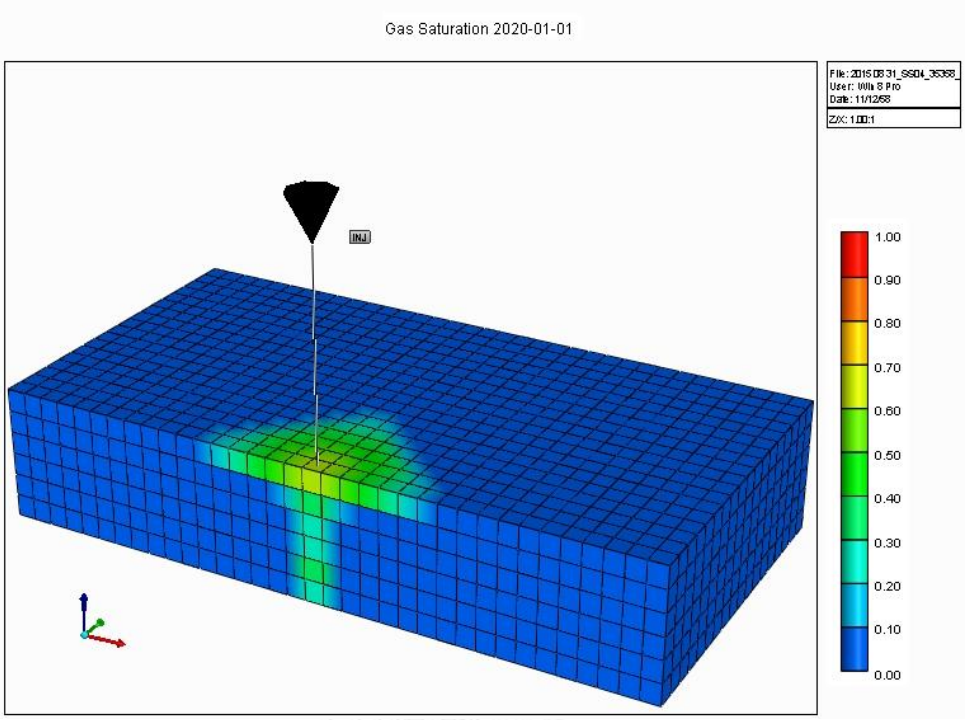

b.

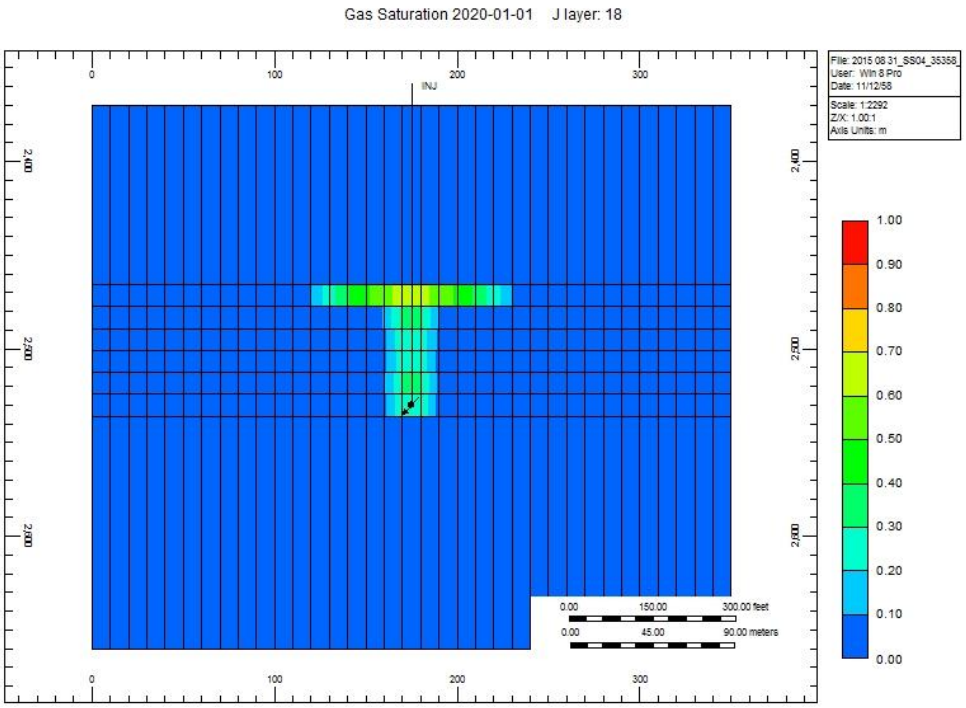

Figure B 12 (a) 3D view, 5 year injection and (b) side view, 5 year injection at. 2465.83-2535.94 m.

a.

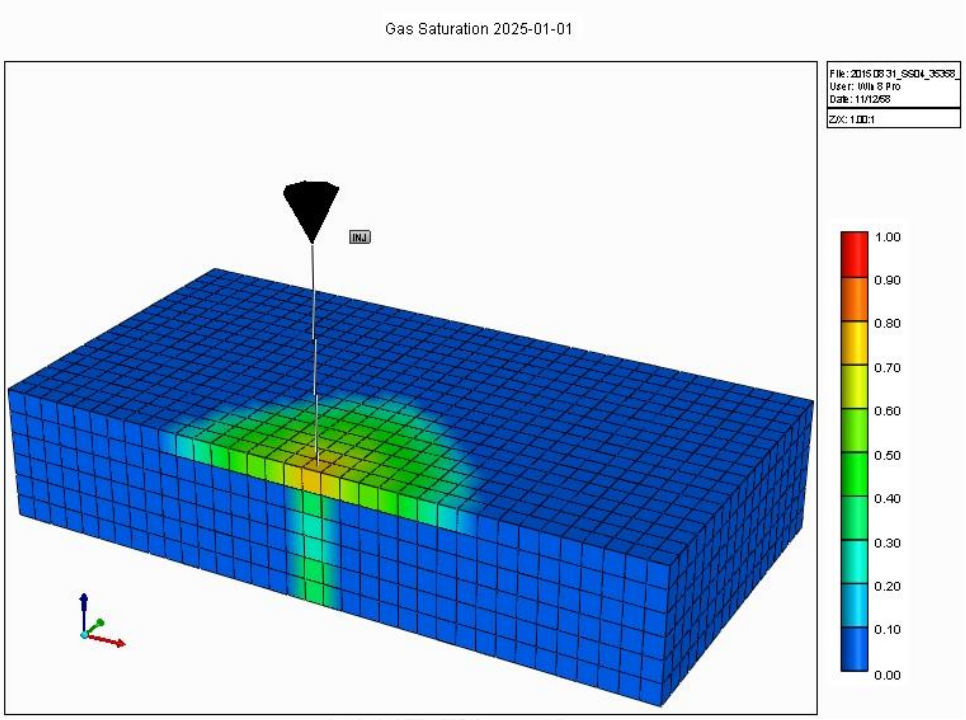

b.

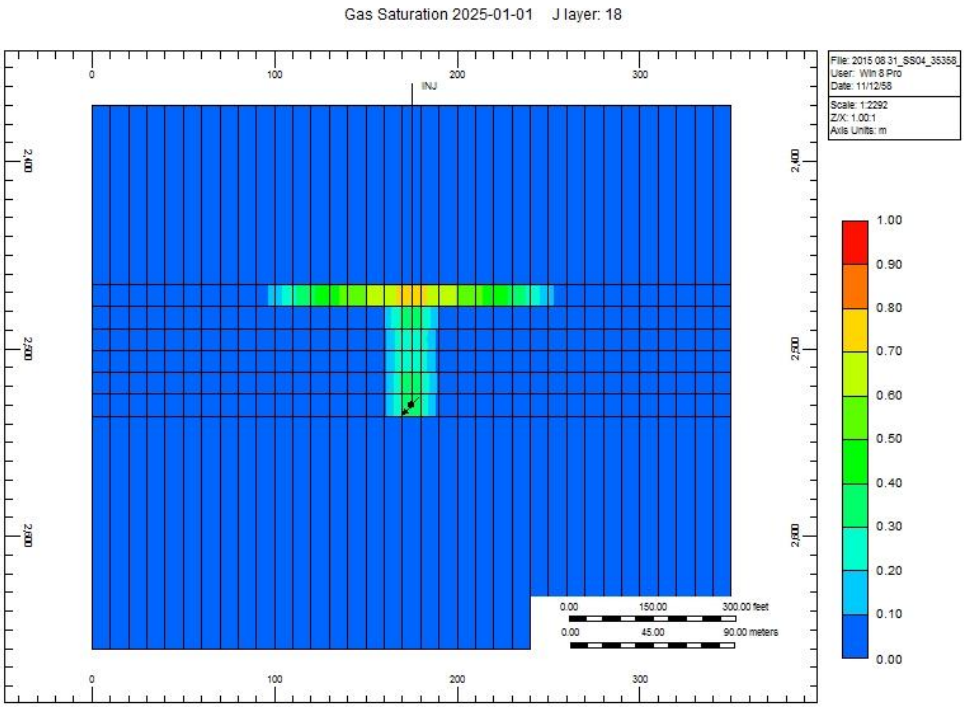

Figure B 13 (a) 3D view, 10 year injection and (b) side view, 10 year injection at. 2465.83-2535.94 m.

a.

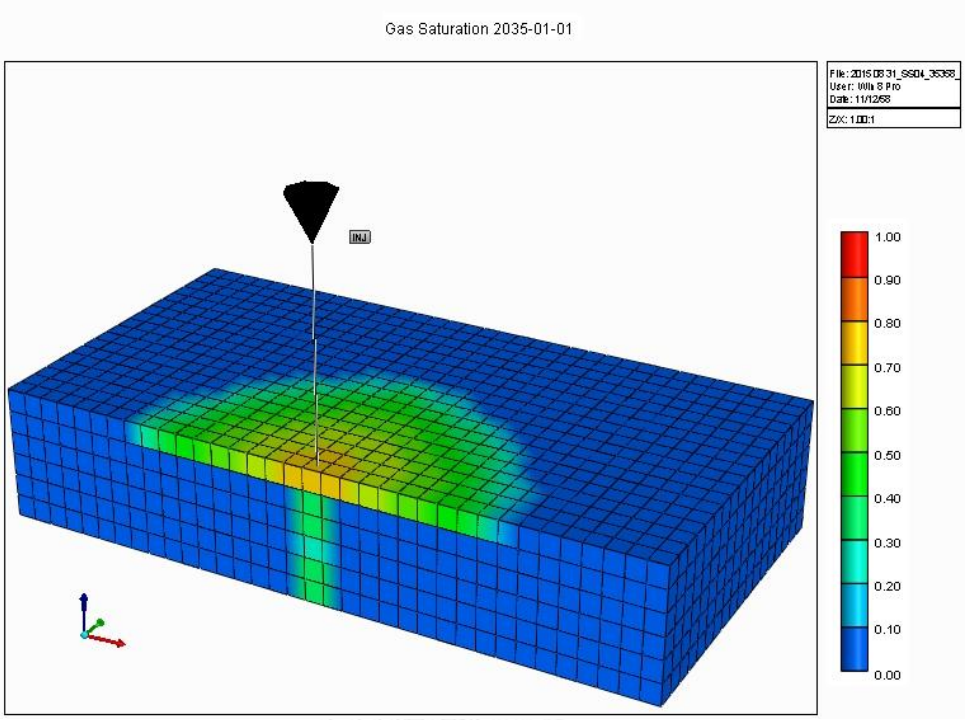

b.

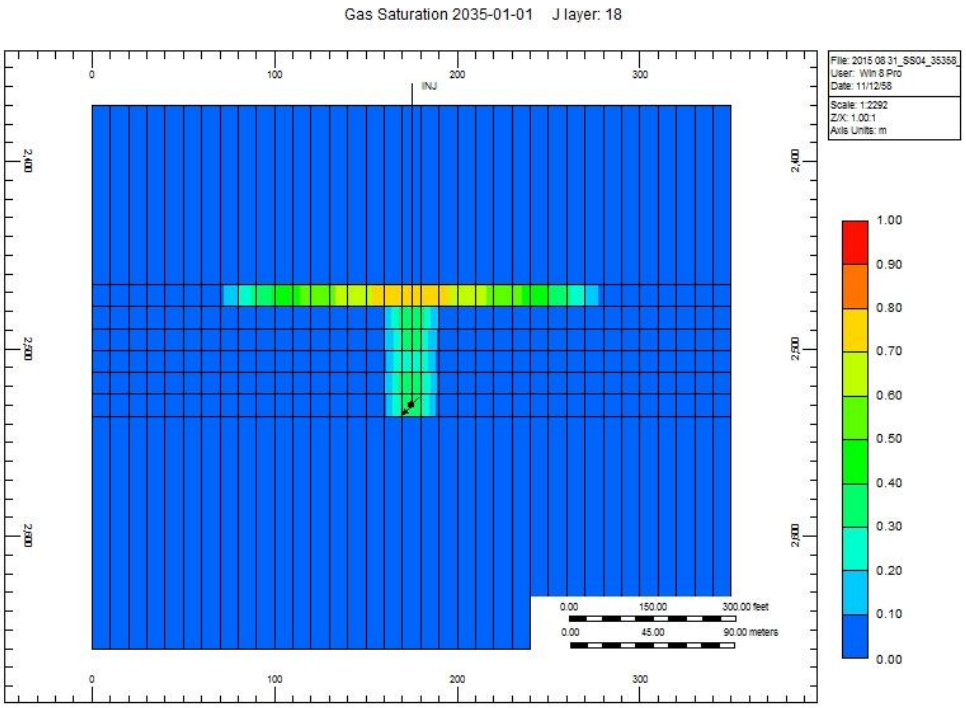

Figure B 14 (a) 3D view, 20 year injection and (b) side view, 20 year injection at. 2465.83-2535.94 m.

a.

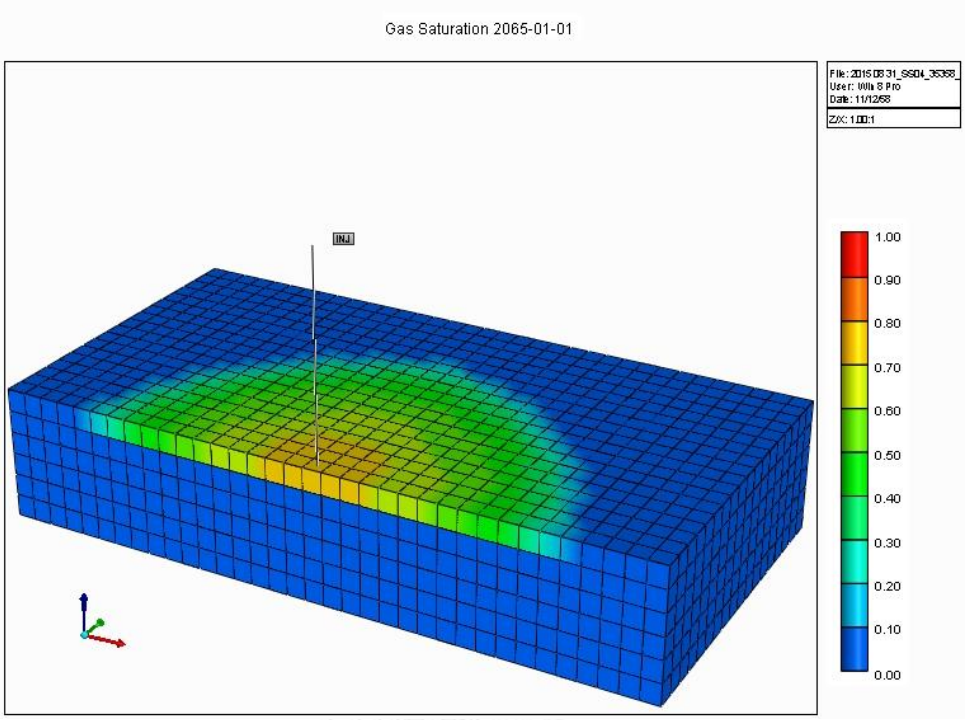

b.

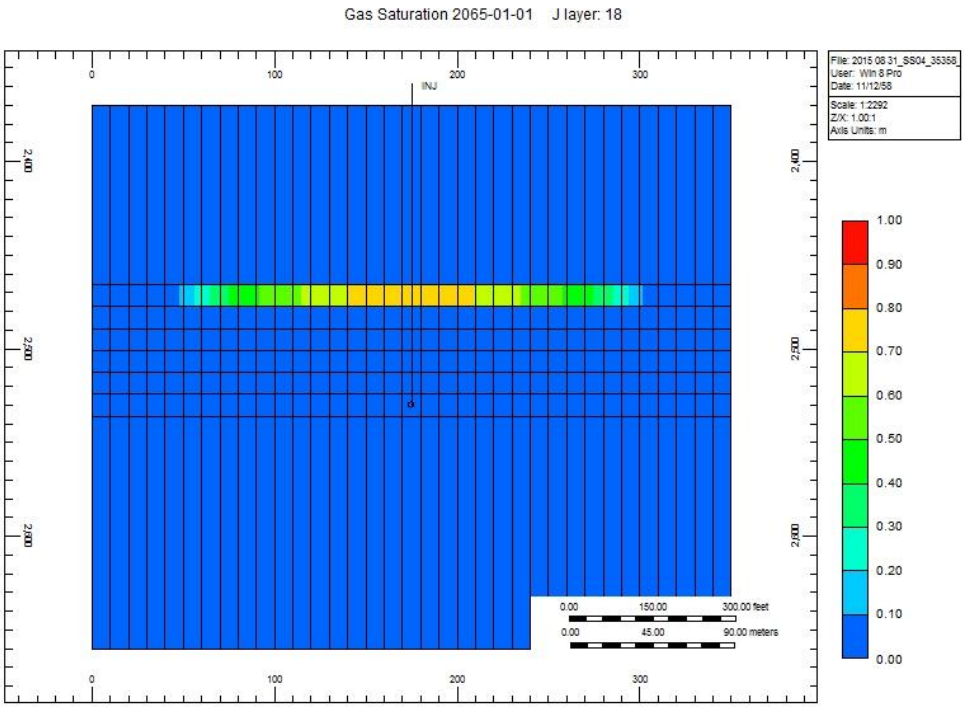

Figure B 15 (a) 3D view, 50 year injection and (b) side view, 50 year injection at. 2465.83-2535.94 m.

a.

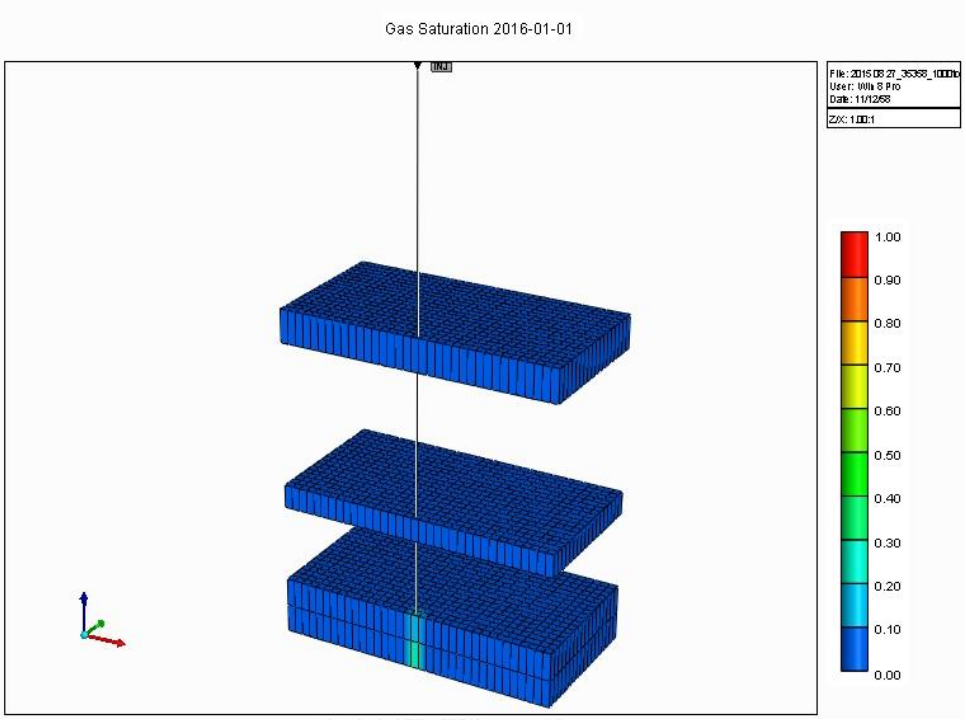

b.

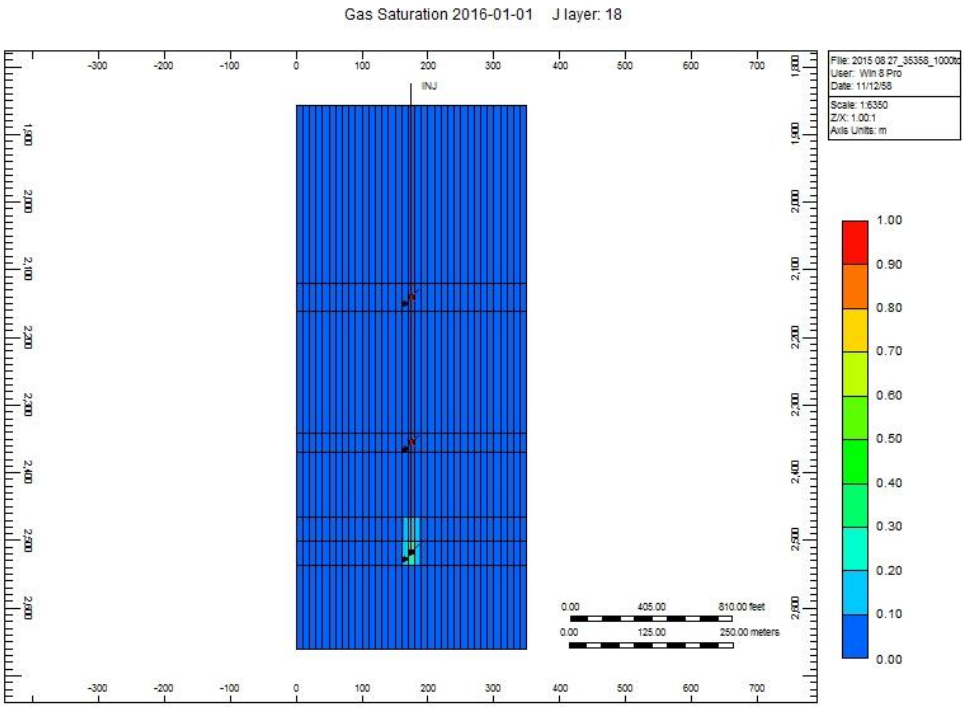

Figure B 16 (a) 3D view, 1 year injection and (b) side view, 1 year injection at. all layer.

a.

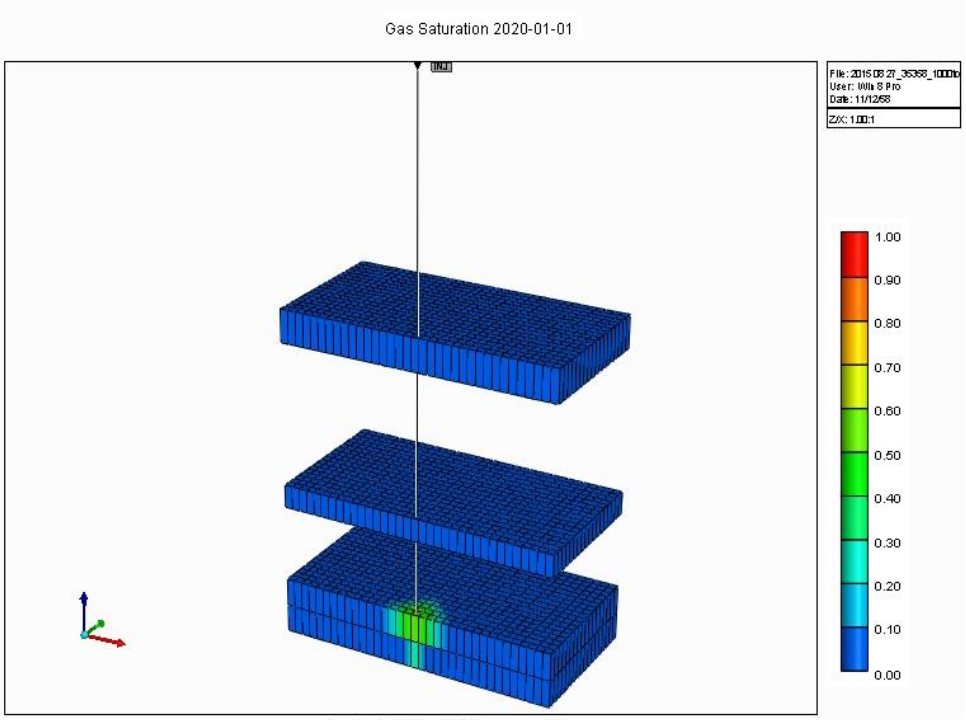

b.

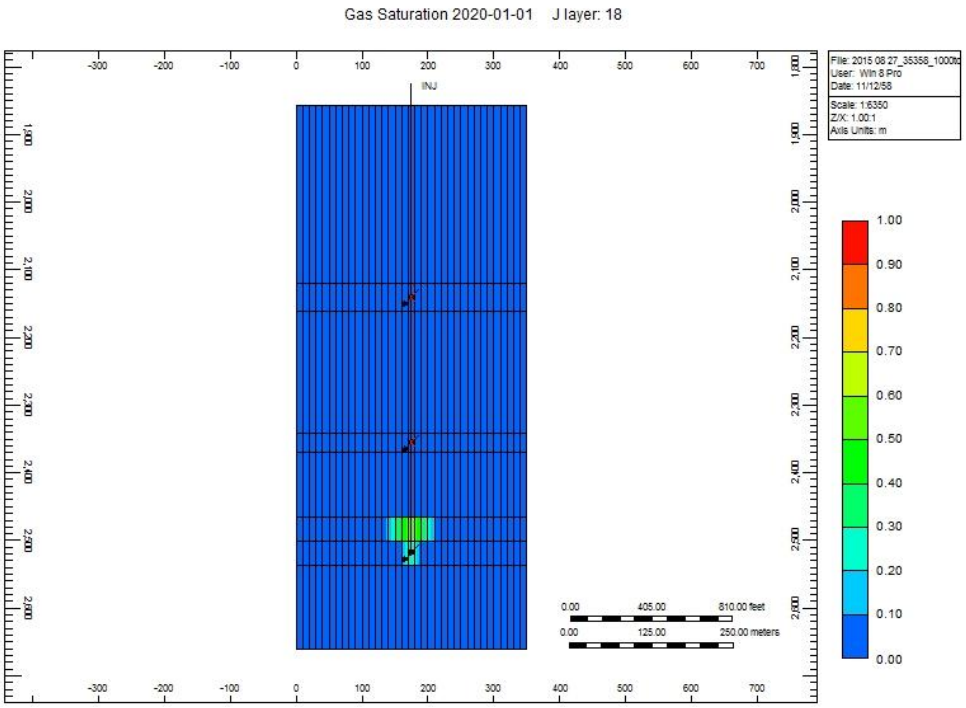

Figure B 17 (a) 3D view, 5 year injection and (b) side view, 5 year injection at. all layer

a.

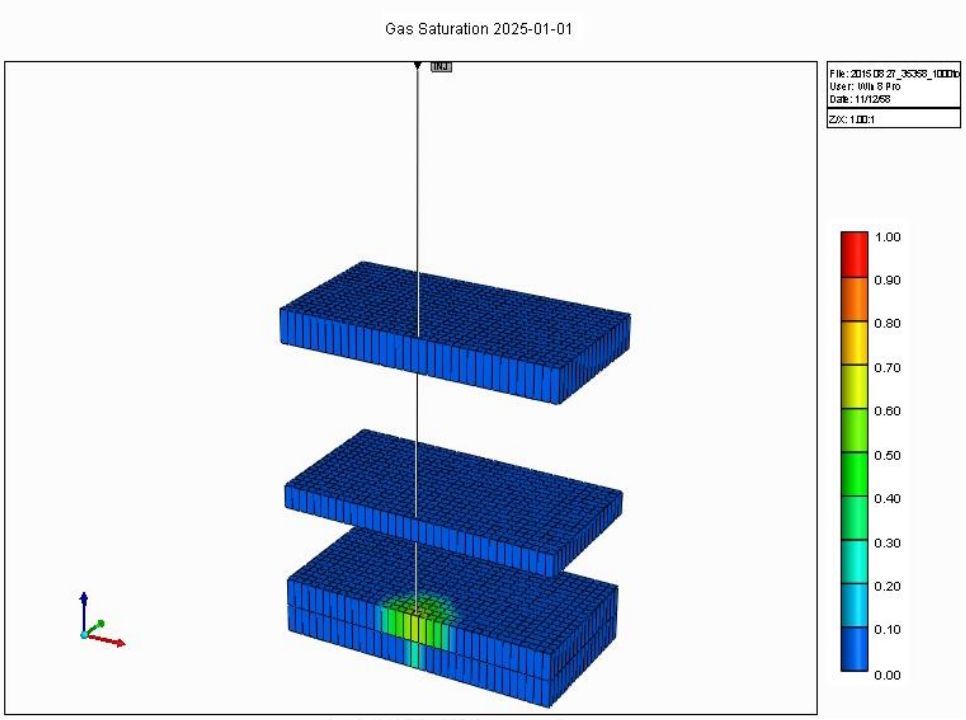

b.

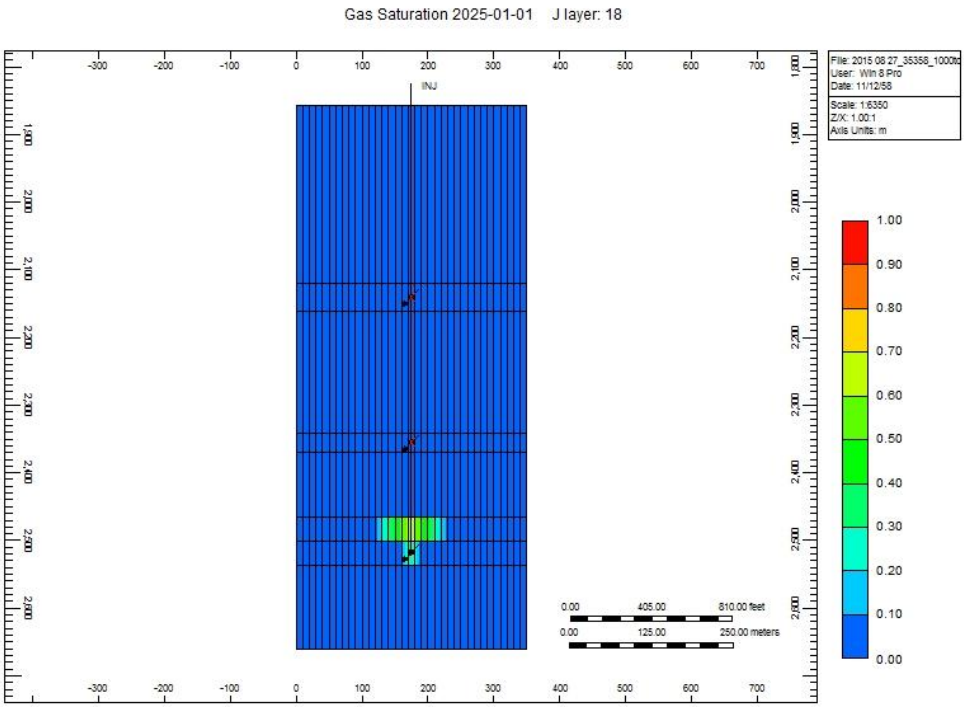

Figure B 18 (a) 3D view, 10 year injection and (b) side view, 10 year injection at. all layer

a.

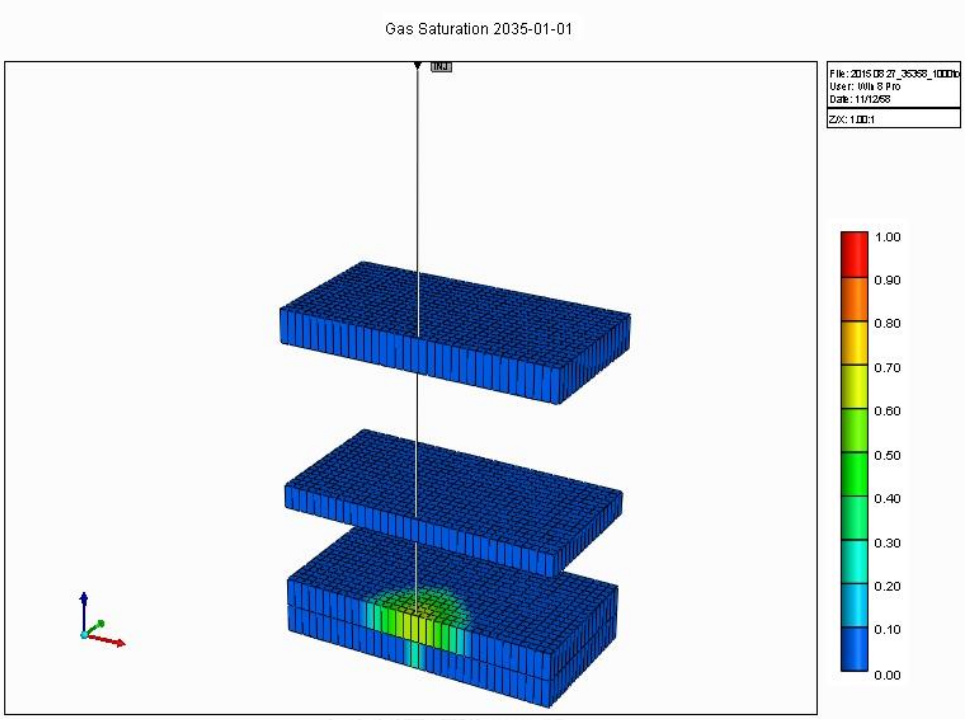

b.

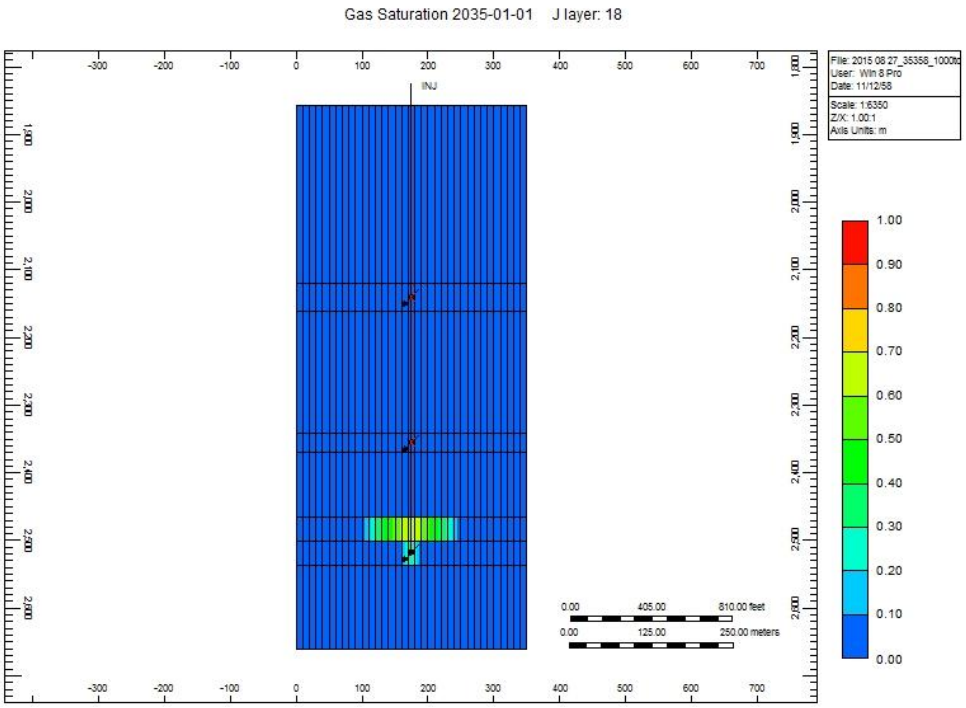

Figure B 19 (a) 3D view, 20 year injection and (b) side view, 20 year injection at. all layer

a.

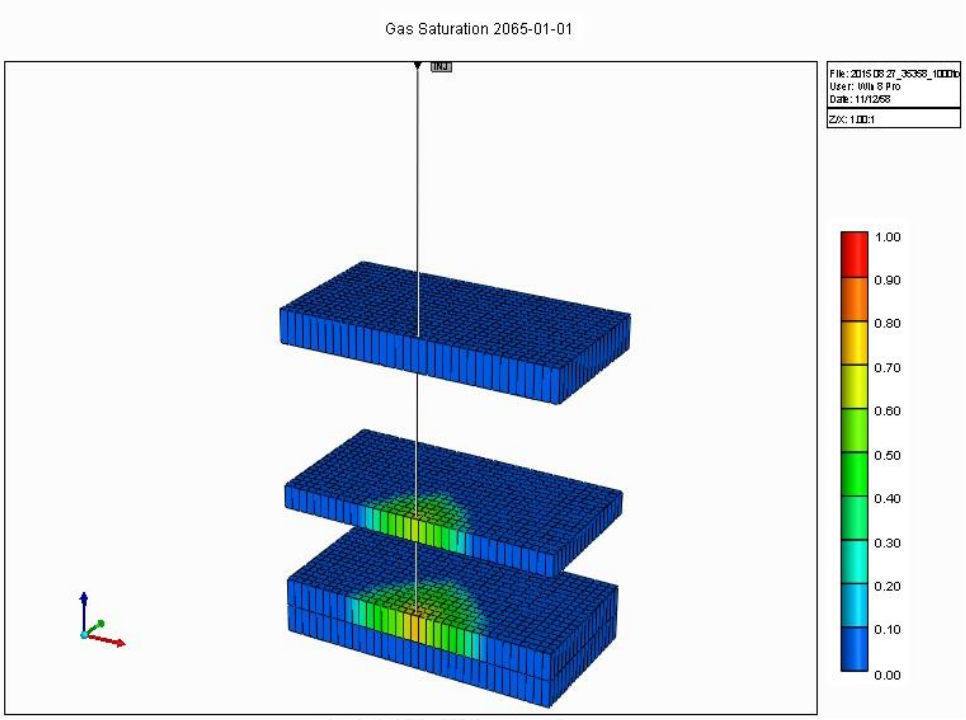

b.

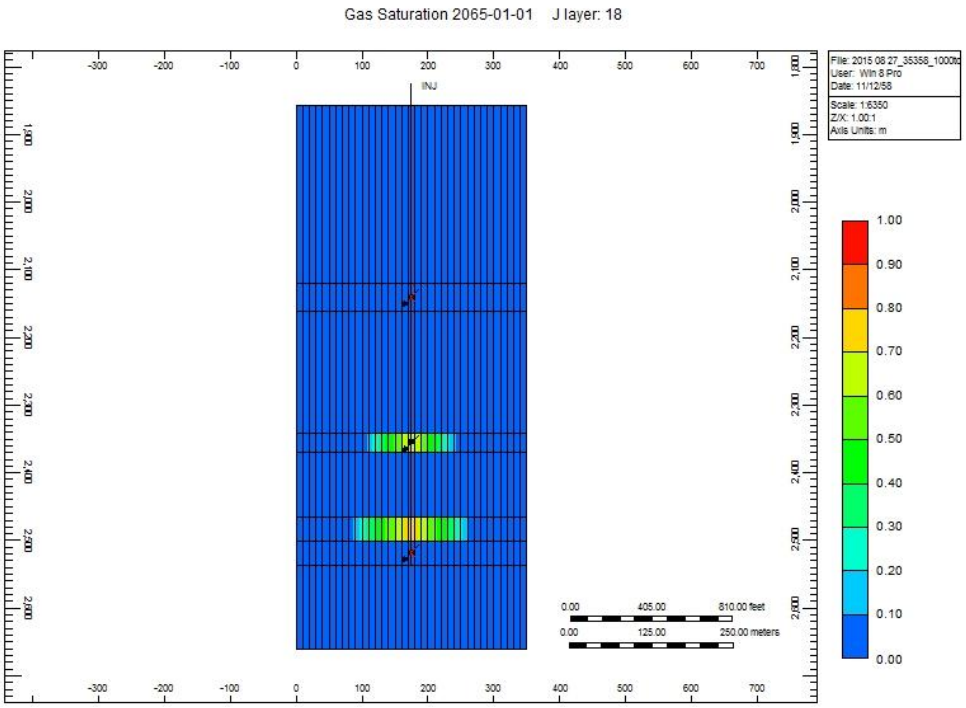

Figure B 20 (a) 3D view, 50 year injection and (b) side view, 50 year injection at. all layer

FA-SS-35-04 at the rate of injection at 2000 tons/day

a.

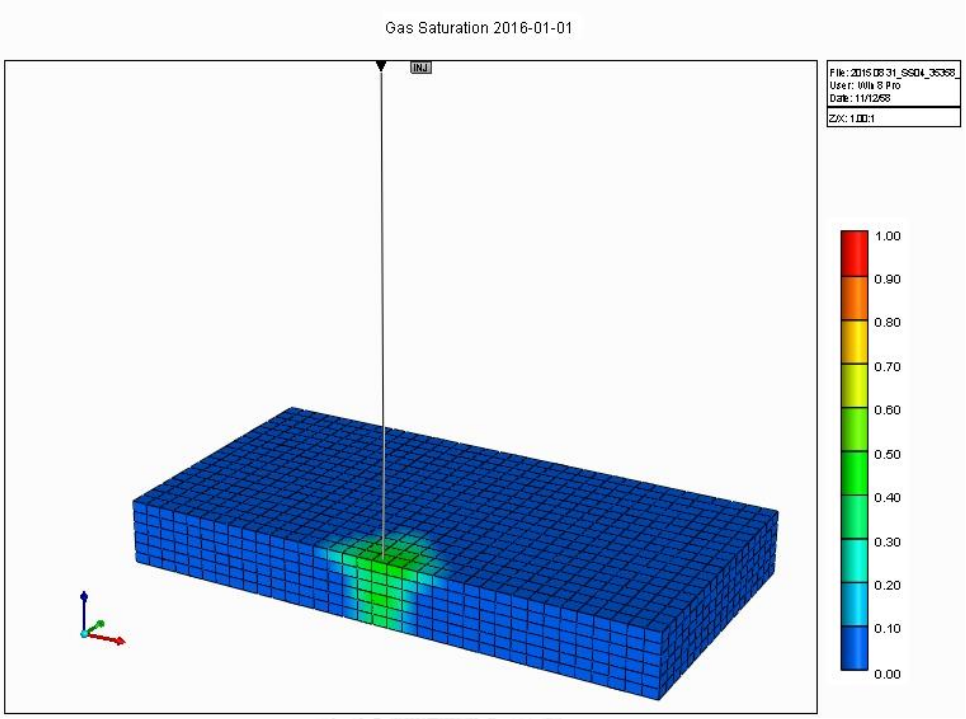

b.

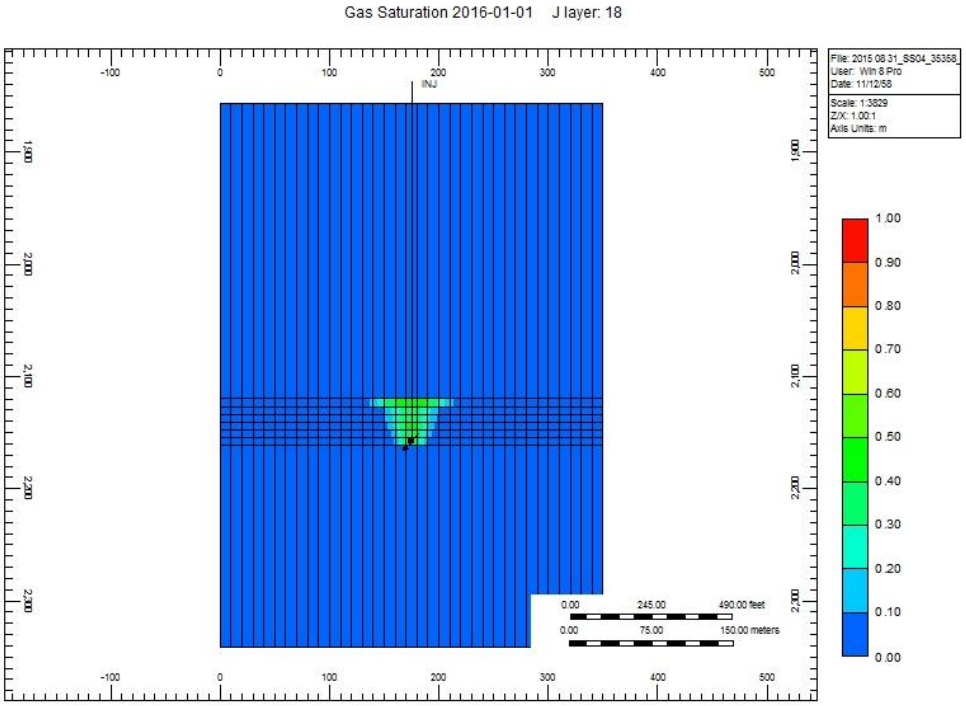

Figure B 1 (a) 3D view, 1 year injection and (b) side view, 1 year injection at. 2119.88-2161.03 m.

a.

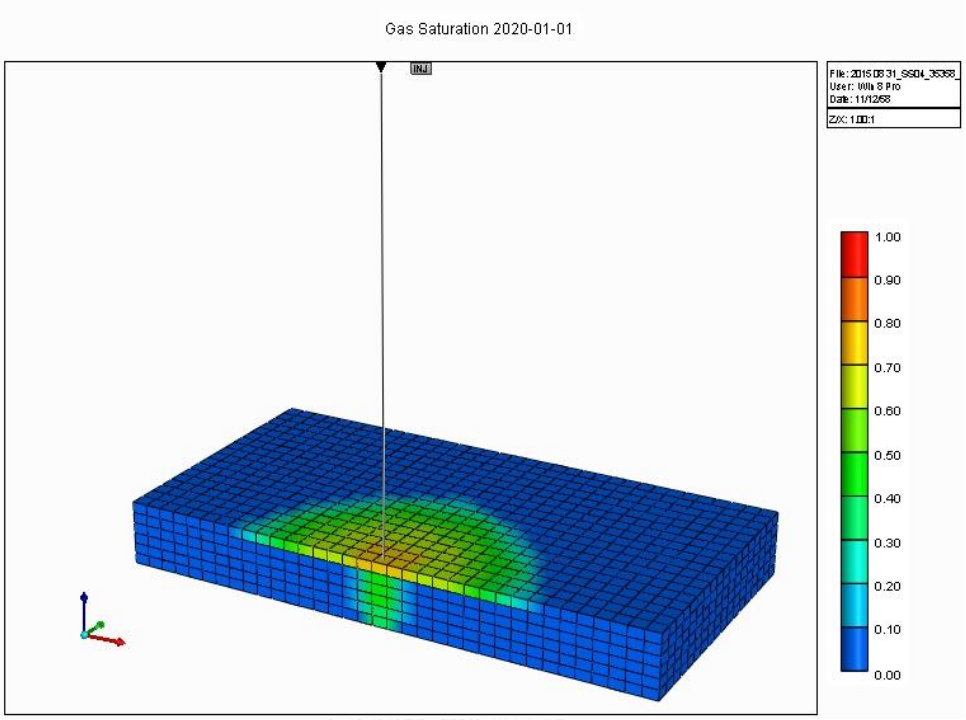

b.

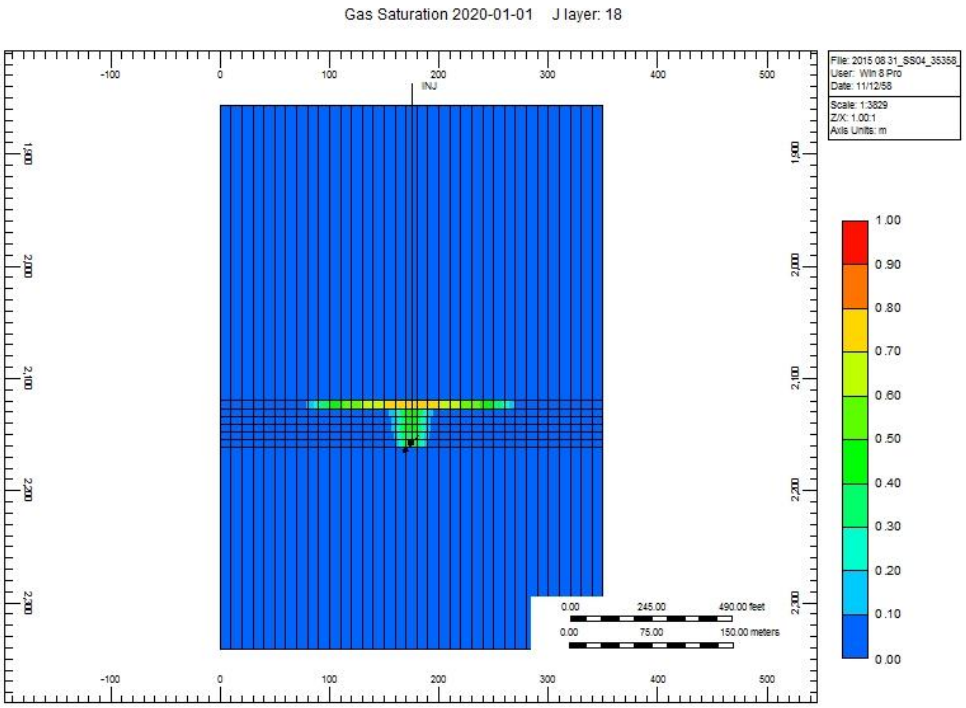

Figure B 22 (a) 3D view, 5 year injection and (b) side view, 5 year injection at. 2119.88-2161.03 m.

a.

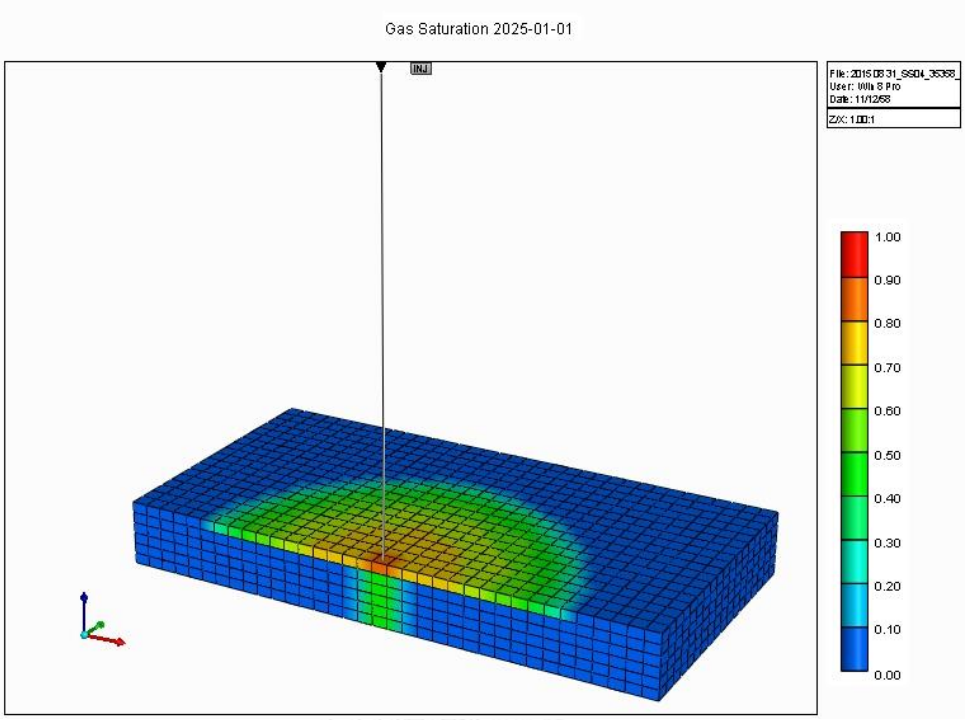

b.

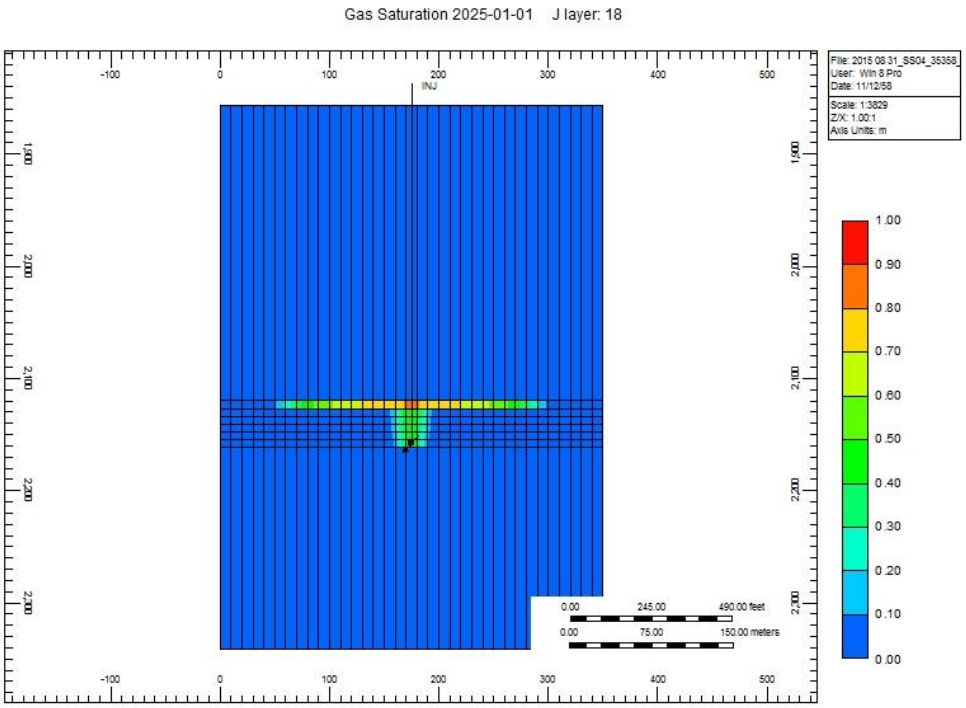

Figure B 23 (a) 3D view, 10 year injection and (b) side view, 10 year injection at. 2119.88-2161.03 m.

a.

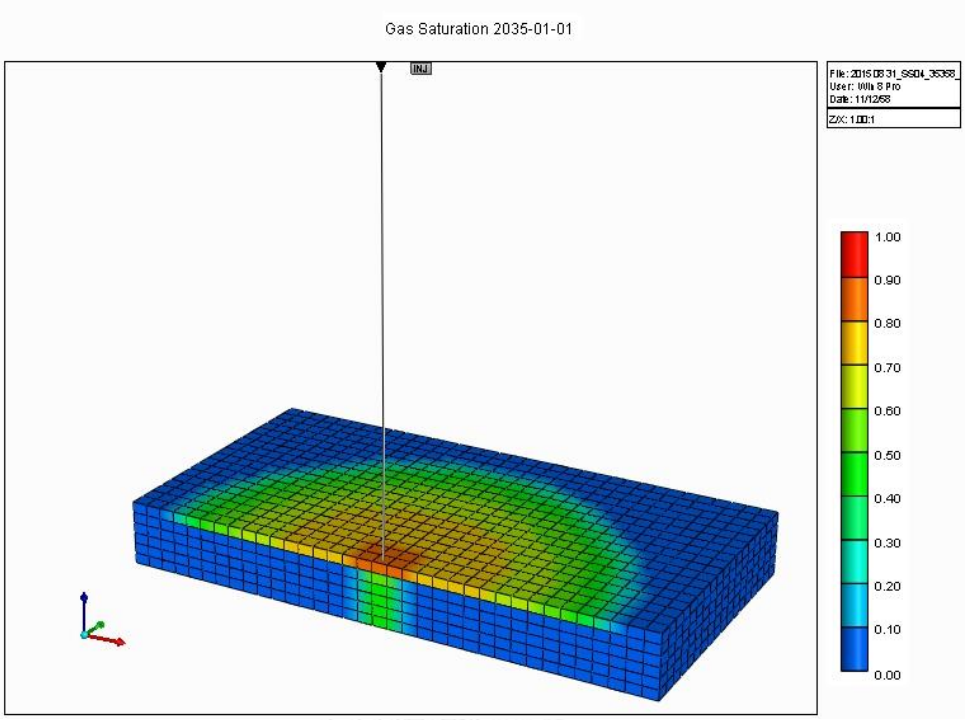

b.

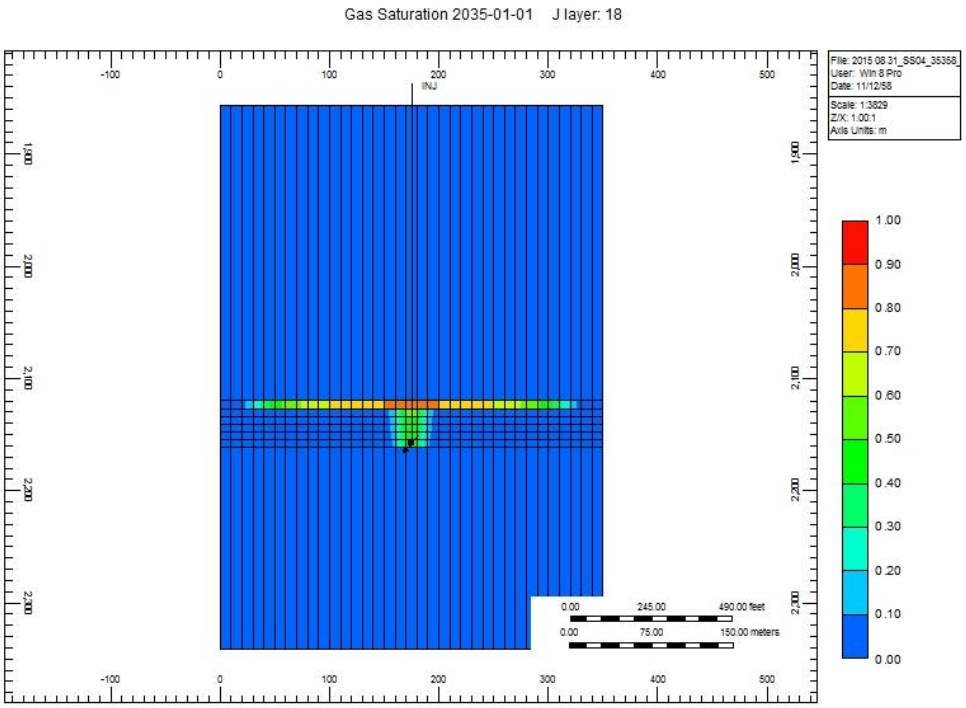

Figure B 24 (a) 3D view, 20 year injection and (b) side view, 20 year injection at. 2119.88-2161.03 m.

a.

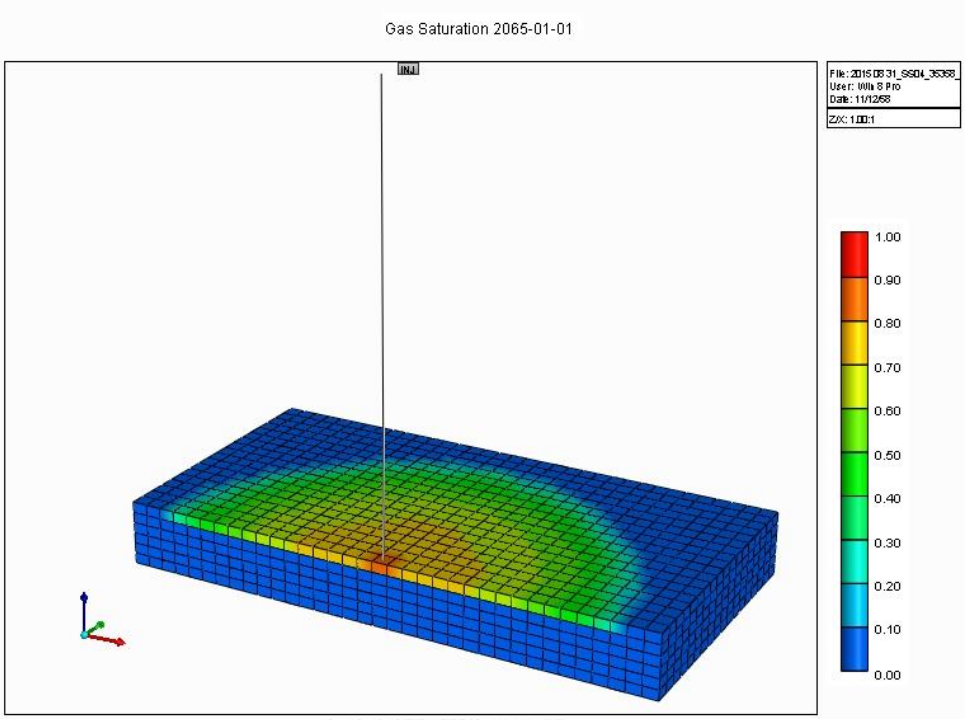

b.

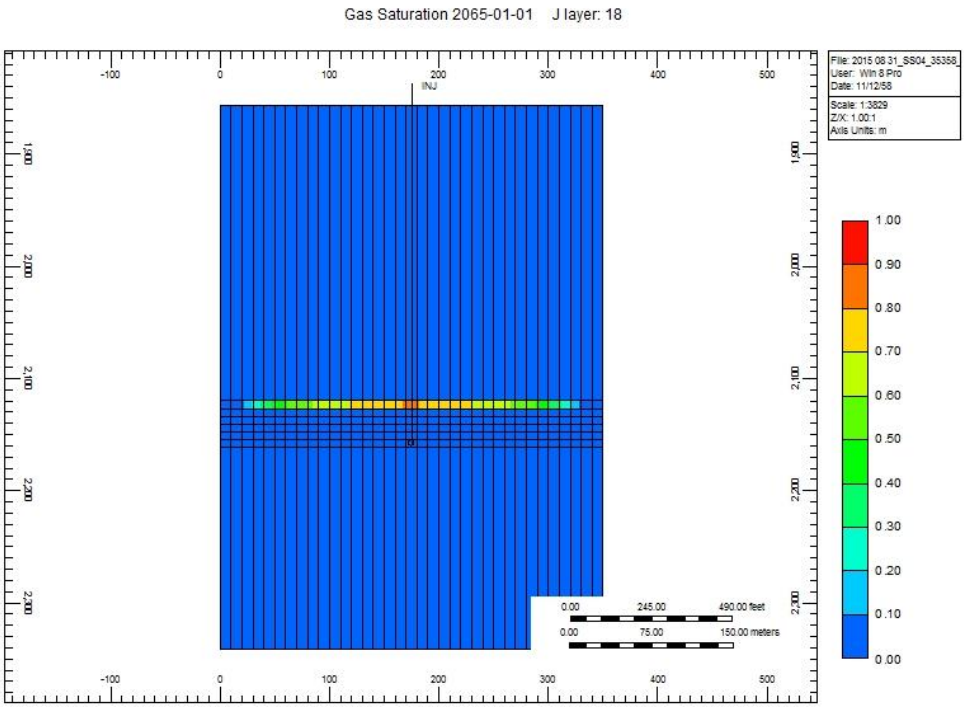

Figure B 25 (a) 3D view, 50 year injection and (b) side view, 50 year injection at. 2119.88-2161.03 m.

a.

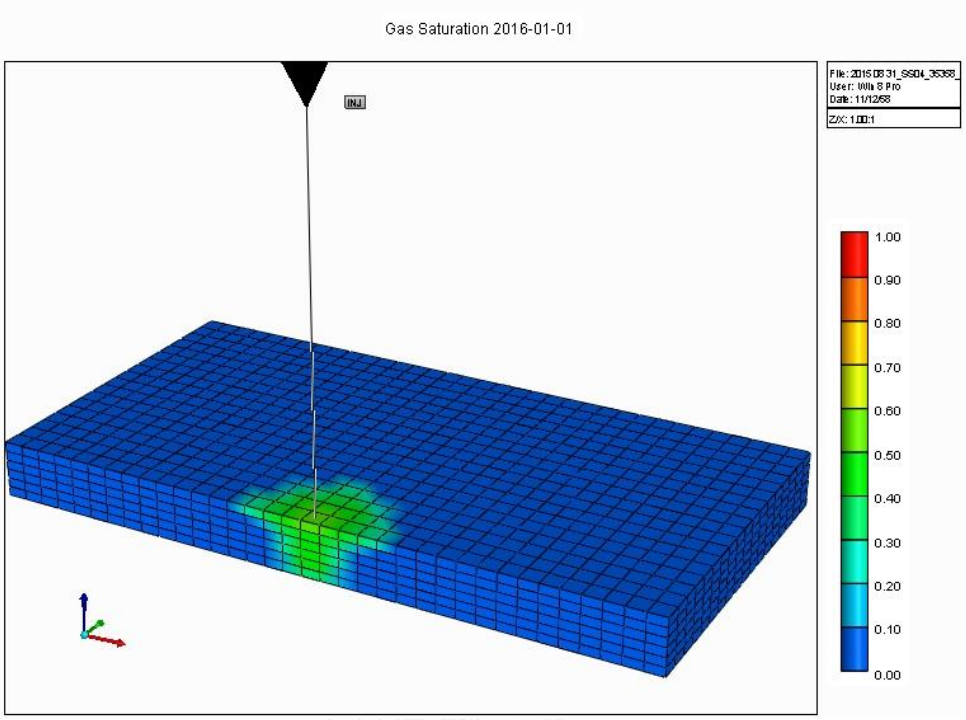

b.

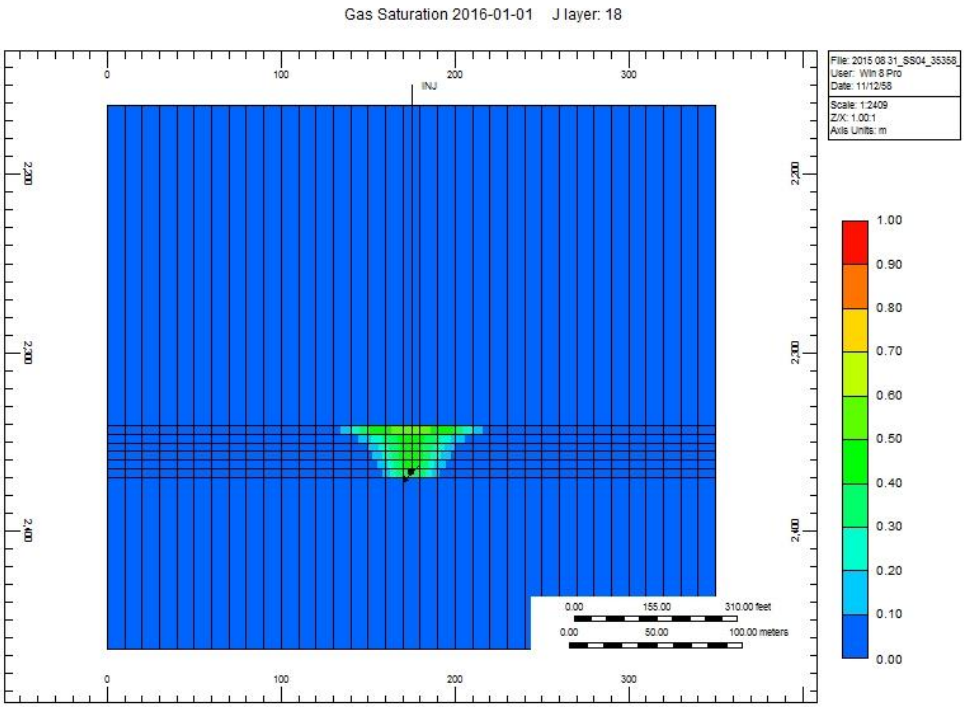

Figure B 26 (a) 3D view, 1 year injection and (b) side view, 1 year injection at. 2340.86-2369.82 m.

a.

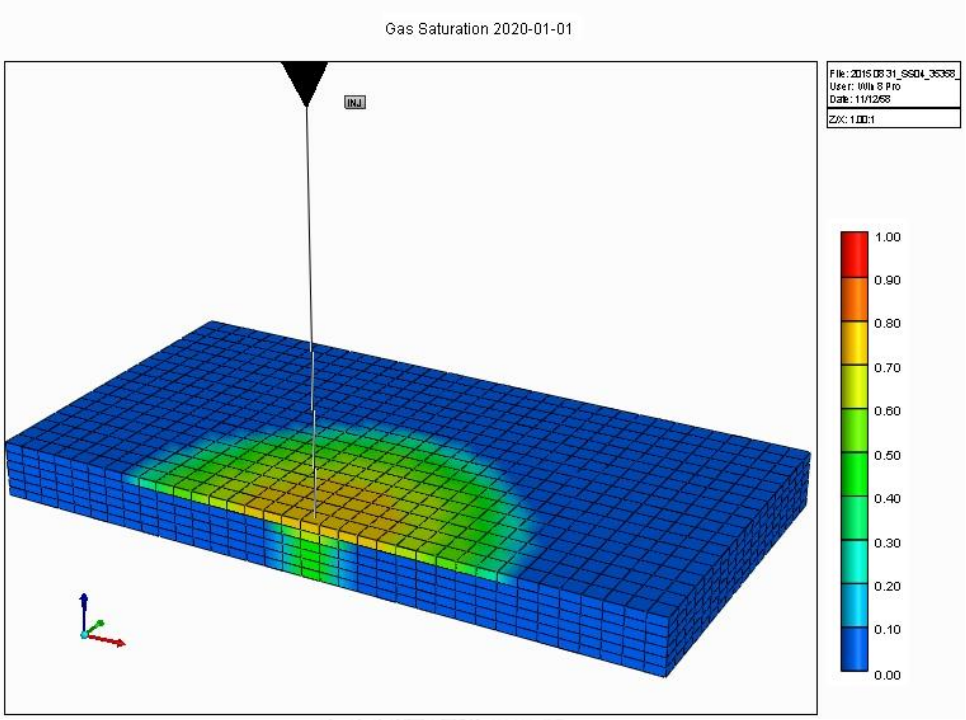

b.

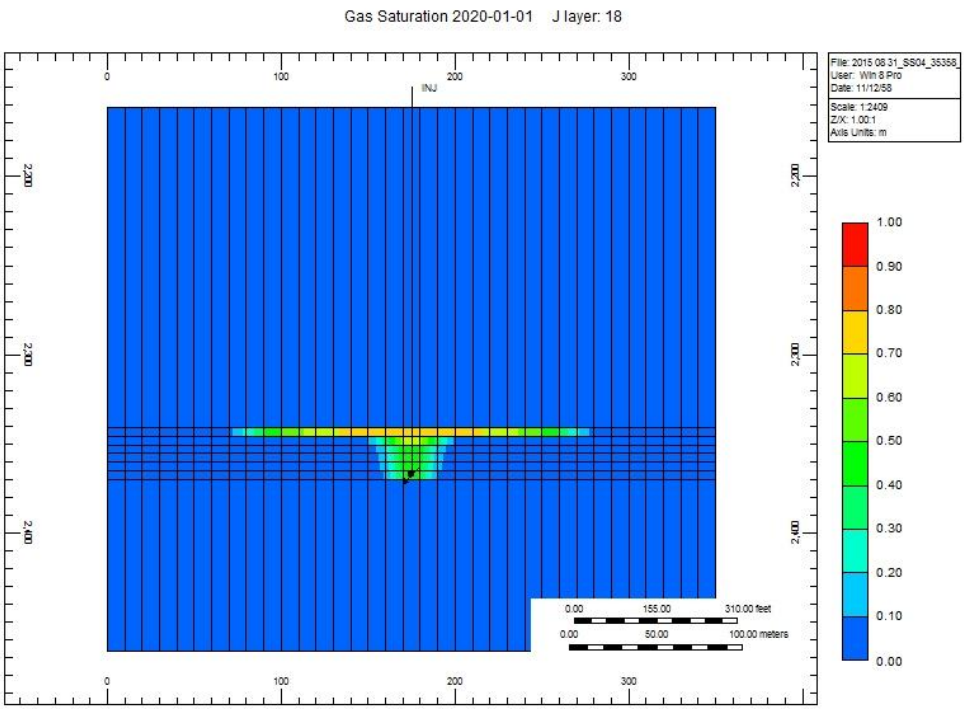

Figure B 27 (a) 3D view, 5 year injection and (b) side view, 5 year injection at. 2340.86-2369.82 m.

a.

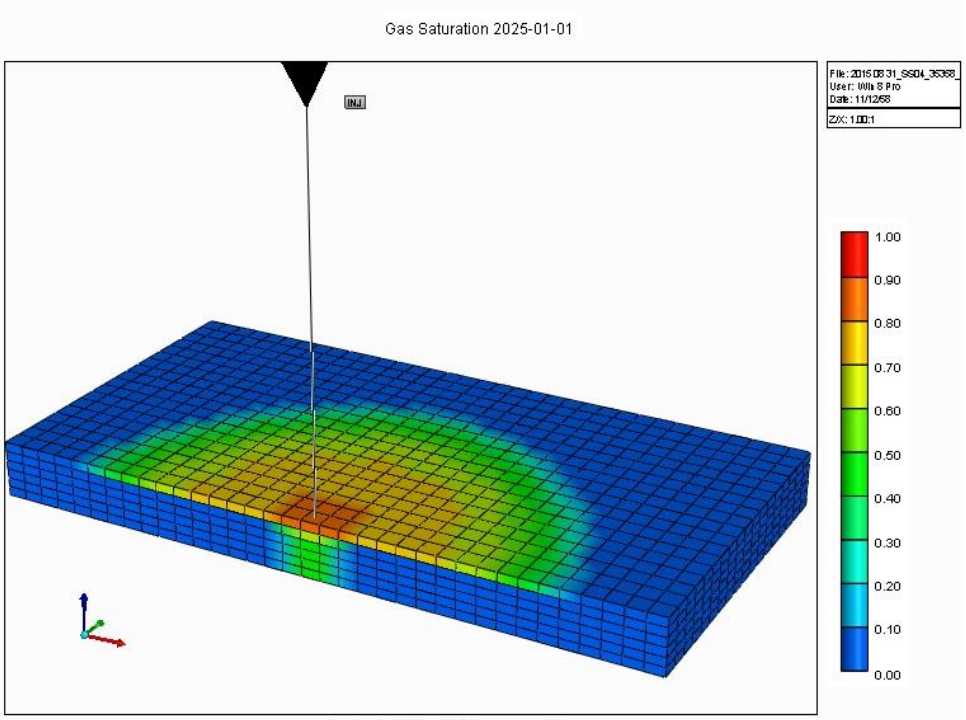

b.

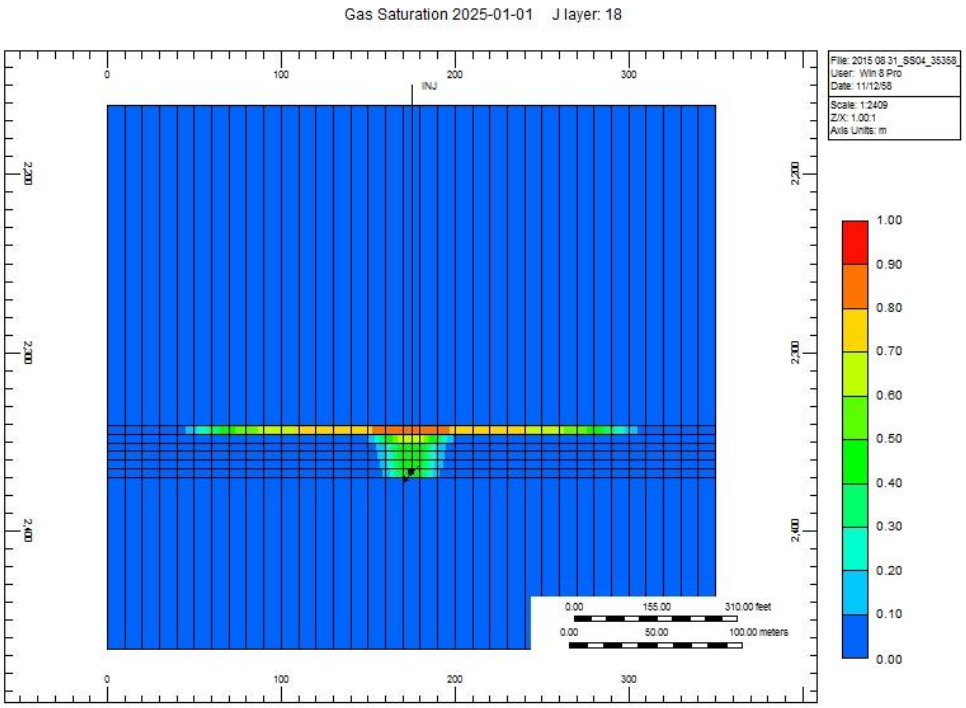

Figure B 28 (a) 3D view, 10 year injection and (b) side view, 10 year injection at. 2340.86-2369.82 m.

a.

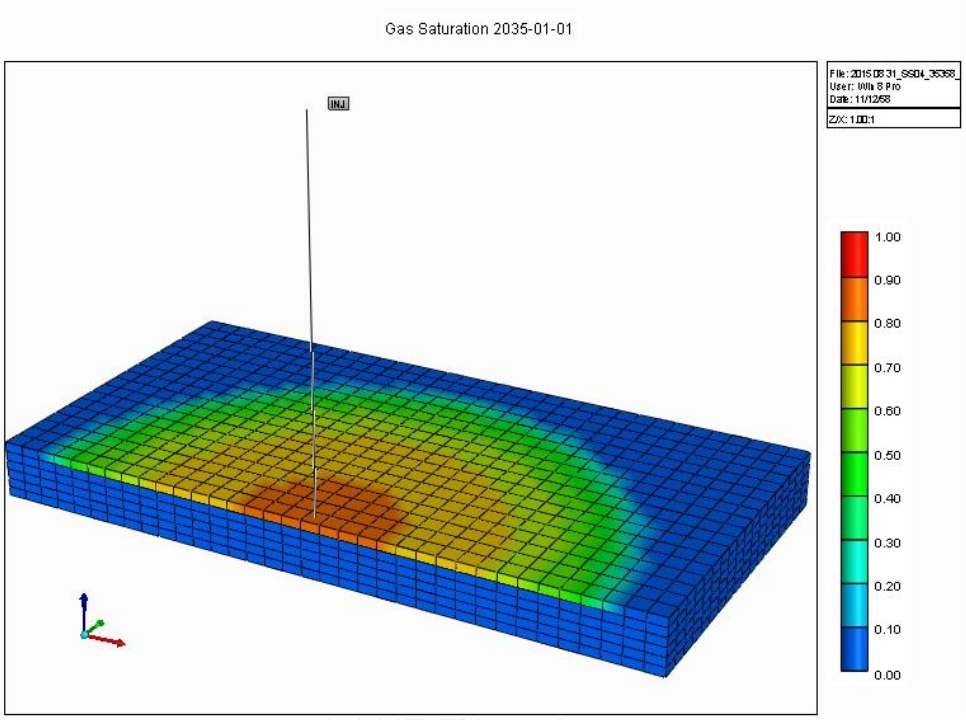

b.

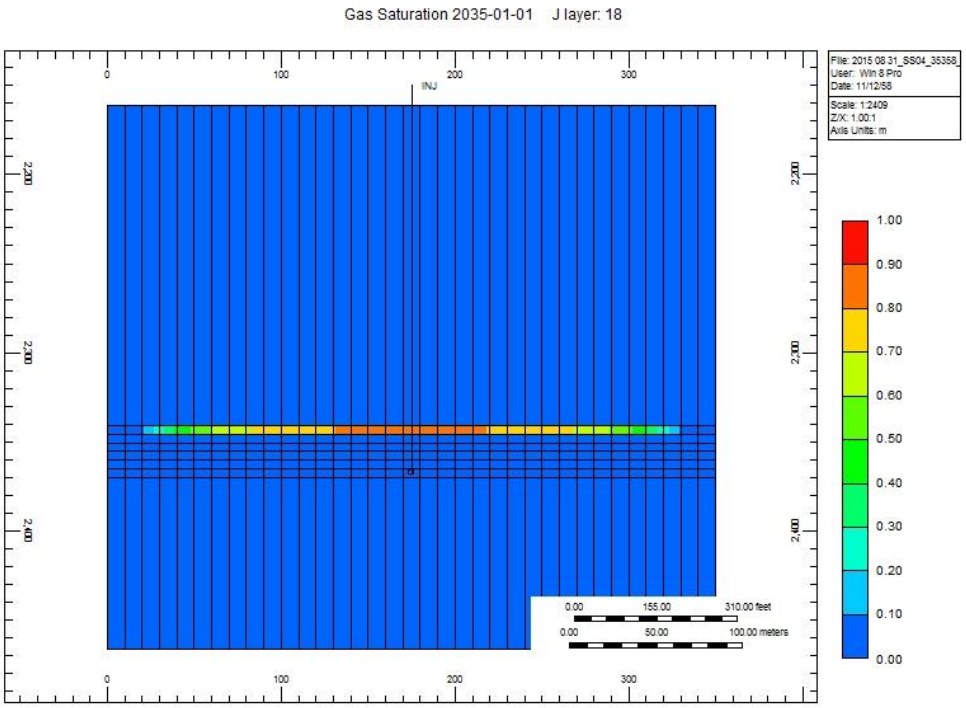

Figure B 29 (a) 3D view, 20 year injection and (b) side view, 20 year injection at. 2340.86-2369.82 m.

a.

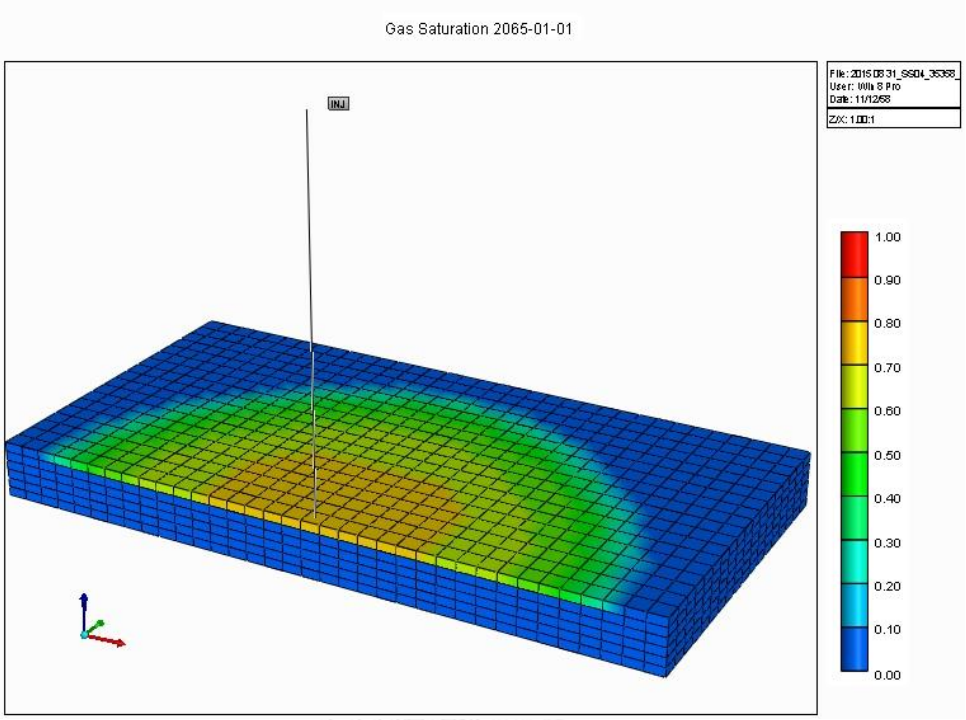

b.

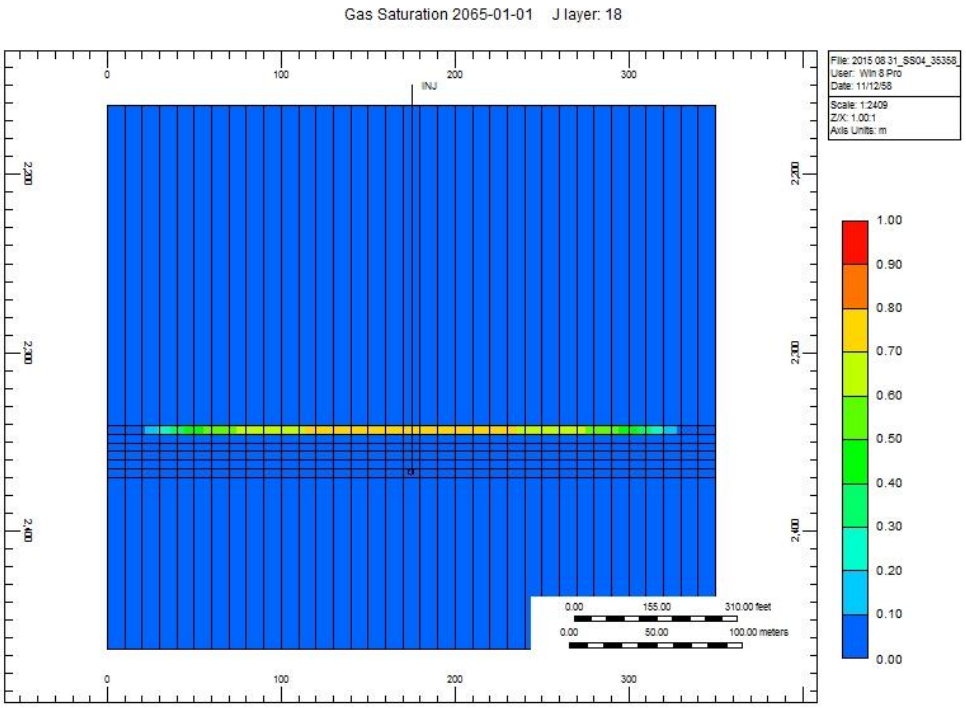

Figure B 30 (a) 3D view, 50 year injection and (b) side view, 50 year injection at. 2340.86-2369.82 m.

a.

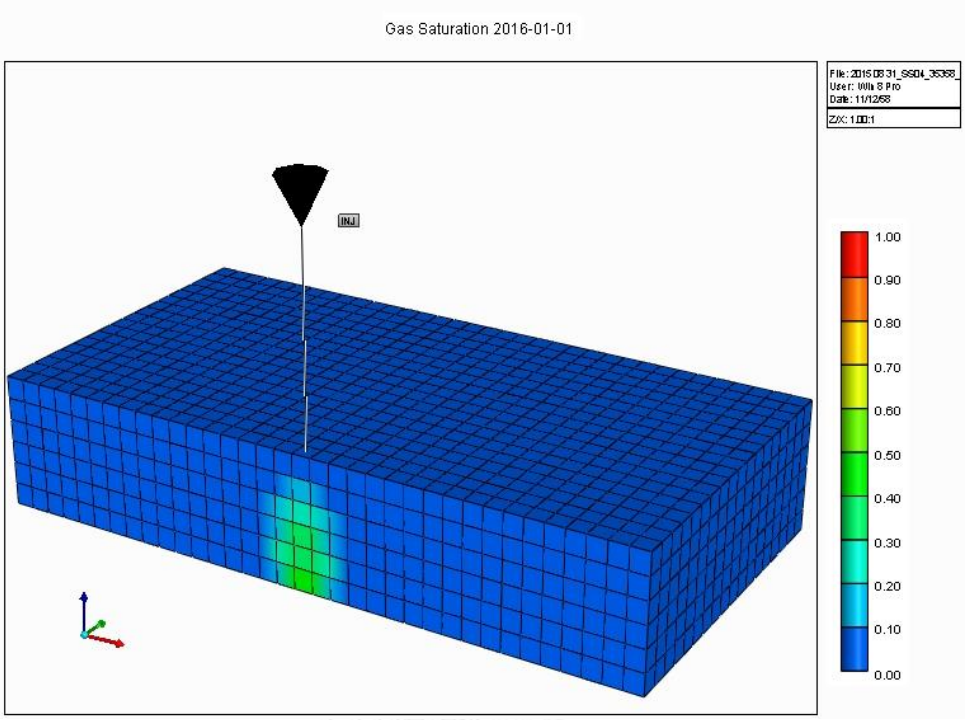

b.

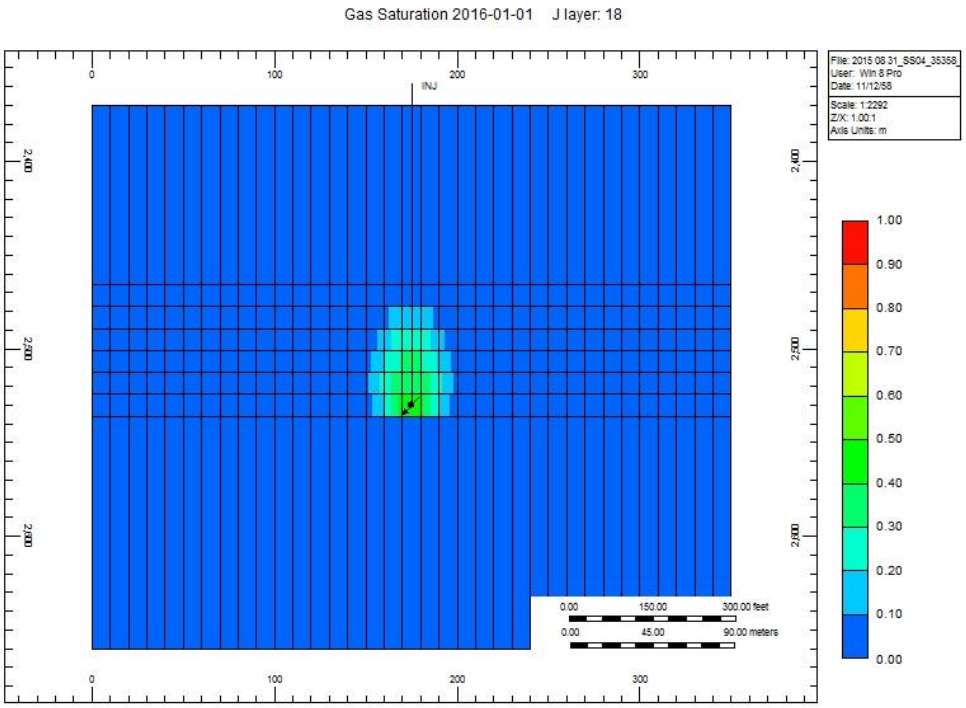

Figure B 31 (a) 3D view, 1 year injection and (b) side view, 1 year injection at. 2465.83-2535.94 m.

a.

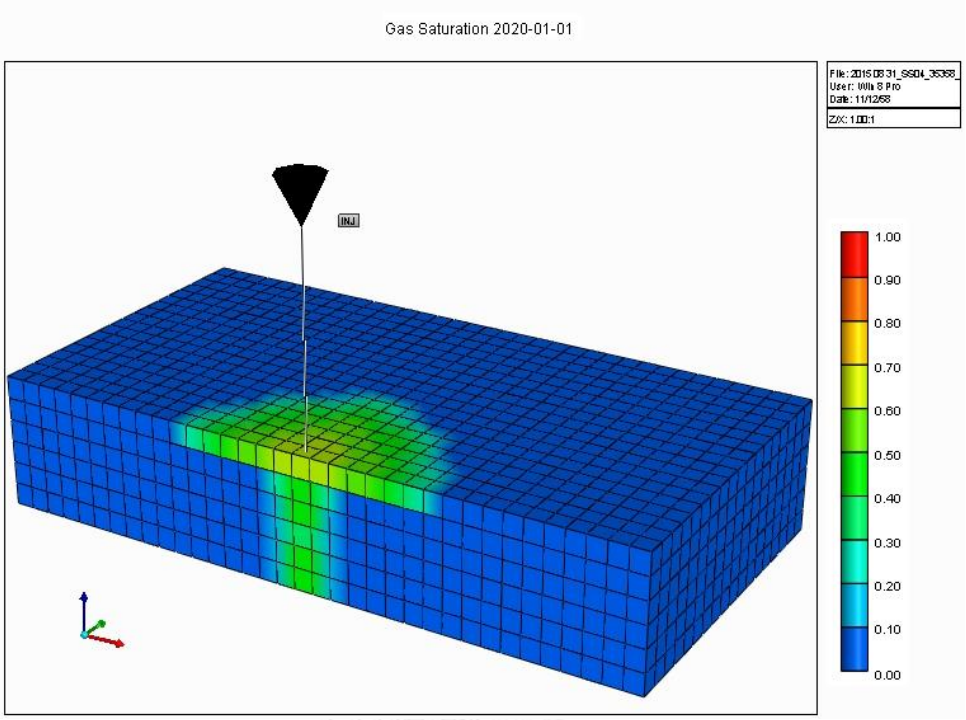

b.

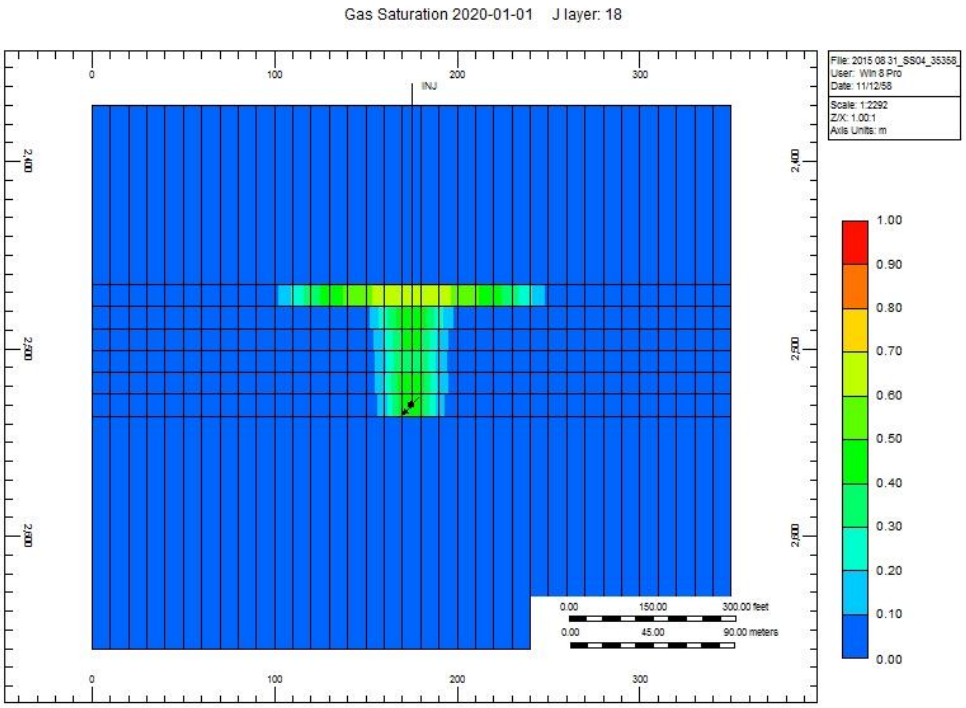

Figure B 32 (a) 3D view, 5 year injection and (b) side view, 5 year injection at. 2465.83-2535.94 m.

a.

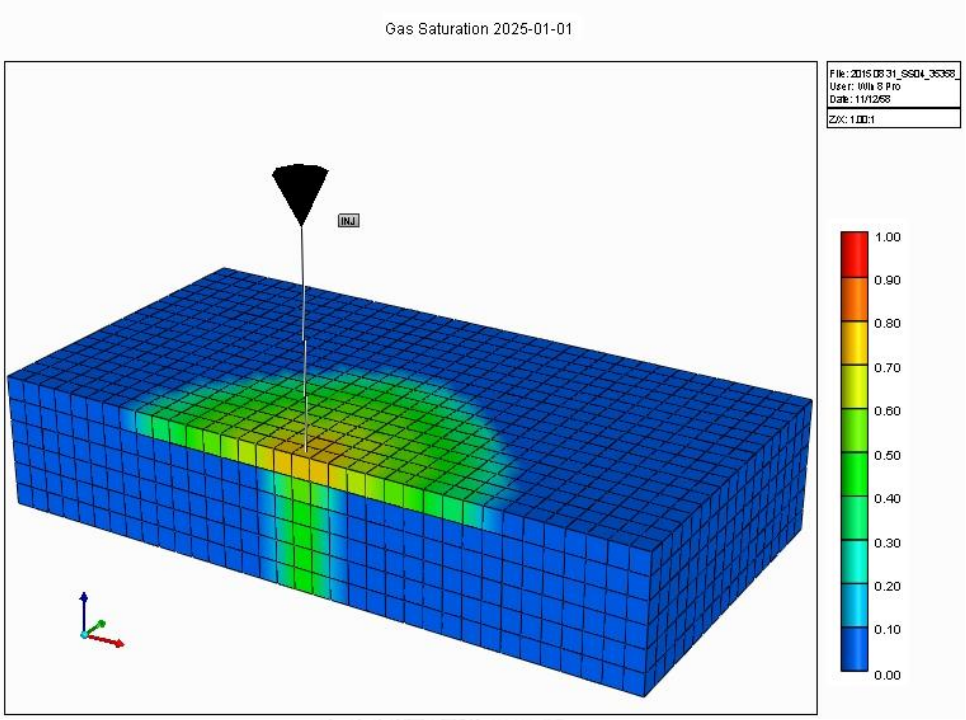

b.

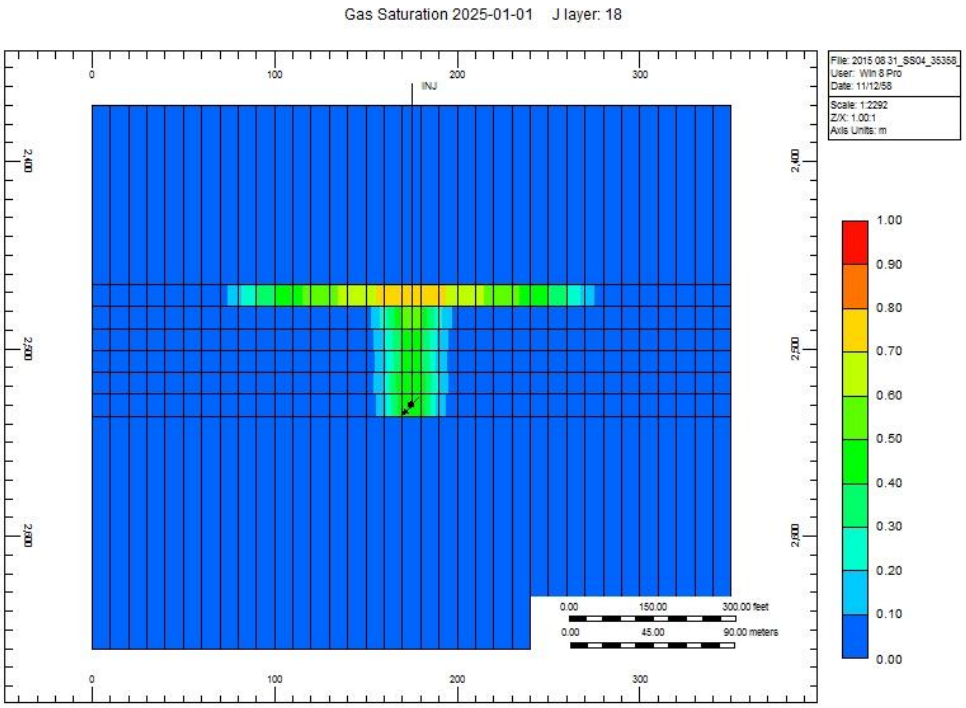

Figure B 33 (a) 3D view, 10 year injection and (b) side view, 10 year injection at. 2465.83-2535.94 m.

a.

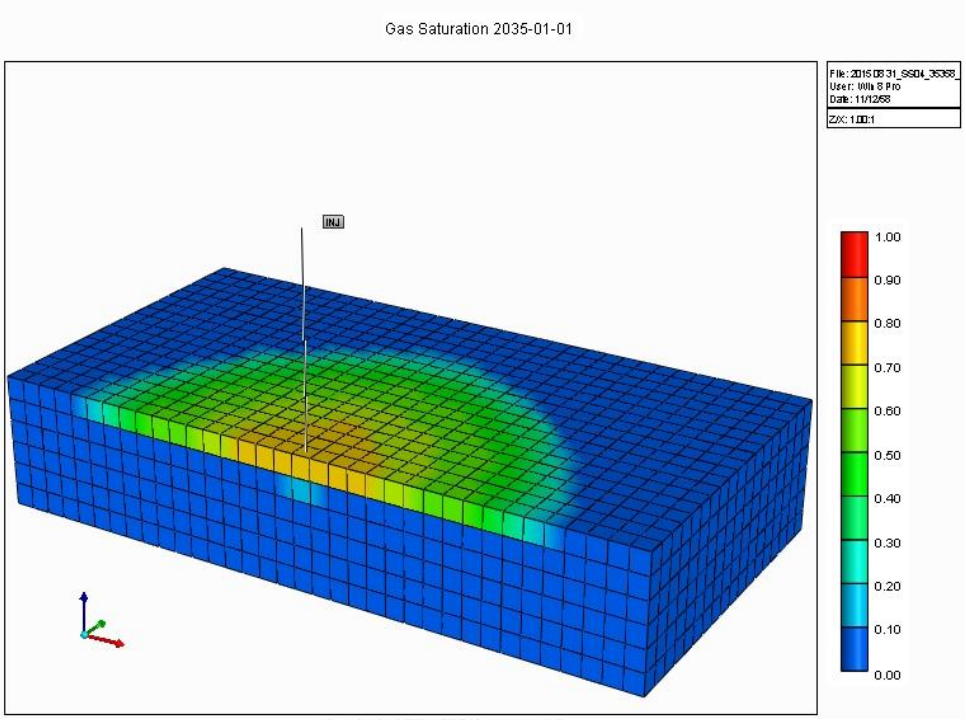

b.

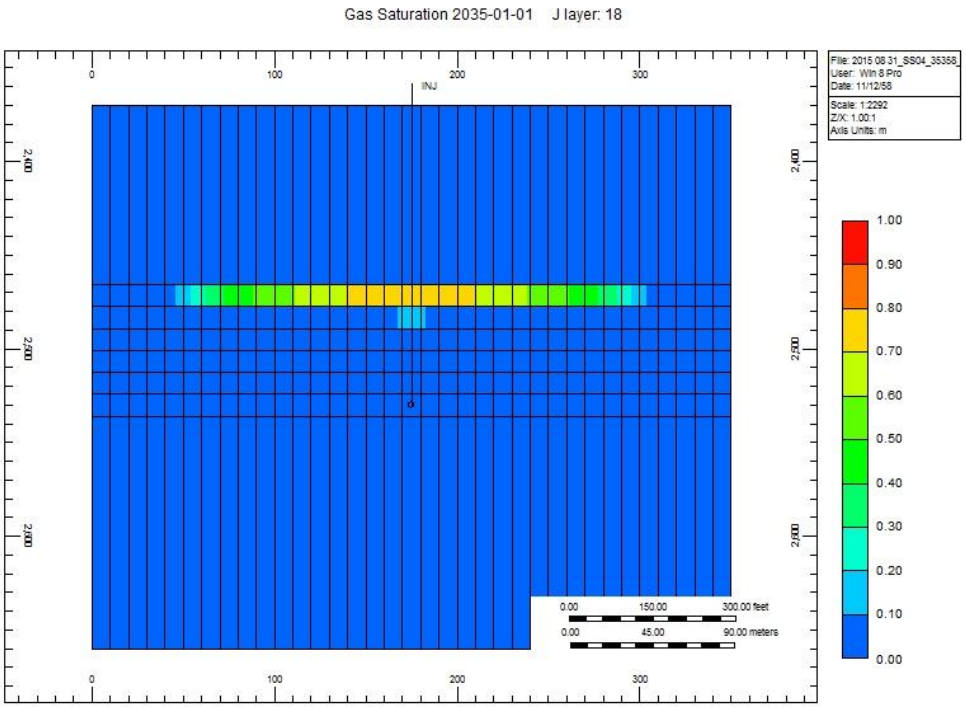

Figure B 34 (a) 3D view, 20 year injection and (b) side view, 20 year injection at. 2465.83-2535.94 m.

a.

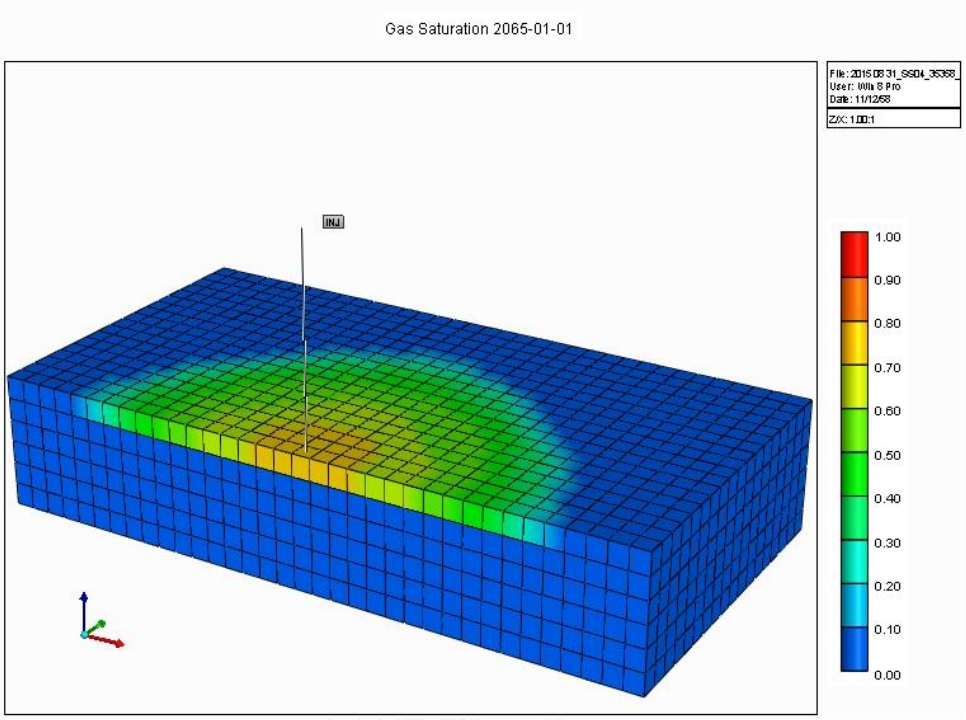

b.

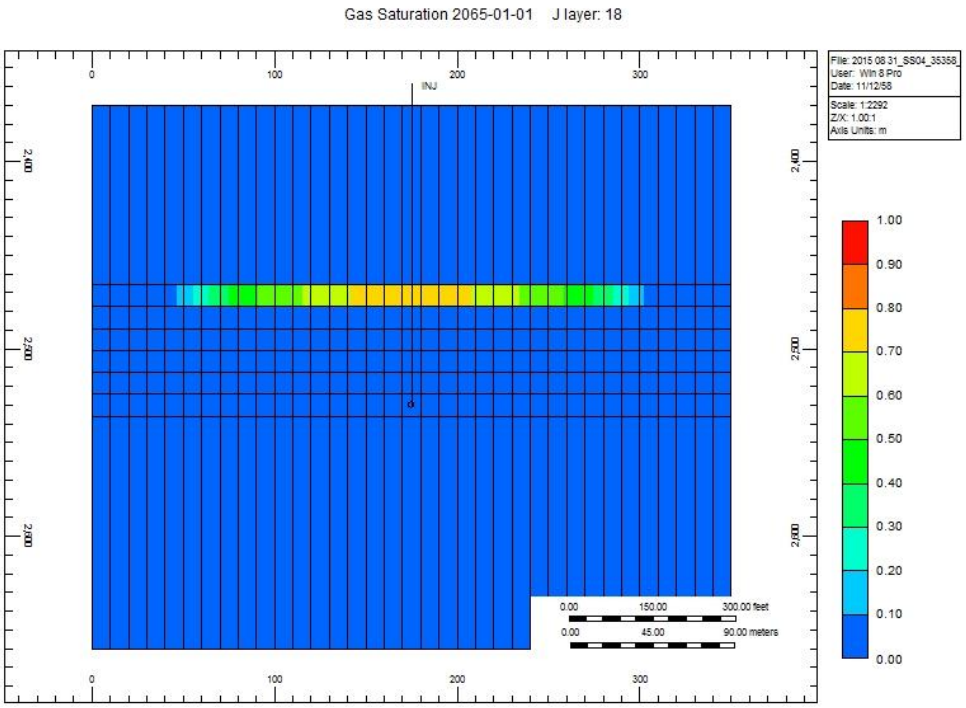

Figure B 35 (a) 3D view, 50 year injection and (b) side view, 50 year injection at. 2465.83-2535.94 m.

a.

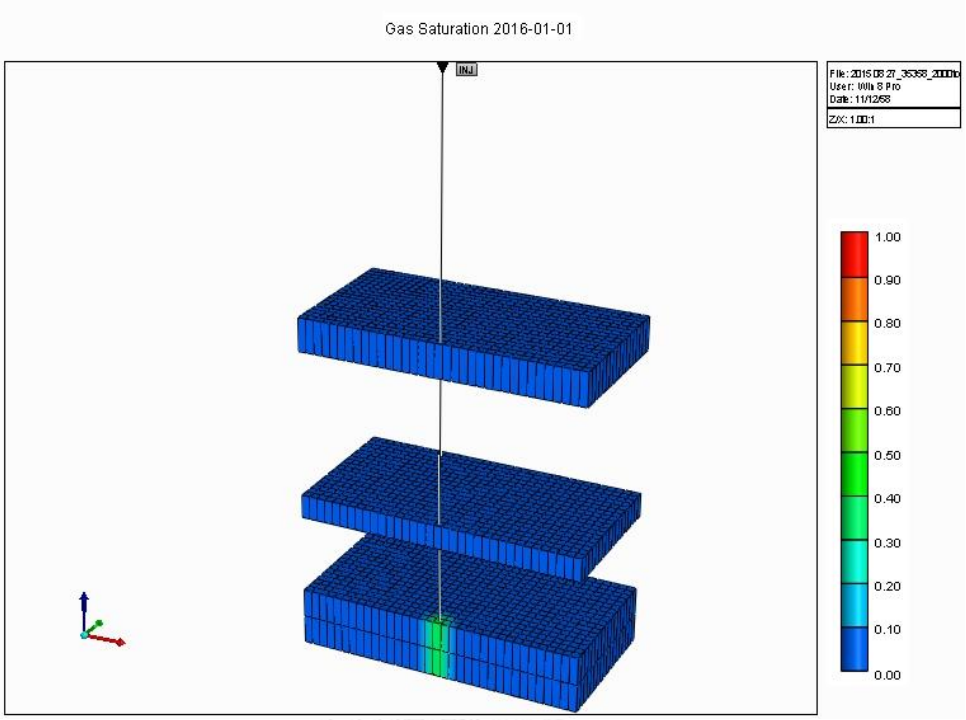

b.

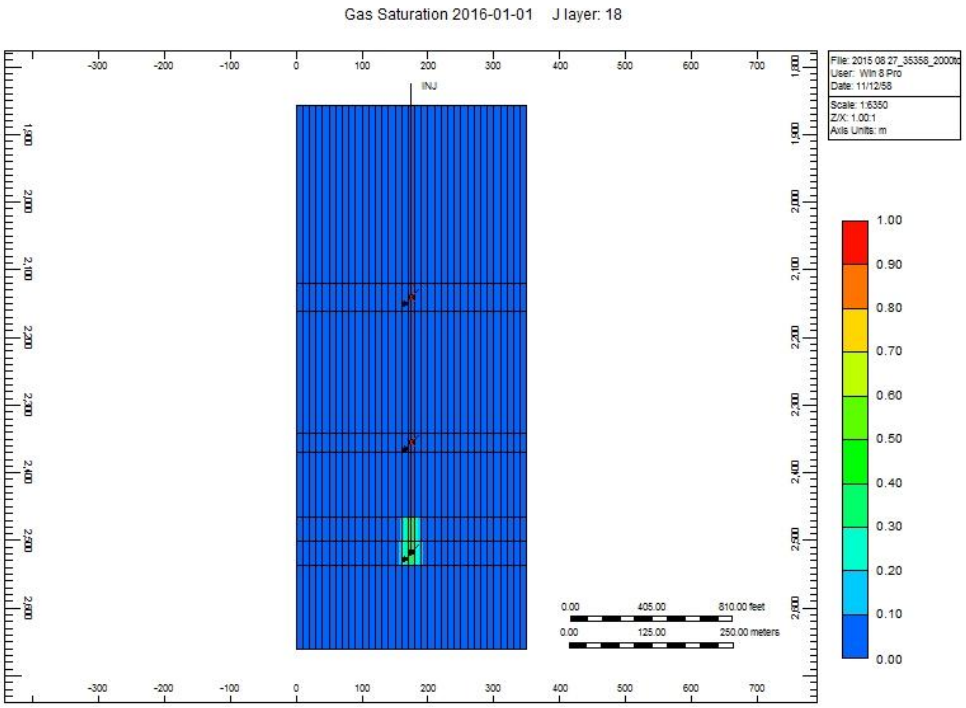

Figure B 36 (a) 3D view, 1 year injection and (b) side view, 1 year injection at. all layer.

a.

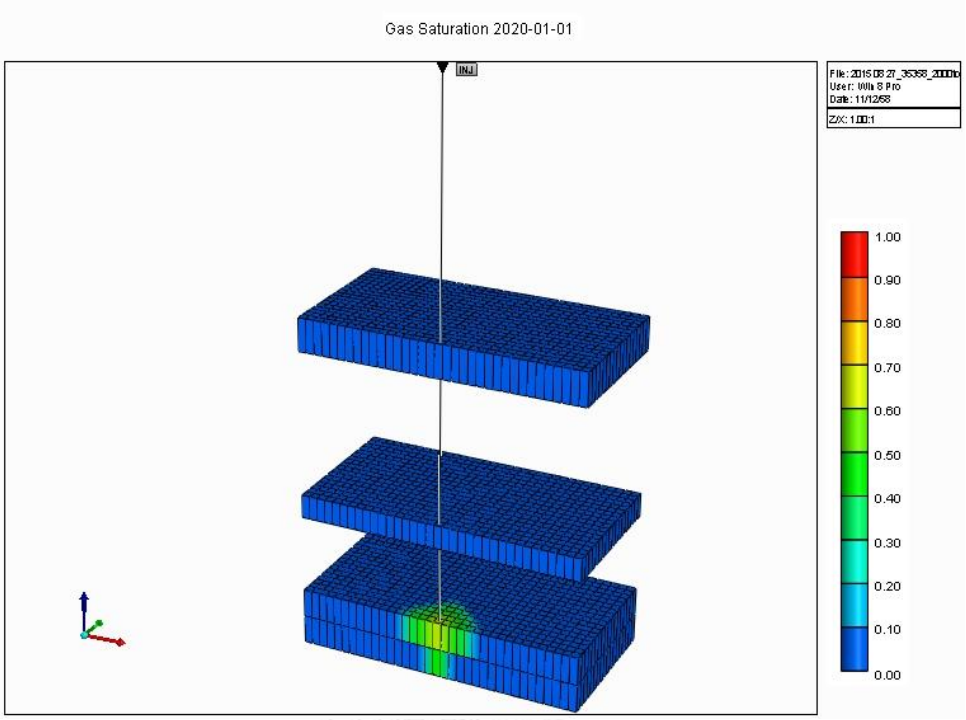

b.

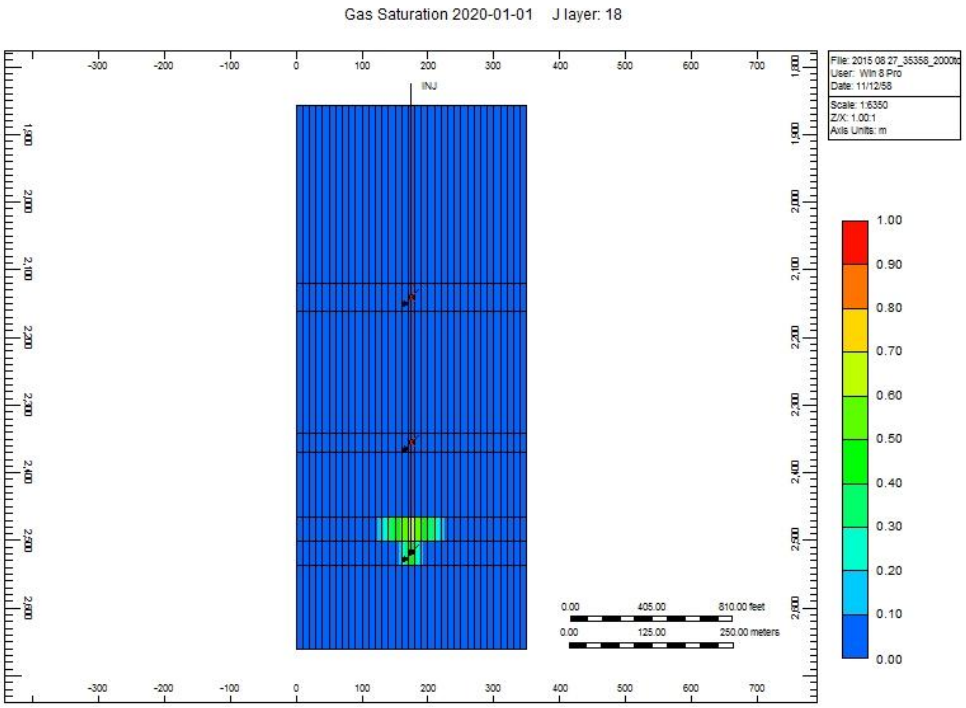

Figure B 37 (a) 3D view, 5 year injection and (b) side view, 5 year injection at. all layer

a.

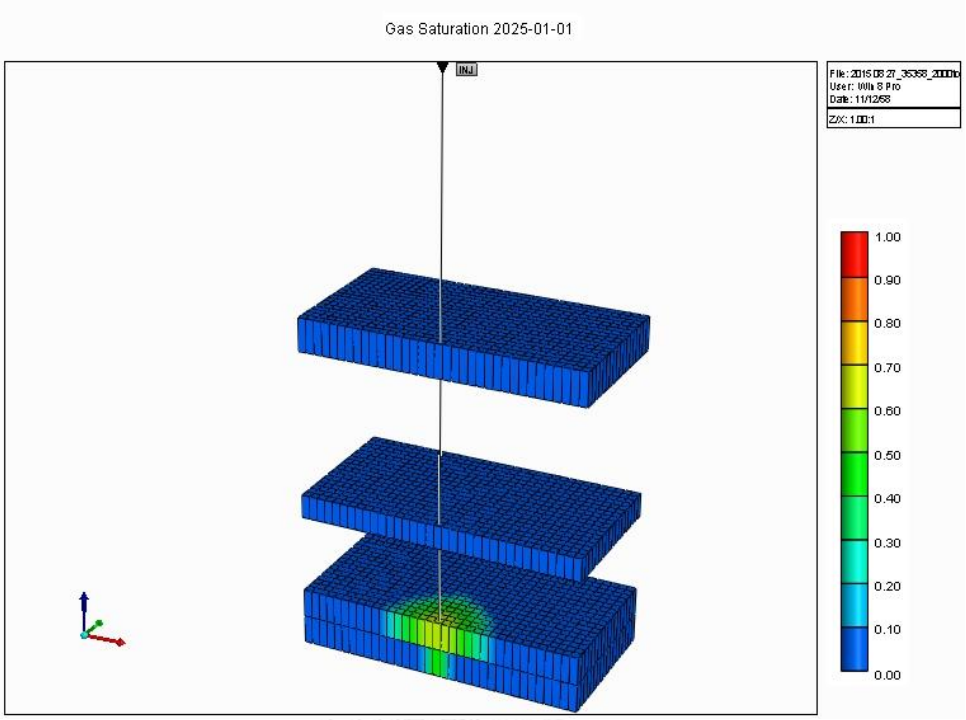

b.

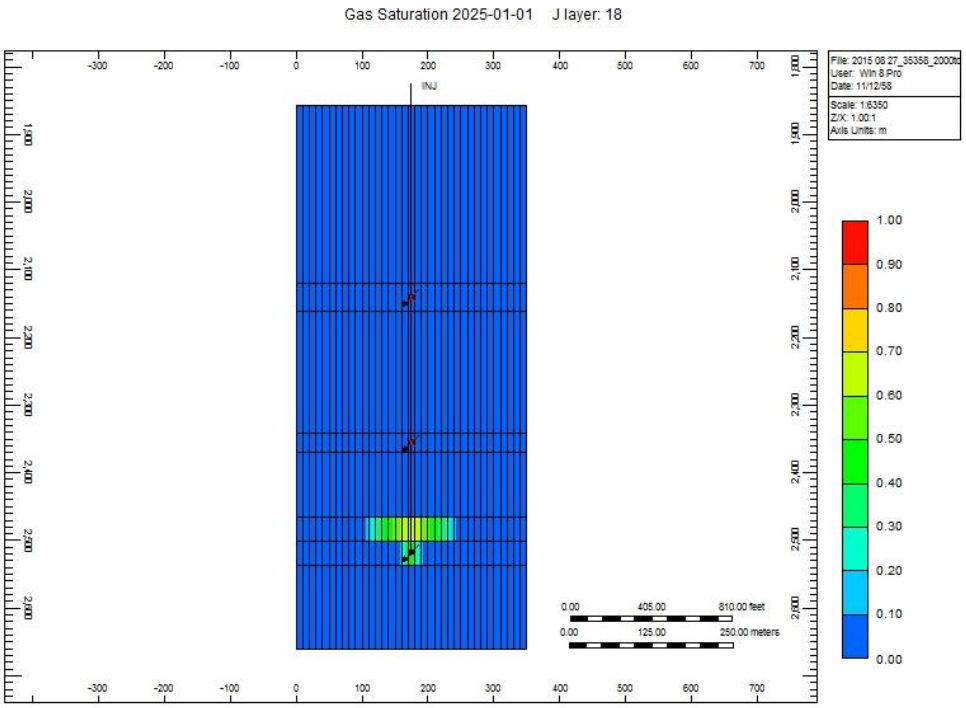

Figure B 38 (a) 3D view, 10 year injection and (b) side view, 10 year injection at. all layer

a.

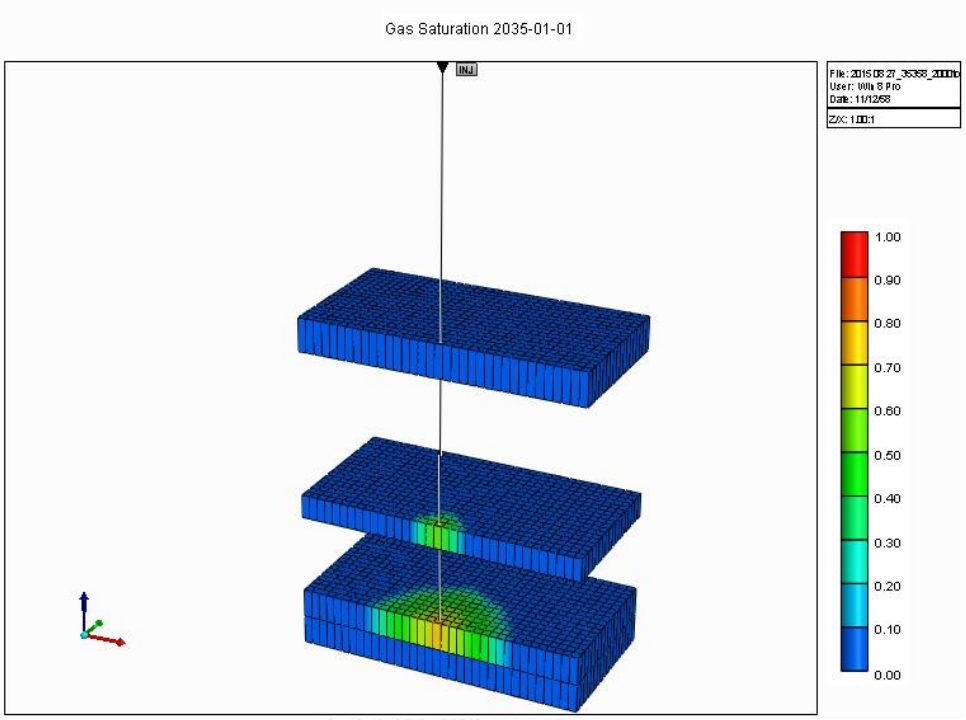

b.

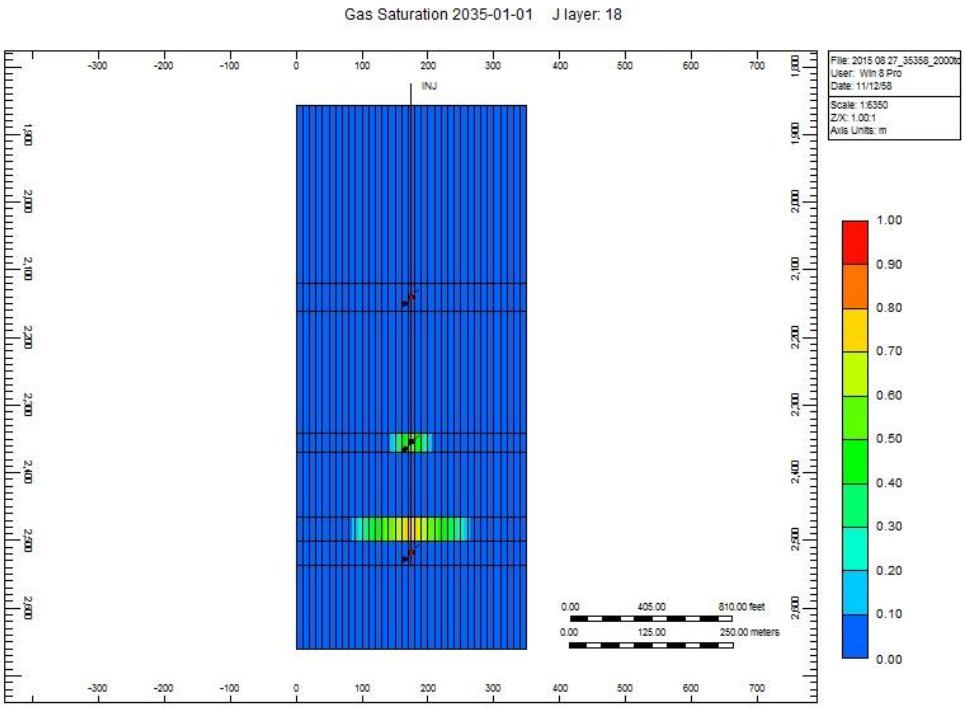

Figure B 39 (a) 3D view, 20 year injection and (b) side view, 20 year injection at. all layer

a.

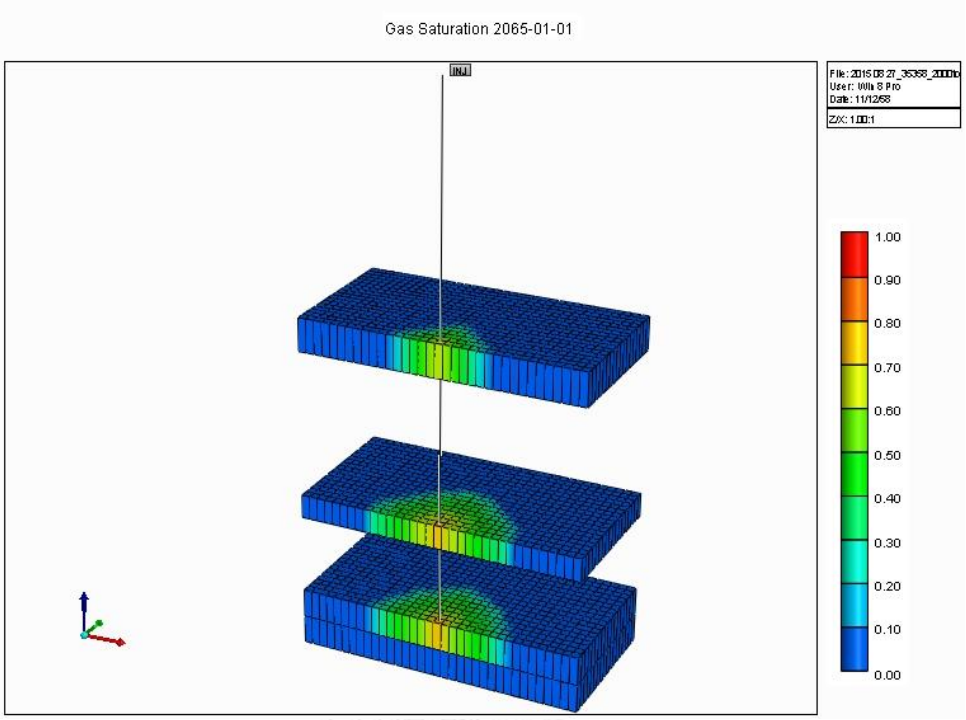

b.

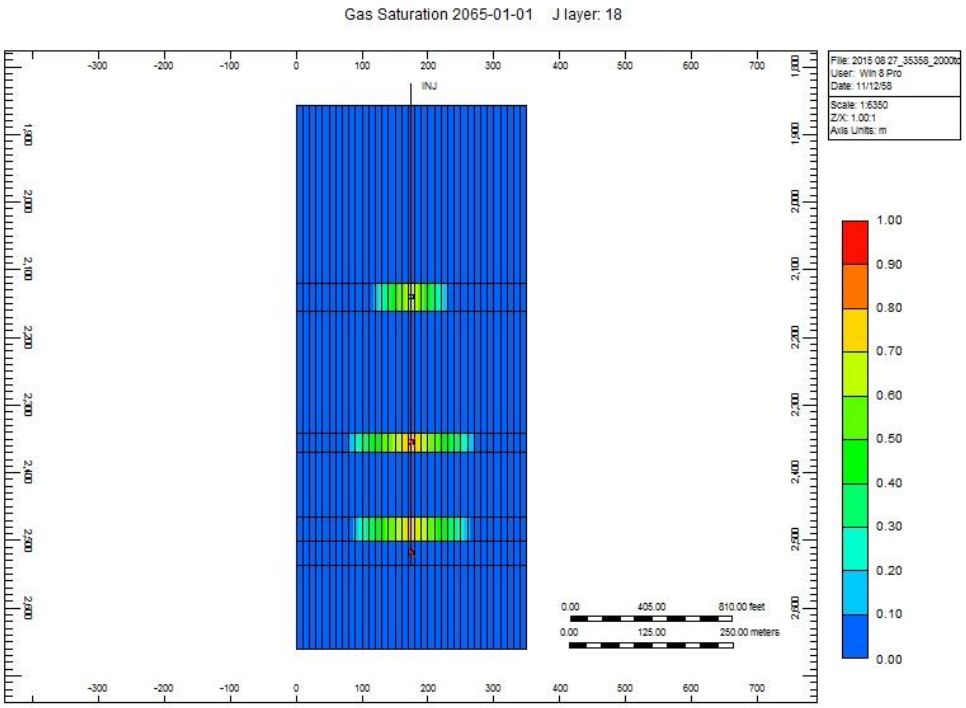

Figure B 40 (a) 3D view, 50 year injection and (b) side view, 50 year injection at. all layer

FA-SS-35-04 at the rate of injection at 4000 tons/day

a.

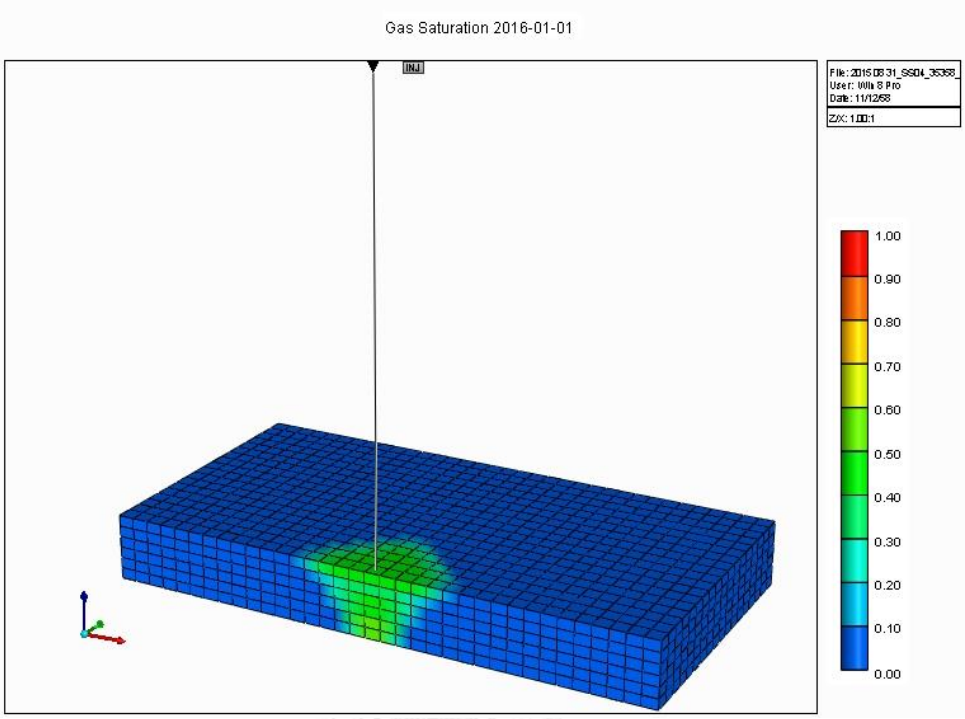

b.

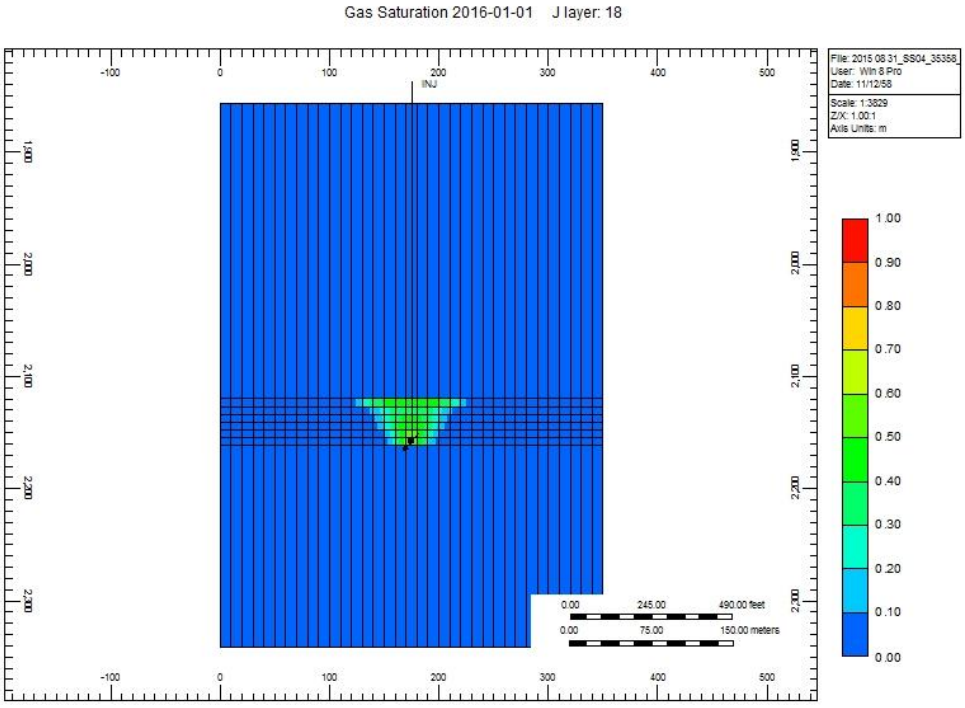

Figure B 41 (a) 3D view, 1 year injection and (b) side view, 1 year injection at. 2119.88-2161.03 m.

a.

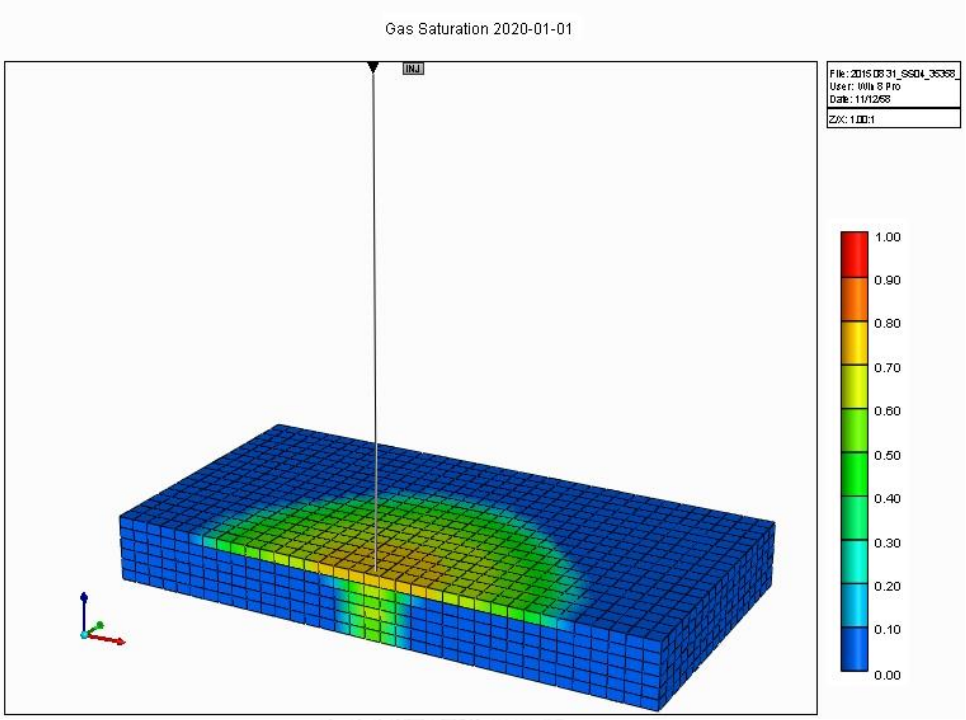

b.

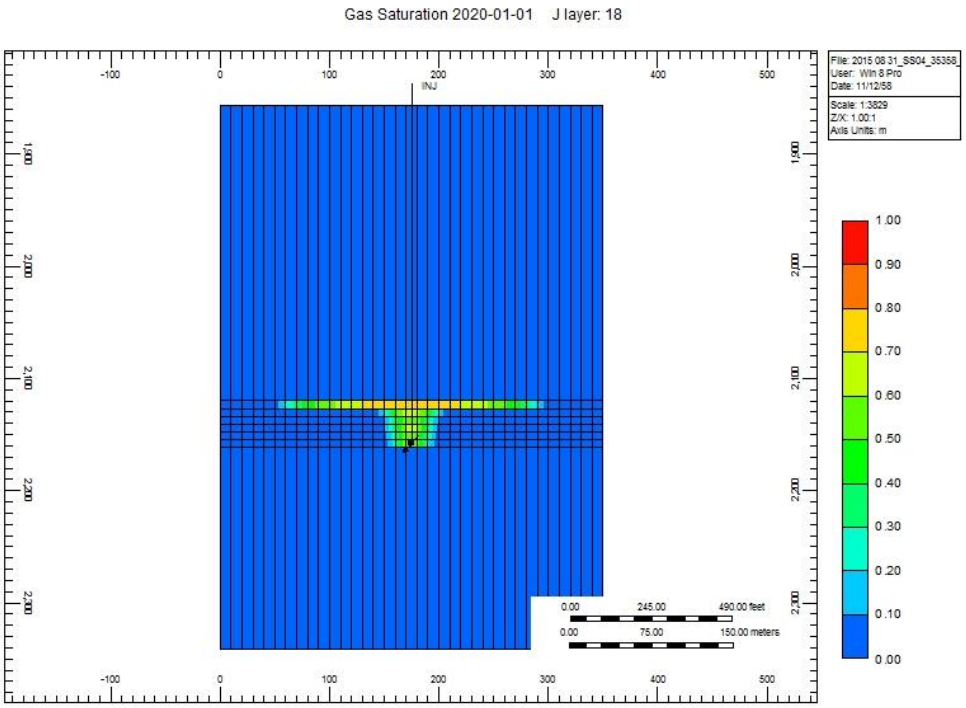

Figure B 42 (a) 3D view, 5 year injection and (b) side view, 5 year injection at. 2119.88-2161.03 m.

a.

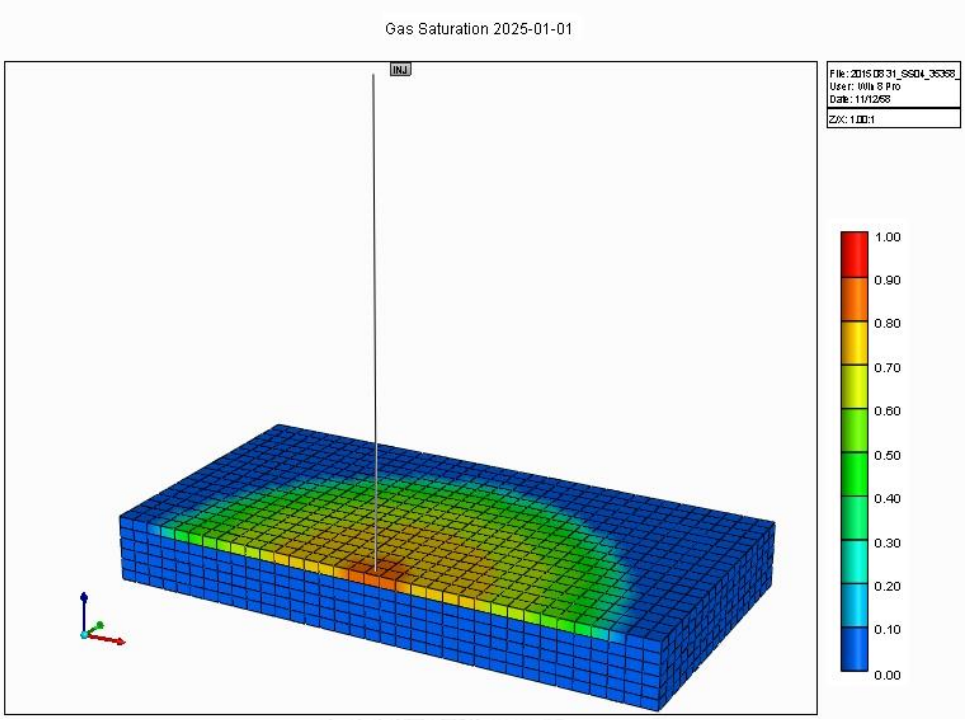

b.

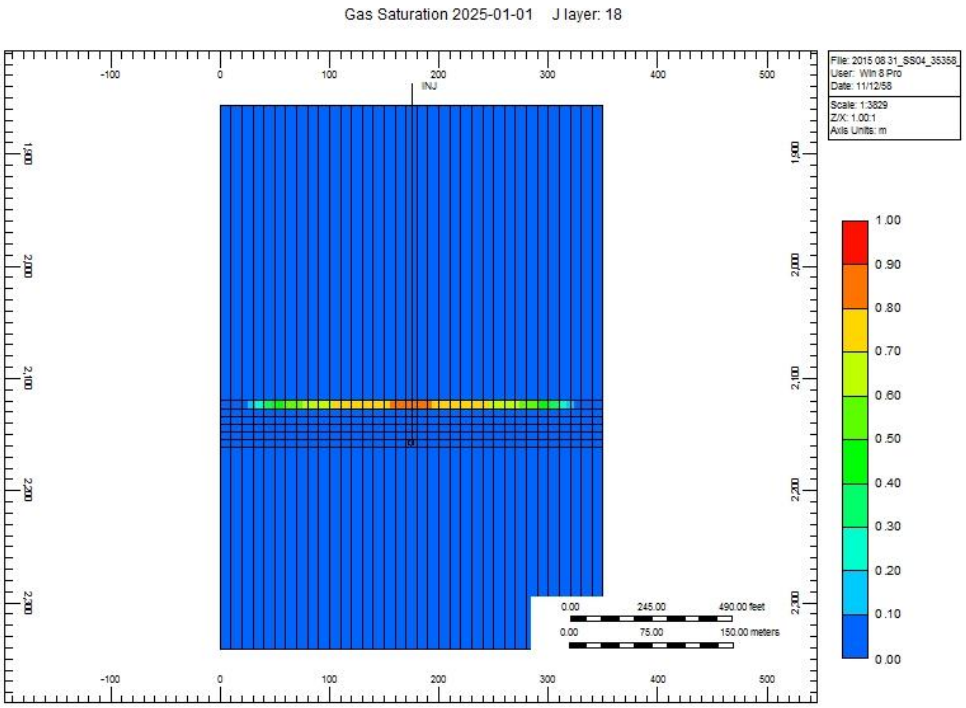

Figure B 43 (a) 3D view, 10 year injection and (b) side view, 10 year injection at. 2119.88-2161.03 m.

a.

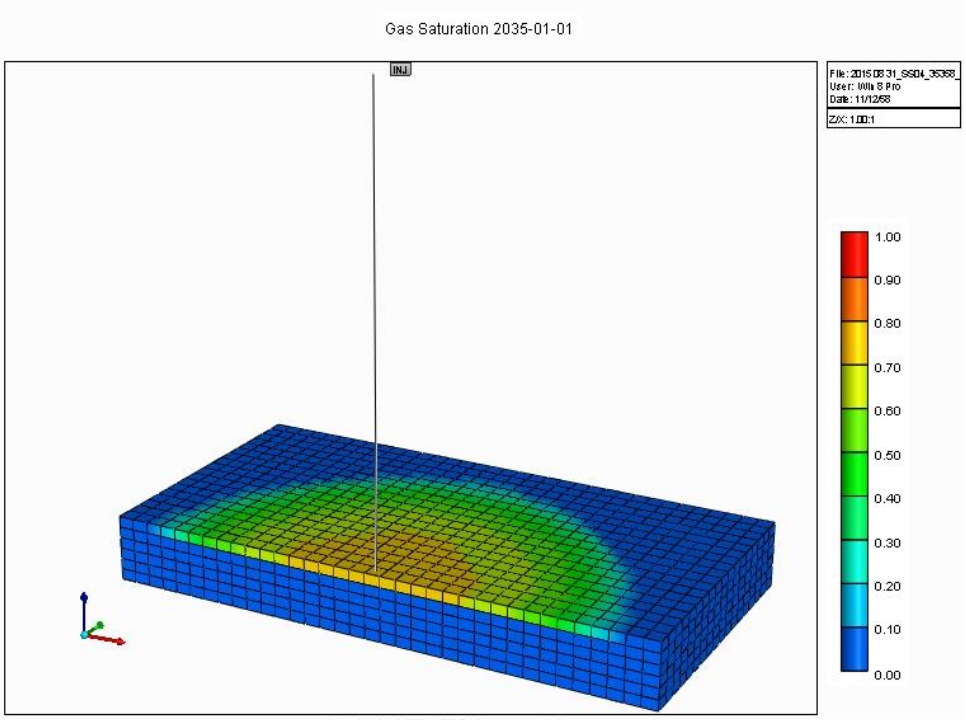

b.

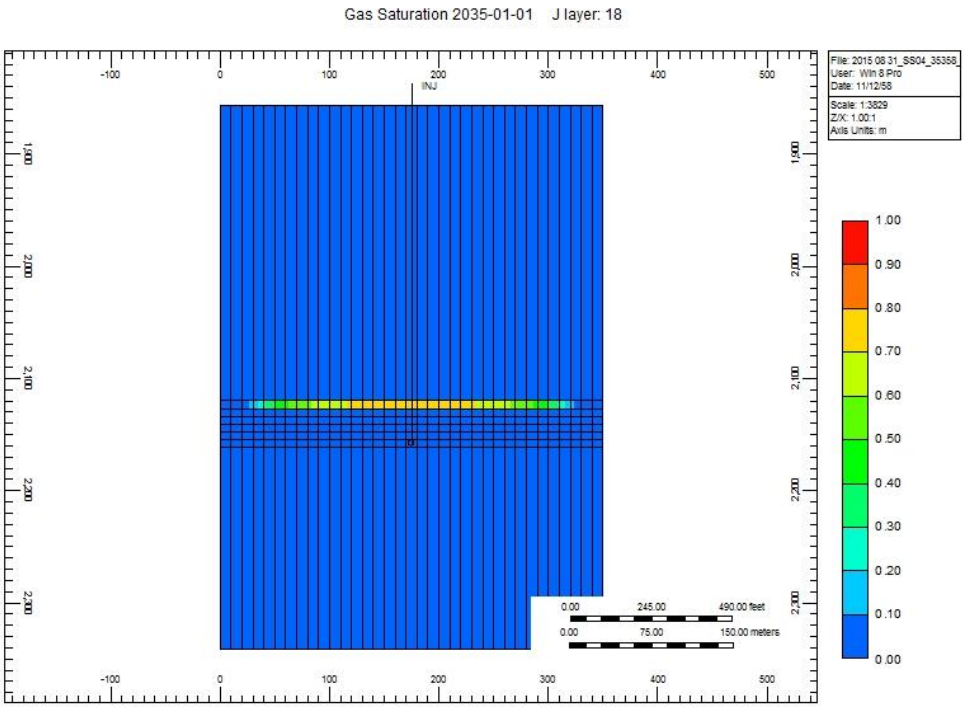

Figure B 44 (a) 3D view, 20 year injection and (b) side view, 20 year injection at. 2119.88-2161.03 m.

a.

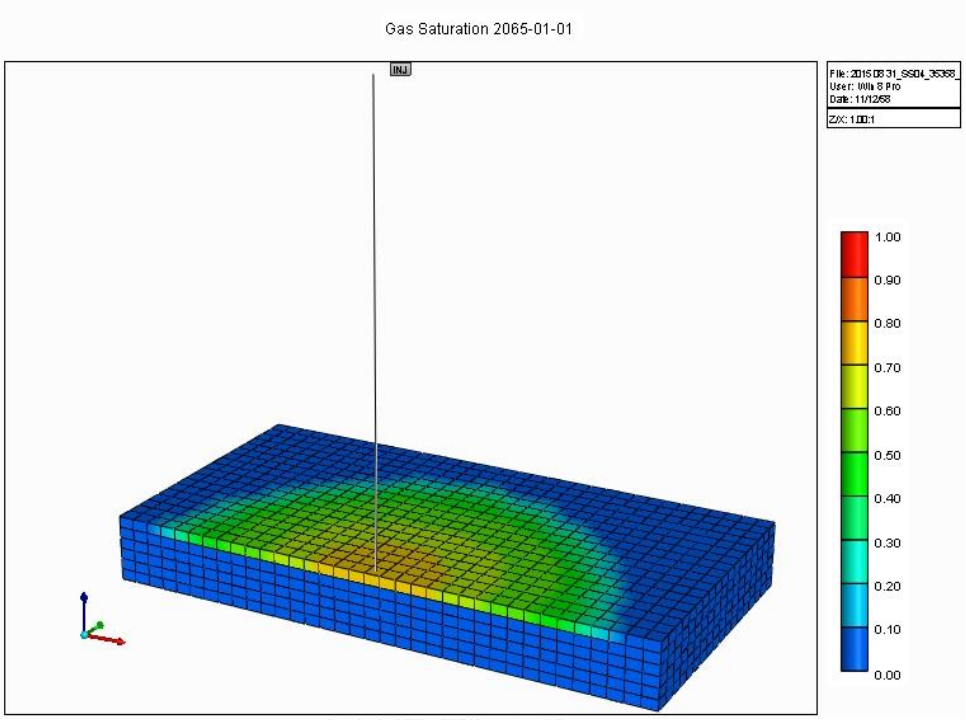

b.

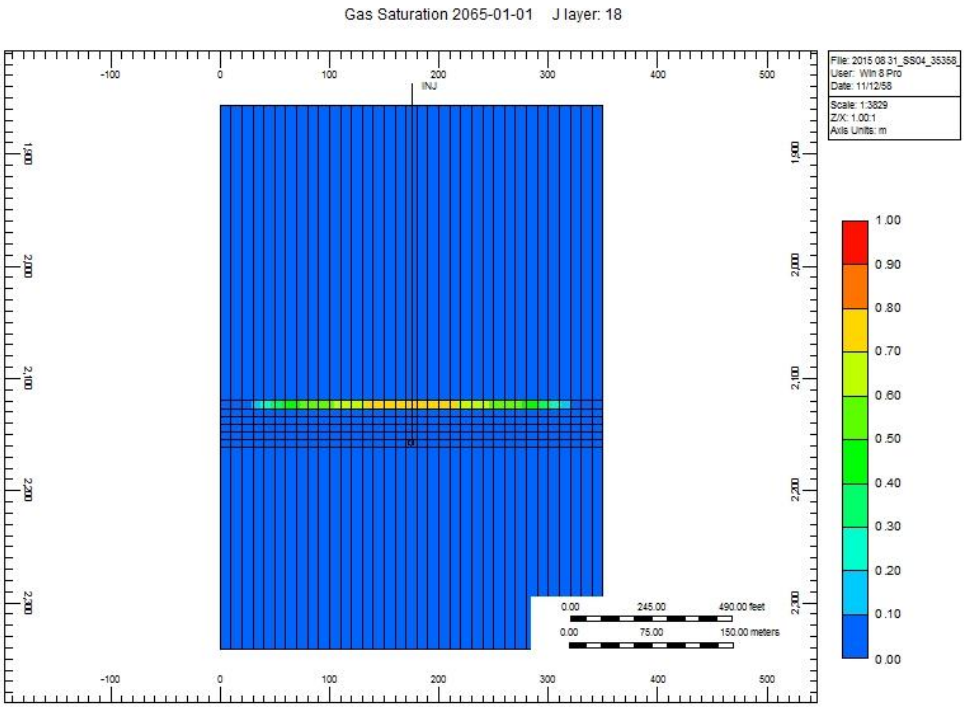

Figure B 45 (a) 3D view, 50 year injection and (b) side view, 50 year injection at. 2119.88-2161.03 m.

a.

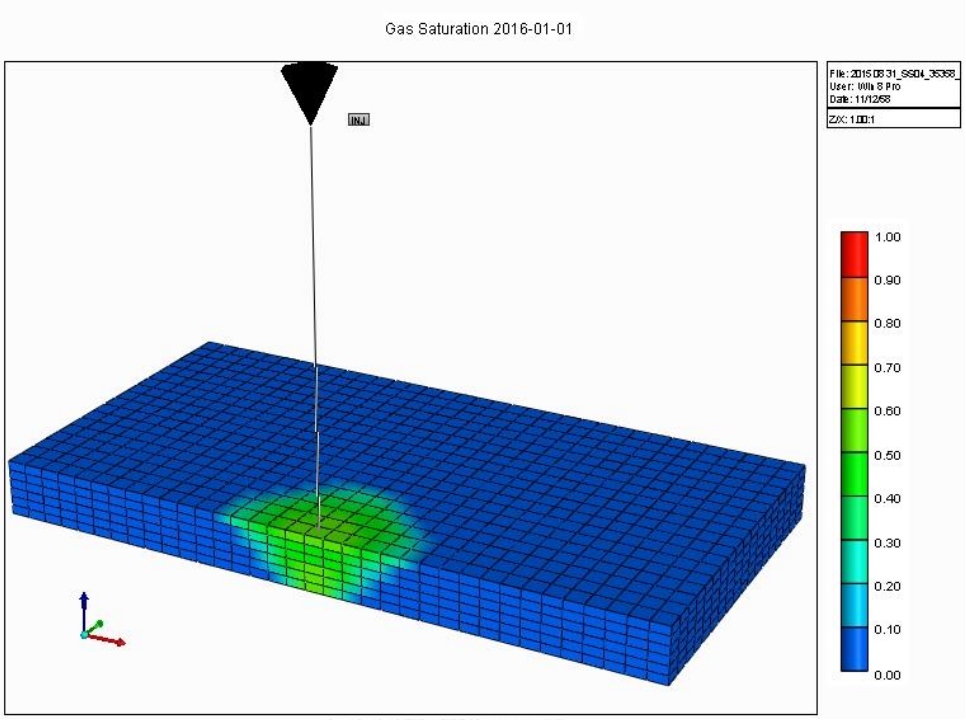

b.

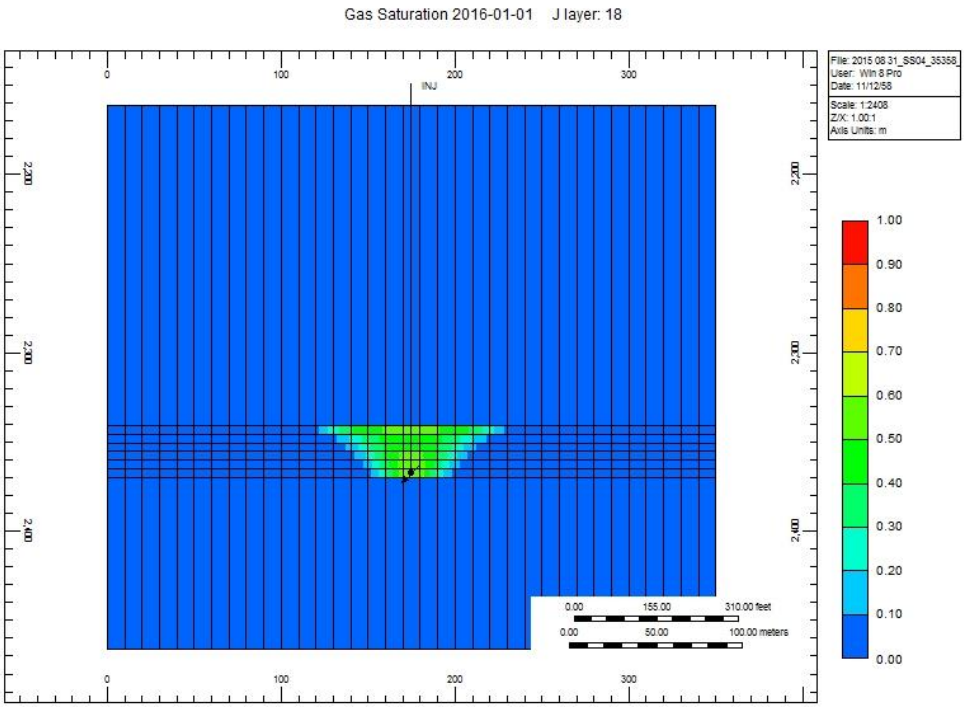

Figure B 46 (a) 3D view, 1 year injection and (b) side view, 1 year injection at. 2340.86-2369.82 m.

a.

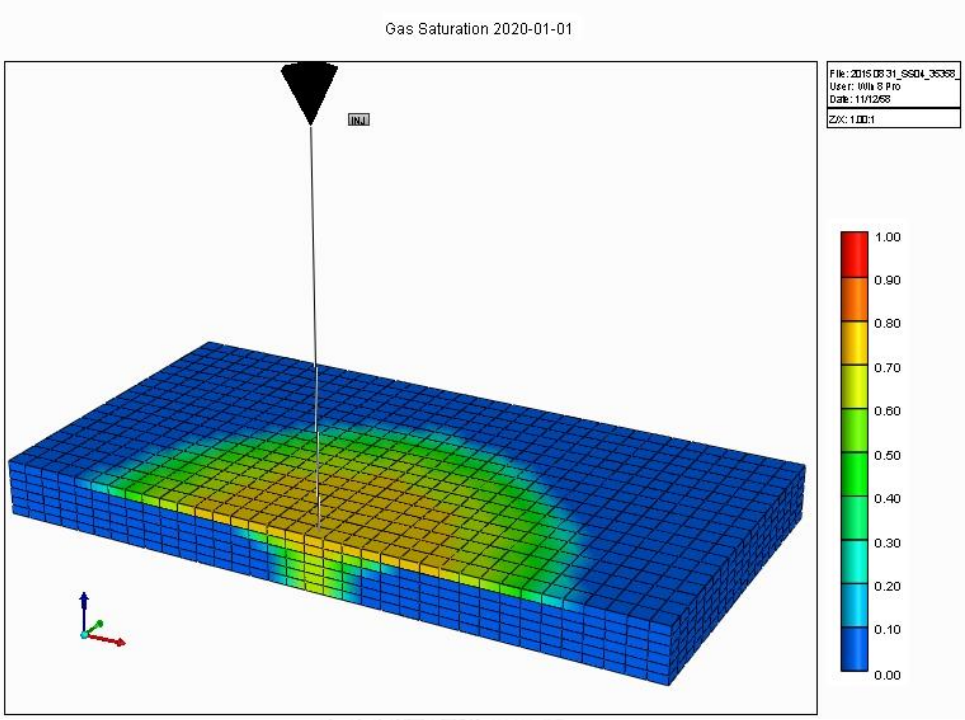

b.

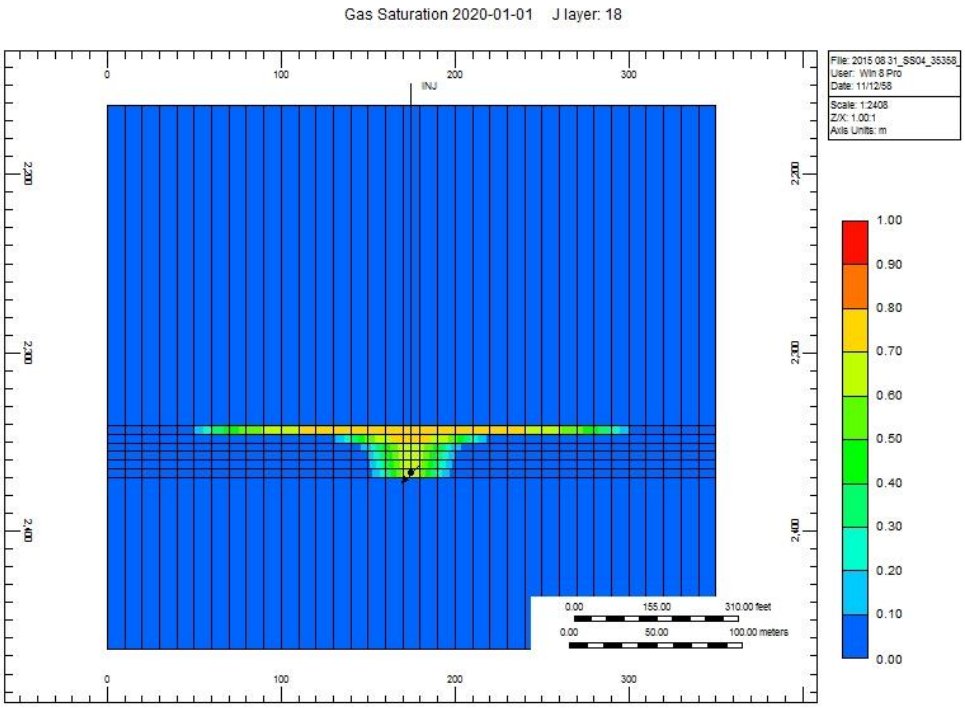

Figure B 47 (a) 3D view, 5 year injection and (b) side view, 5 year injection at. 2340.86-2369.82 m.

a.

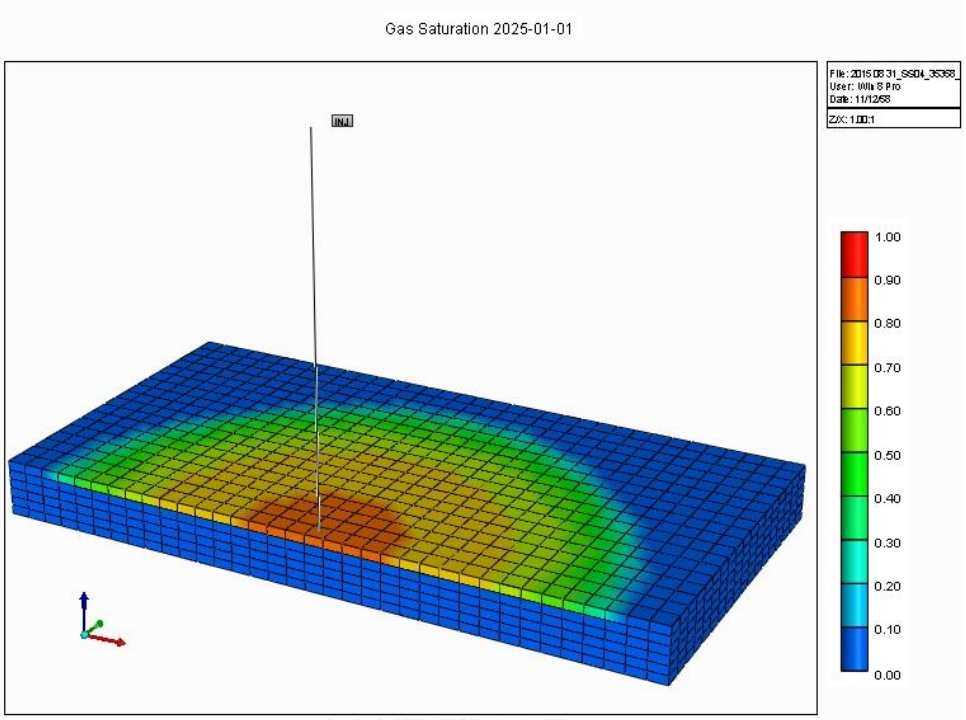

b.

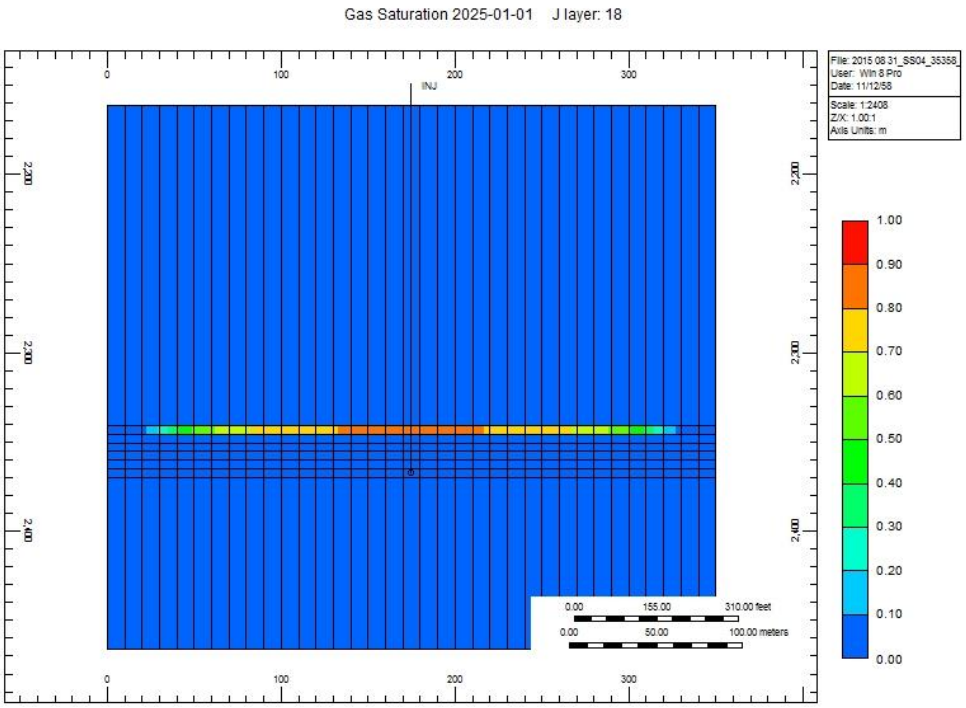

Figure B 48 (a) 3D view, 10 year injection and (b) side view, 10 year injection at. 2340.86-2369.82 m.

a.

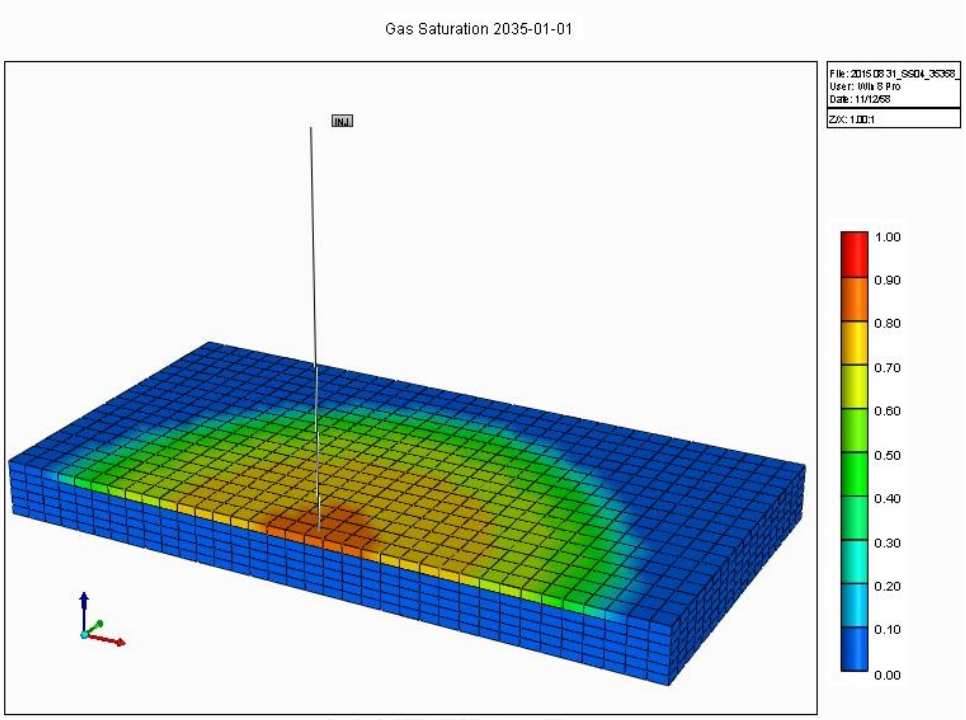

b.

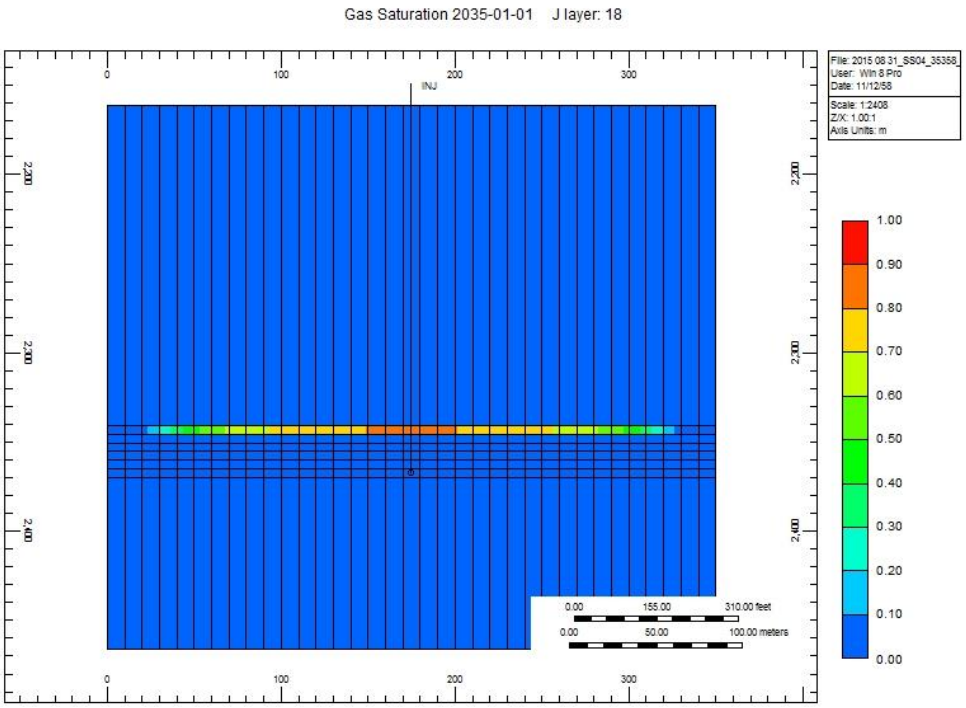

Figure B 49 (a) 3D view, 20 year injection and (b) side view, 20 year injection at. 2340.86-2369.82 m.

a.

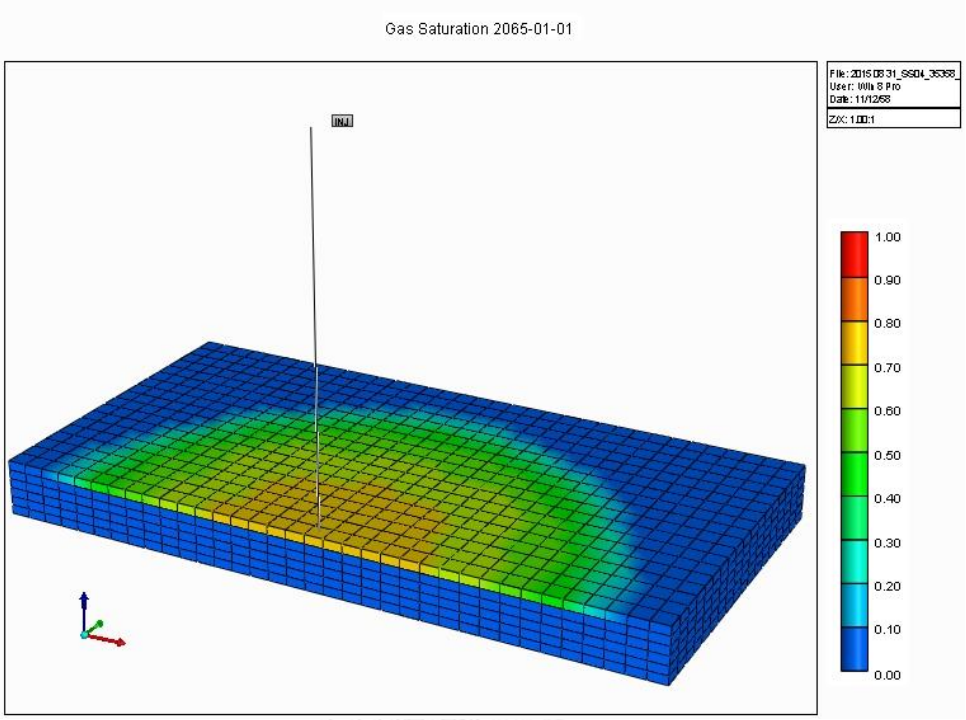

b.

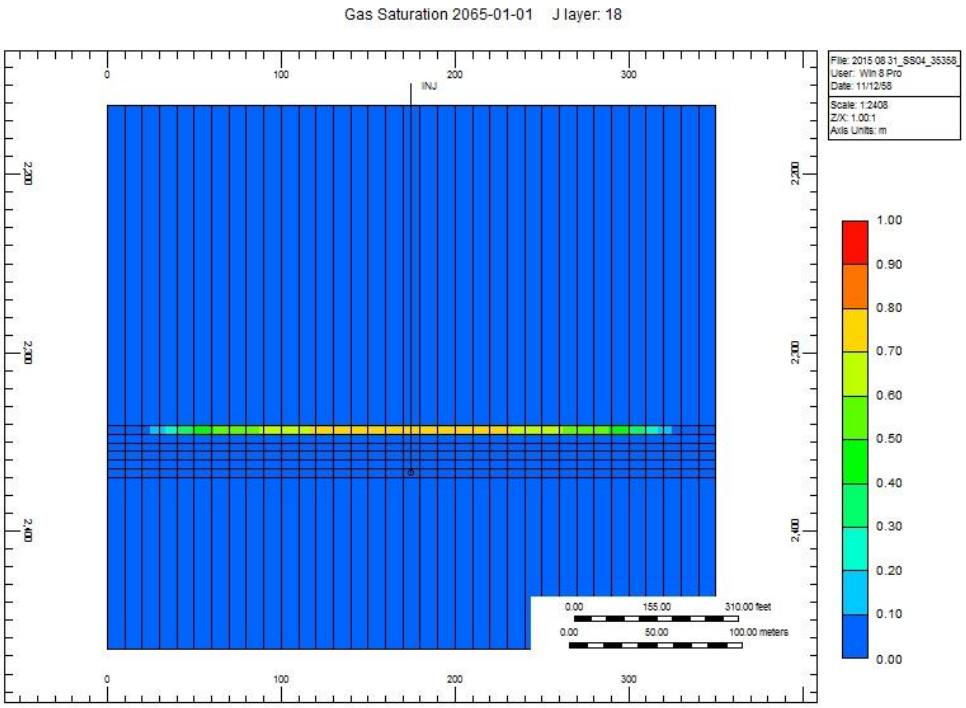

Figure B 50 (a) 3D view, 50 year injection and (b) side view, 50 year injection at. 2340.86-2369.82 m.

a.

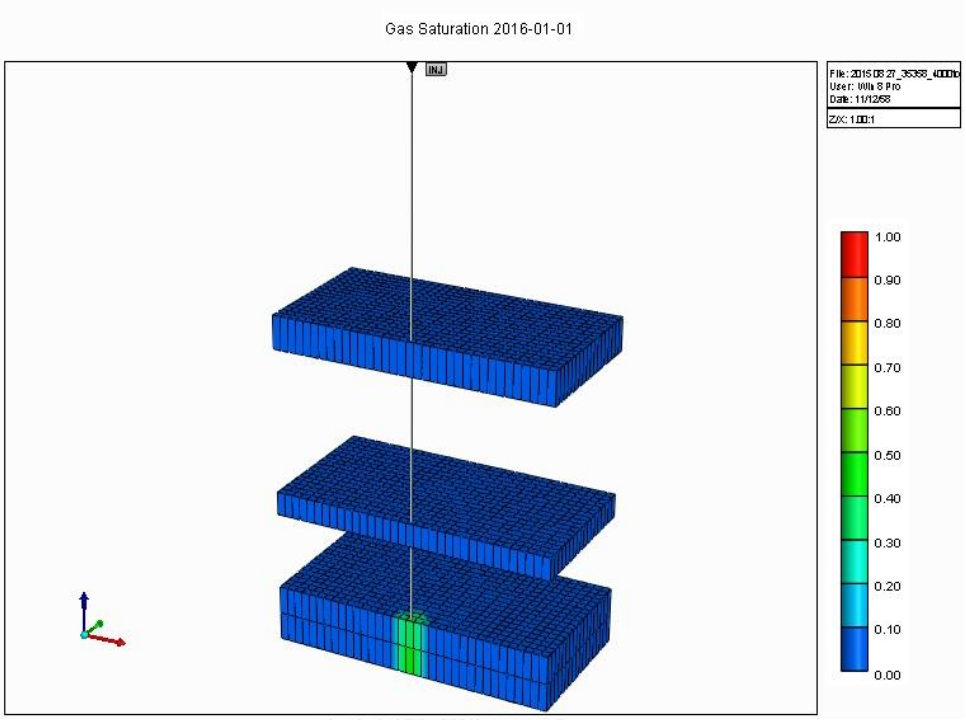

b.

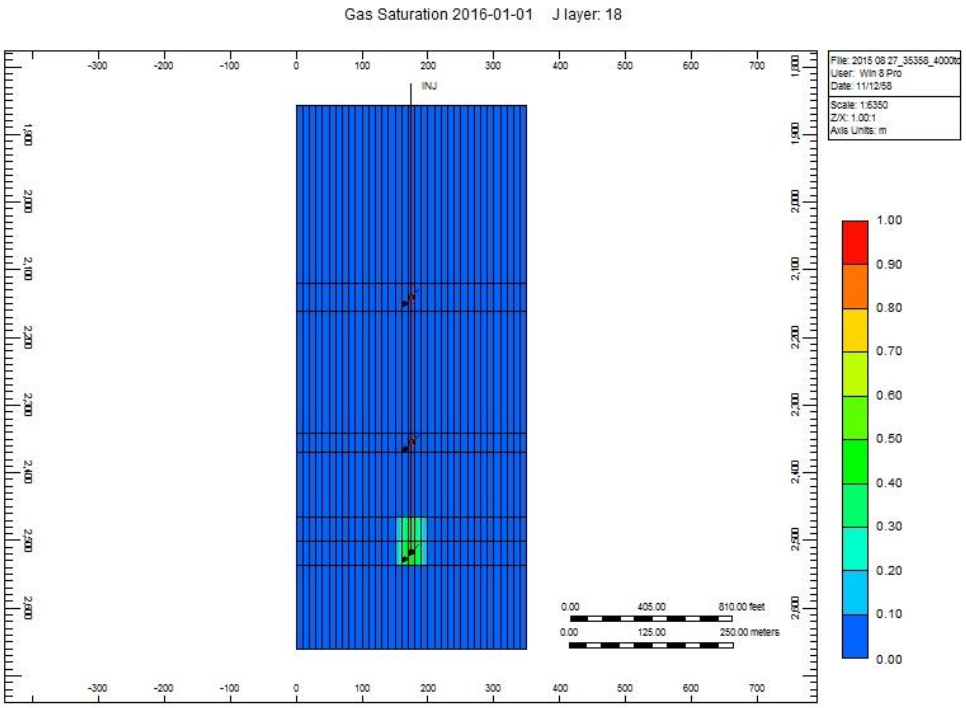

Figure B 51 (a) 3D view, 1 year injection and (b) side view, 1 year injection at. all layer.

a.

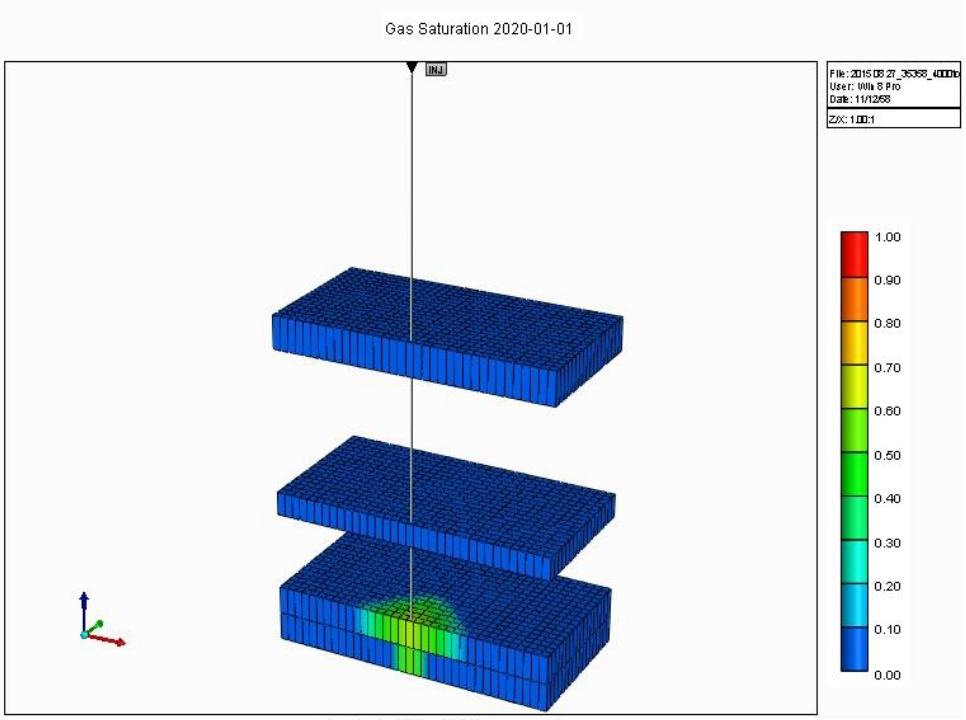

b.

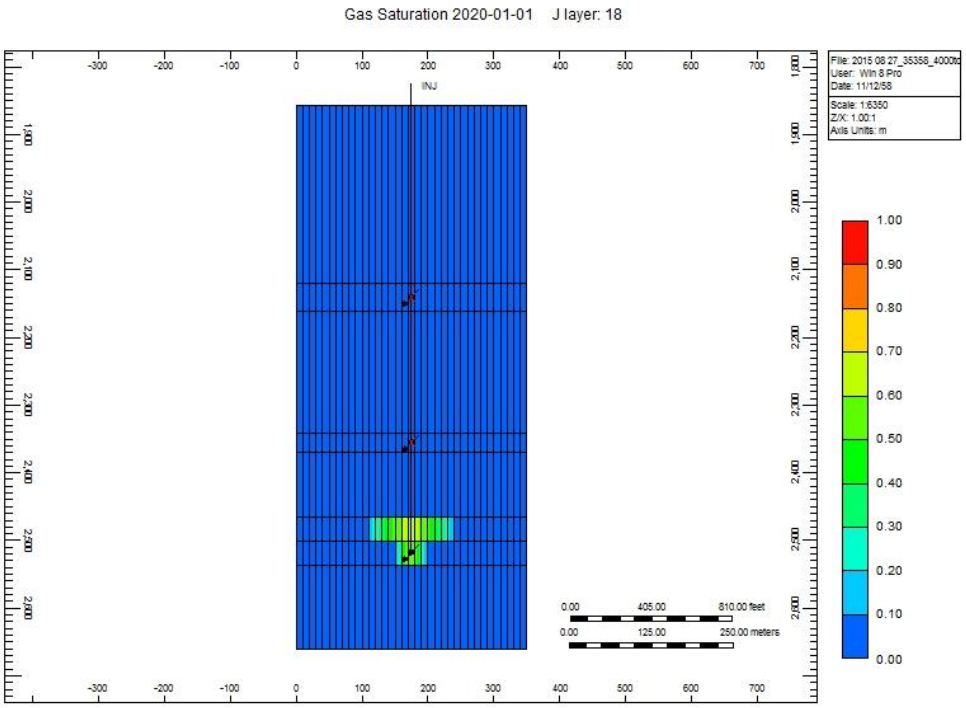

Figure B 52 (a) 3D view, 5 year injection and (b) side view, 5 year injection at. all layer

a.

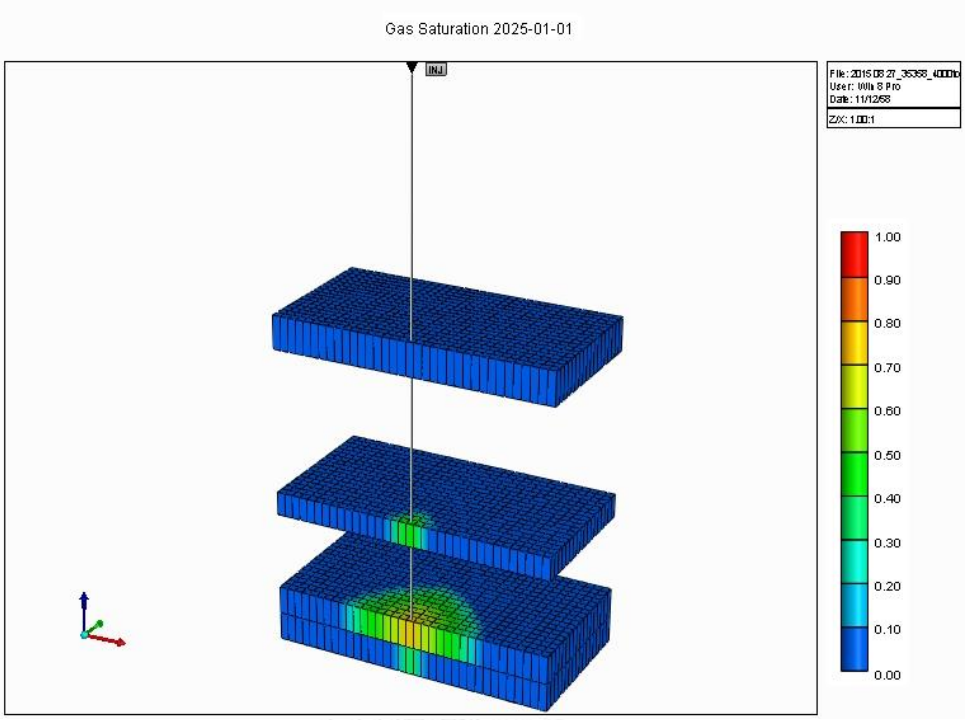

b.

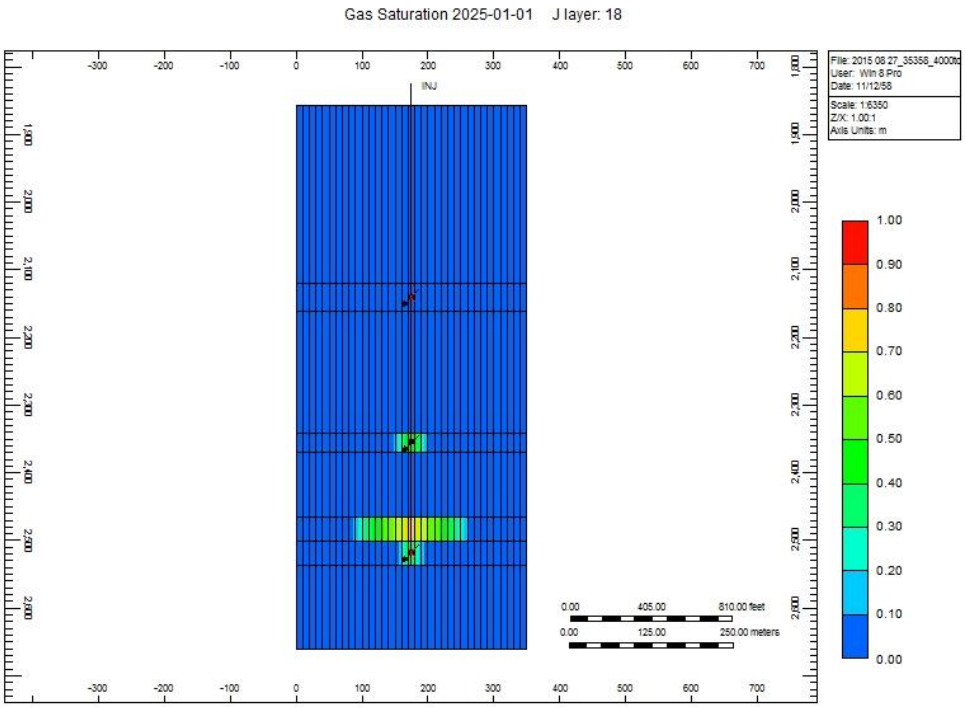

Figure B 53 (a) 3D view, 10 year injection and (b) side view, 10 year injection at. all layer

a.

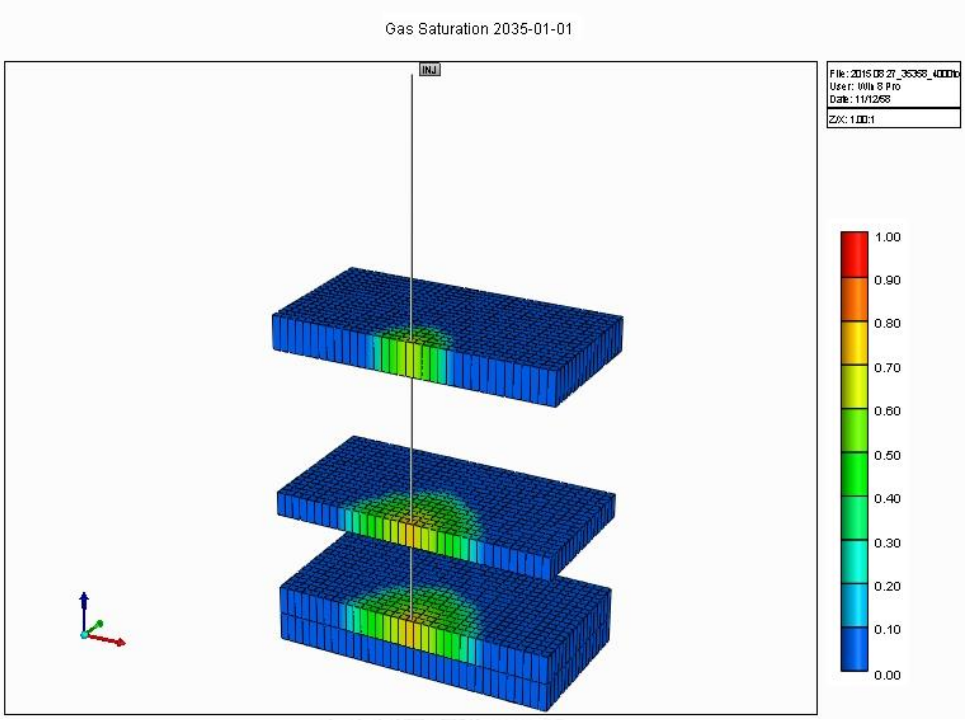

b.

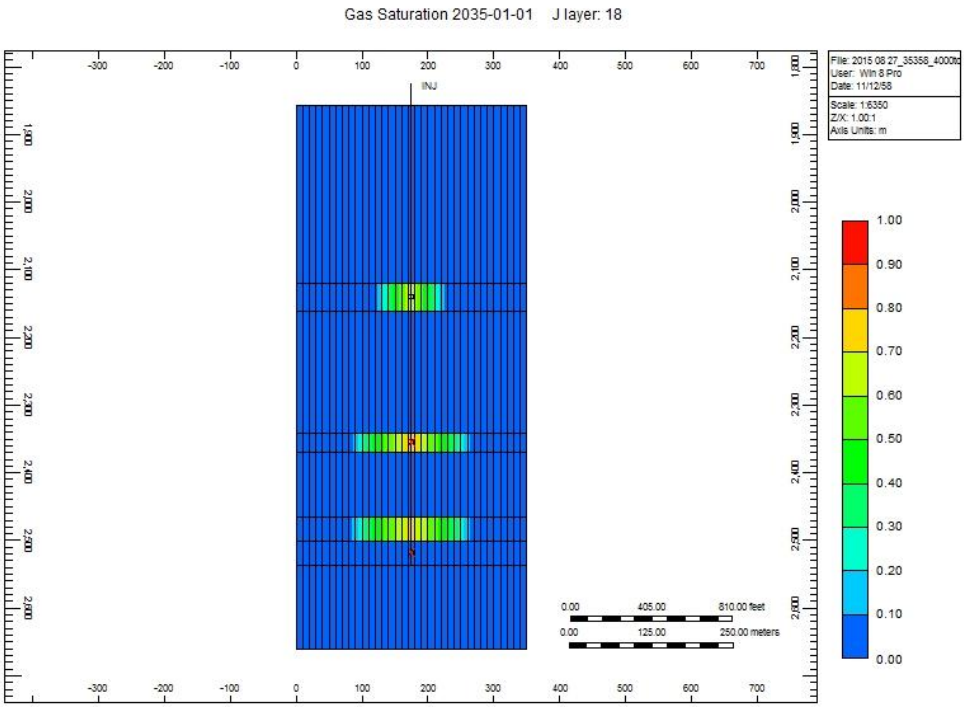

Figure B 54 (a) 3D view, 20 year injection and (b) side view, 20 year injection at. all layer

a.

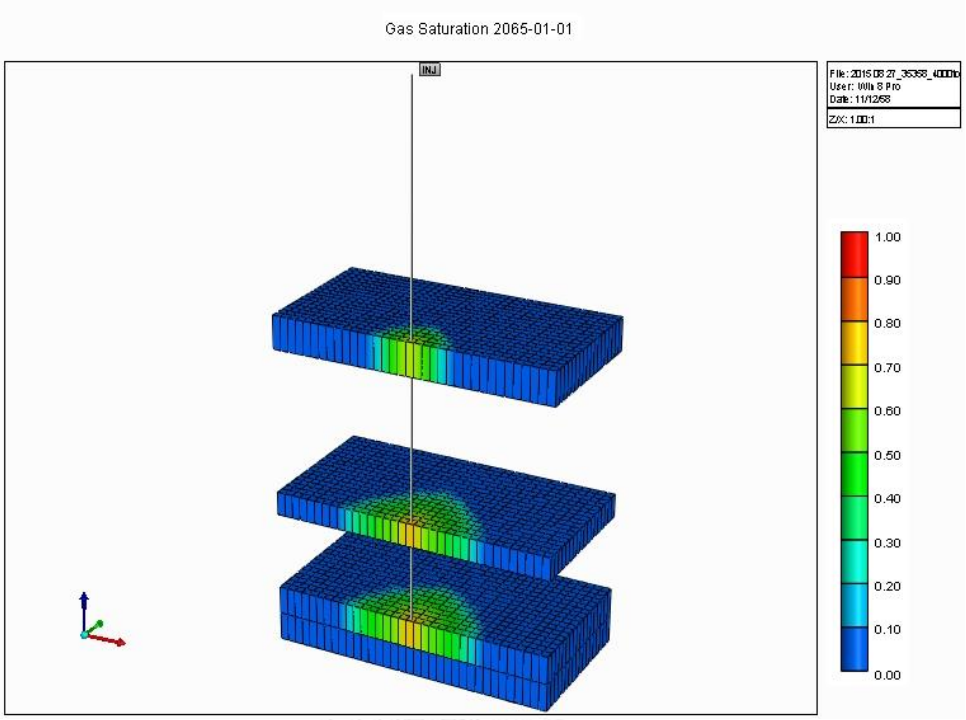

b.

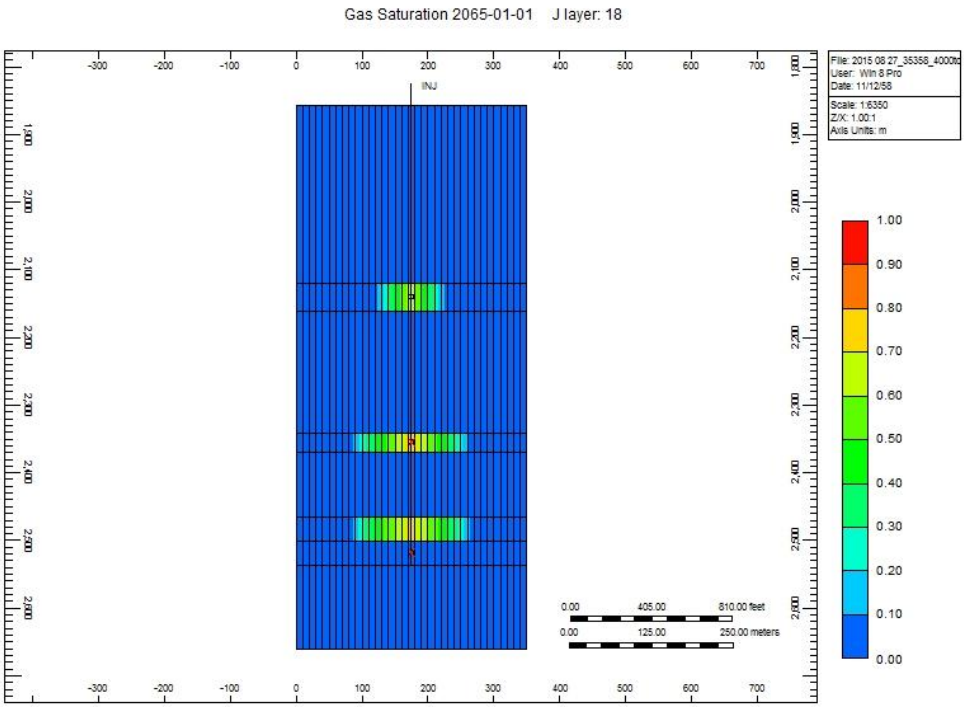

Figure B 55 (a) 3D view, 50 year injection and (b) side view, 50 year injection at. all layer

VITA

Miss Noppawan Ruanman was born on July 4, 1988 in Lampang province, Thailand. She received her Bachelor's Degree of Science (Geology) from Department of Geological Science, Faculty of Science, Chiang Mai University (CMU) in 2010. After graduating, she had worked in Department of Marine and Coastal Resources around 7 months. In 2012, she continued her in Master of Georesources Engineering program at Department of Mining and Petroleum Engineering, Faculty of Engineering, Chulalongkron University.